

	Research and Development Program on Seismic Ground Motion	Ref : SIGMA-2012-D3-38 Version : 01
	CONFIDENTIAL <i>Restricted to SIGMA scientific partners and members of the consortium, please do not pass around</i>	Date : 26/04/2012 Page : 74



Evaluation of the relevance of the numerical simulation approach for site effect estimation: lessons of the Euroseistest Verification and Validation Project (E2VP) - phase 1 and perspectives for phase 2.

Emeline MAUFROY, Emmanuel CHALJUB,
 Pierre-Yves BARD, Fabrice HOLLENDER
 (and many other collaborators)

(26 April 2012 – Version 1)

AUTHORS		REVIEW		APPROVAL	
NOM	DATE and VISA	NOM	DATE and VISA	NOM	DATE and VISA
E. Maufroy (ISTerre)		A. Pecker (Geodynamique et Structures) Scientific Committee	In written review attached	F. Hollender WP Leader	
		R. Paolucci (Politecnico di Milano) Scientific Committee	In written review attached	G. Senfaute SIGMA Project Leader	

DISSEMINATION: Authors; Steering Committee; Work Package leaders, Scientific Committee, Archiving.

	<p>Research and Development Program on Seismic Ground Motion</p> <p>CONFIDENTIAL <i>Restricted to SIGMA scientific partners and members of the consortium, please do not pass around</i></p>	<p>Ref : SIGMA-2012-D3-38 Version : 01</p> <hr/> <p>Date : 26/04/2012 Page : 74</p>
--	--	---

Summary

The estimation of site effects within the framework of a seismic hazard study can involve the use of different approaches, both empiric and numeric. However, in context of low or moderate seismicity, the use of empirical approaches may be difficult to implement due to the lack of representative earthquakes. In this context, the use of numerical tools becomes essential.

Before using the ground motion simulation codes within the framework of civil engineering design purposes, it was requisite to evaluate them. This evaluation is one of the essential tasks scheduled in SIGMA-WP3, in close collaboration with the Cashima project (co-funded by CEA and ILL).

Previous “benchmark” exercises were already done. Our need was to focus on sedimentary basin contexts (due to the situation of sites of possible future applications). One previous work was done for the ESG’2006 meeting and concerned the Grenoble basin (Chaljub et al., 2006; Chaljub et al., 2010). Nevertheless, this last work focused on comparisons between simulation (“verification procedure”) and not comparisons between simulation and real data (“validation procedure”).

Hence, it was necessary to continue the effort on a site where the validation could be possible. This was the motivation of the E2VP.

The first phase of the E2VP (E2VP-1) was conducted between autumn 2007 (preparation tasks) and June 2010 (final meeting). Indeed, the work continued, especially on the verification part with the computation of “canonical cases” (simulations over simple geometries that were built to better understand the differences observed during the verification work of E2VP-1). These “canonical cases” were the link between the two phases of the project.

The second phase of E2VP (E2VP-2) was lunched on February 2012 (Kickoff meeting) and aims to proceed the validation work, especially to better access uncertainties and identify their origins.

This report presents the results of E2VP-1 and of canonical cases. It also briefly presents the schedule of E2VP-2.

Evaluation of the relevance of the numerical simulation approach for site effect estimation: lessons of the Euroseistest Verification and Validation Project (E2VP) - phase 1 and perspectives for phase 2.

Emeline MAUFROY, Emmanuel CHALJUB,
Pierre-Yves BARD, Fabrice HOLLENDER
(and many other collaborators)

(26 April 2012 – Version 1)



TABLE OF CONTENTS

1 INTRODUCTION	6
1.1 CONTEXT AND PLACE OF E2VP WITHIN THE CASHIMA AND SIGMA PROJECTS.....	6
1.2 OBJECTIVES OF THE E2VP-1	6
1.3 CHOICE OF THE RIGHT SITE	7
1.4 HOW TO EVALUATE THE ACCORDANCE BETWEEN TWO SIGNALS (REAL OR SIMULATED): A MATTER OF POINT OF VIEW	8
1.5 PARTICIPATING TEAMS	9
1.6 PROJECT ORGANIZATION	10
2 THE GEOLOGICAL MODEL OF THE MYGDONIAN BASIN	11
2.1 GEOLOGICAL CONTEXT OF THE EUROSEISTEST SITE	11
2.2 GEOLOGICAL, GEOPHYSICAL AND GEOTECHNICAL CHARACTERIZATION.....	12
2.3 GEOMETRIC MODEL CONSTRUCTION	12
3 VERIFICATION OF THE ACCURACY OF THE 3D NUMERICAL METHODS.....	14
3.1 NUMERICAL METHODS	14
3.2 MODEL AND SOURCE CONFIGURATIONS.....	15
3.3 METHOD OF COMPARISON BETWEEN NUMERICAL PREDICTIONS.....	16
3.4 SITE EFFECTS AND GROUND MOTION NUMERICAL PREDICTIONS IN THE MYGDONIAN BASIN.....	18
3.4.1 3D SIMULATIONS OF THE GROUND MOTION CAUSED BY A VIRTUAL CENTRAL EVENT	18
3.4.2 VISCO-ELASTIC SIMULATIONS IN MODEL A.....	18
3.4.3 ELASTIC SIMULATIONS IN MODEL A	20
3.4.4 ELASTIC SIMULATIONS IN MODEL B.....	24
3.4.5 CONCLUSIONS OF THE 3D VERIFICATION EXERCISE	24
3.5 CANONICAL CASES.....	29
3.5.1 HOMOGENEOUS HALFSPACE WITH HIGH V_p/V_s RATIO (CAN1)	29
3.5.2 LAYERED HALFSPACE (CAN2 AND CAN3).....	36
3.5.3 CANONICAL BASIN WITH DIFFERENT SIDES (CAN4 AND CAN5).....	43

4	2D VERIFICATION: LINEAR AND NONLINEAR CASES	48
5	VALIDATION OF THE NUMERICAL DATA FOR REALISTIC APPLICATIONS	52
5.1	COMPARISON WITH LOCAL EARTHQUAKE RECORDINGS FOR VALIDATION OF THE GROUND MOTION NUMERICAL PREDICTIONS	52
5.2	CONCLUSIONS OF VALIDATION	61
6	SENSITIVITY STUDIES, 2D AND 3D CASES.....	63
6.1	SENSITIVITY TO MODEL GEOMETRY: EFFECT OF SURFACE TOPOGRAPHY	63
6.2	SENSITIVITY TO DAMPING.....	65
6.3	SENSITIVITY TO VELOCITY MODEL: EFFECT OF AN ALTERED SURFACE LAYER WITHIN ROCK	67
6.4	SENSITIVITY TO VELOCITY MODEL: IMPACT OF THE REPRESENTATION OF THE SEDIMENTS, LAYERING OR GRADIENT.....	68
6.5	WRAP-UP OF SENSITIVITY RESULTS.....	70
7	CONCLUSION OF E2VP PHASE 1 AND PERSPECTIVES FOR PHASE 2	71
7.1	CONCLUSION OF E2VP PHASE 1	71
7.2	PERSPECTIVES FOR E2VP PHASE 2	73
7.2.1	ESTIMATION OF THE INFLUENCE OF GEOLOGICAL AND SOURCE PARAMETER UNCERTAINTIES ON THE NUMERICAL SIMULATION UNCERTAINTIES.....	73
7.2.2	ESTIMATING GROUND MOTION VARIABILITY USING SIMULATIONS	73
7.2.3	ESTIMATING "SINGLE-STATION SIGMA" WITH REAL ACCELEROMETRIC DATA.....	73
7.2.4	OTHER ISSUES	74
7.2.5	VALIDATION WORK ON DISTANT EVENTS.....	74
7.2.6	UNTIL WHICH FREQUENCY ARE THE DETERMINISTIC MODELING APPROACHES RELEVANT?.....	74
8	REFERENCES	75

1 INTRODUCTION

1.1 CONTEXT AND PLACE OF E2VP WITHIN THE CASHIMA AND SIGMA PROJECTS

The estimation of site effects within the framework of a seismic hazard study can involve the use of different approaches, both empiric and numeric. However, in context of low or moderate seismicity, the use of empirical approaches may be difficult to implement due to the lack of representative earthquakes. In this context, the use of numerical tools becomes essential.

Before using the ground motion simulation codes within the framework of civil engineering design purposes, it was requisite to evaluate them. Previous “benchmark” exercises were already done. Our need within the Cashima project (and later, the Sigma project) was to focus on sedimentary basin contexts (due to the situation of sites of possible future applications). One previous work was done for the ESG’2006 meeting and concerned the Grenoble basin (Chaljub *et al.*, 2006; Chaljub *et al.*, 2010). Nevertheless, this last work focused on comparisons between simulation (“verification procedure”) and not comparisons between simulation and real data (“validation procedure”).

Hence, it was necessary to continue the effort on a site where the validation could be possible. This was the motivation of the E2VP.

The first phase of the E2VP (E2VP-1) was conducted between autumn 2007 (preparation tasks) and June 2010 (final meeting). Indeed, the work continued, especially on the verification part with the computation of “canonical cases” (simulations over simple geometries that were built to better understand the differences observed during the verification work of E2VP-1). These “canonical cases” were the link between the two phases of the project.

The second phase of E2VP (E2VP-2) was lunched on February 2012 (Kickoff meeting) and aims to proceed the validation work, especially to better access uncertainties and identify their origins.

This report presents the results of E2VP-1 and of canonical cases. It also briefly presents the schedule of E2VP-2.

1.2 OBJECTIVES OF THE E2VP-1

During the last decades, an important effort has been dedicated to develop accurate and computationally efficient numerical methods to predict earthquake ground motion in heterogeneous media. The progress in methods and the increasing capability of computers have made it technically feasible to calculate realistic seismograms for frequencies of interest in seismic design applications.

In order to foster the use of numerical simulation in practical prediction, it is important to

1. evaluate the accuracy of current numerical methods when applied to realistic 2D or 3D applications where no reference solution exists (E2VP: “verification” part) and
2. to quantify the agreement between recorded and numerically simulated earthquake ground motion (E2VP: “validation” part).

A verification exercise for numerical simulation of earthquake ground motion in alpine valleys has been previously organized (Chaljub *et al.*, 2006). This exercise revealed that the 3D numerical simulations were far from being a “press-button approach”. It was only after a few more years of collaborative work that four teams succeeded in getting close predictions, which were analyzed with objective quantitative misfit criteria (Tsuno *et al.*, 2006; Chaljub *et al.*, 2010). Among the lessons learned during this process it was clear that several predictions by different numerical methods were needed in realistic situations where no reference solution exists, and that no single method could be considered as best for all important medium-wavefield configurations in terms of accuracy and computational efficiency.

With the aim of extending this initial work on verification and to advance the validation process, it was decided in 2008 to launch the Euroseistest Verification and Validation Project (E2VP) – an ongoing international collaborative work, organized jointly by the Aristotle University of Thessaloniki, Greece, the Cashima research project (supported by the French nuclear agency, CEA, and the Laue-Langevin Institute, ILL, Grenoble), and the Joseph Fourier University, Grenoble, France.

1.3 CHOICE OF THE RIGHT SITE

The first step of the project was to identify a test site. The ideal site should have:

- a good preexisting geological, geophysical and geotechnical characterization in order to produce a realistic model of the medium;
- availability of many seismic event recordings from many different stations (for the validation process);
- a global framework in which all of these information could be used without restriction in a large collaborative project.

After an international investigation, where thirty sites were mentioned, the site "Euroseistest", located a few tens of kilometers east of Thessaloniki, Greece, was chosen. This site have the advantage of a velocity model already available in both 2D (7-layers model derived from Raptakis *et al.*, 2000) and 3D (3-layers model derived from Manakou *et al.*, 2007). In addition, numerous accelerograms are available.

The target of the project is the Mygdonian basin located in North-Eastern Greece, 30 km ENE of Thessaloniki (see *Figure 1*), in the epicentral area of a magnitude 6.5 event that occurred in 1978.



Figure 1: Location of the Euroseistest and the Mygdonian basin in the NE Greece.

The Mygdonian basin is the place of the so-called "Euroseistest" test site which has been extensively investigated within the framework of various European projects (Euroseistest, Euroseismod, Euroseisrisk, Ismod) and is now maintained by ITSAK and AUTH (Pitilakis *et al.*, 2009). The basin has been shaped by NS extensive tectonics with EW trending normal faults on each side. It is now densely instrumented with surface accelerometers (red triangles in Figure 2), including a vertical array with 6 sensors over 200 m depth at the central TST site.

The project makes use of a new detailed 3D model of the Mygdonian basin about 5 km wide and 15 km long, with sediments thickness reaching about 400 m (see Figure 2 and Manakou *et al.*, 2007).

The velocity structure of the basin is well constrained along a central NS profile crossing TST, from a large number of geophysical and geotechnical measurements (*e.g.* Jongmans *et al.*, 1998), surface and borehole seismic prospecting, electrical soundings and microtremor recordings. The sediment thickness is maximum along this profile at the TST site (197 m) and the velocity increases from 130 m/s at very shallow depth to about 650 m/s at large depth, with a large contrast with the underlying bedrock (2600 m/s). The 3D structure in the whole graben has then been extrapolated from this central profile, taking into account information from many single point microtremor measurements, a few array microtremor recordings, one EW refraction profile, and old deep boreholes drilled for water exploration purposes (Raptakis *et al.*, 2005). In the resulting 3D model, the TST site appears like a saddle-point, with the sediment thickness increasing both eastward and westward, off the central profile which actually corresponds to a buried pass between two thicker sub-basins (see Figure 2).

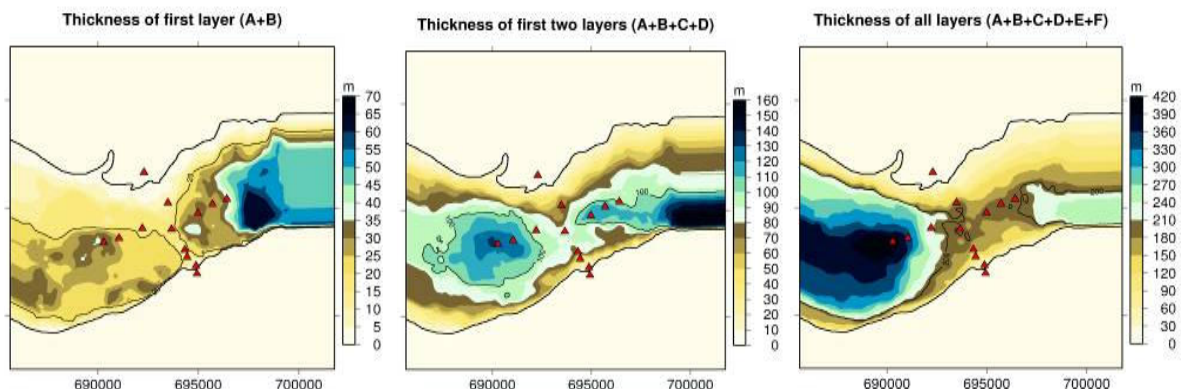


Figure 2: Sediment thickness in the 3D Mygdonian basin model A: first (left), first two (middle) and all layers (right). Note the strong lateral variations and the asymmetries between the northern and southern edges, as well as between the western and eastern sides. The location of the accelerometric array is represented by the red triangles. The central TST site appears as a saddle-point: a maximum in the NS direction and a minimum in the EW direction.

1.4 HOW TO EVALUATE THE ACCORDANCE BETWEEN TWO SIGNALS (REAL OR SIMULATED): A MATTER OF POINT OF VIEW

It is not so simple to determine how to test the reliability of ground motion simulation tools. Of course, this will lead to compare signals between them (simulated signals to simulated signals within the "verification procedure" or real recorded signals to simulated signals within the "validation procedure"). But how to decide the criterion(s) of what is a good agreement or what is a poor agreement?

From the beginning of the E2VP, the experience shows that the agreement within a single set of two signals could appear as (almost) perfection for one person (usually from the engineer community...) and as a complete disaster for the other one (usually from the computational seismology community...), with all intermediate points of view!

Of course these two “end-members” are right in their own referential. We cannot discuss about any agreement without associate it to a given objective. The goal of E2VP is to evaluate the reliability of the simulation tools for civil engineering design purposes. However, even within the civil engineering design context, the choice of the right parameter (or a set of parameters) and the definition of an acceptable agreement threshold is not easy and is one task of its own in the project. Moreover, even if the final target of the project deals with engineer application, the analysis of the results with the seismologist point of view is definitely necessary because it is the only one than can identify (or at least attempt to identify) the reason of discrepancy and thus, can suggest ways of improvement.

In this report, we will try to split all conclusions in two parts in order to give the point of view of both seismologists and engineers. This will result in comparison and discussion starting from synthetic time histories with any attenuation (so, coming from non-realistic cases), to minimalist values such as ratios between two PGA or intensities coming from realistic cases. The two are absolutely essential.

1.5 PARTICIPATING TEAMS

The project involved more than 10 international teams from Europe, China, Japan and USA (see Table 1).

Table 1: Teams and institutions contributing to the E2VP.

Institution	Country	Town	Team acronym
Comenius University of Bratislava	Slovakia	Bratislava	CUB
Université Joseph Fourier	France	Grenoble	UJF
Disaster Prevention Research Institute	Japan	Kyoto	DPRI
Istituto Nazionale di Oceanografia e Geofisica Sperimentale	Italy	Trieste	OGS
National Research Institute for Earth Science and Disaster Prevention	Japan	Tsukuba	NIED
Commissariat à l’Energie Atomique et aux Energies Alternatives	France	Bruyères le Chatel	LDG
Carnegie Mellon University	U.S.A.	Pittsburgh	CMU
Politecnico di Milano	Italy	Milan	POLIMI
Université de Nice – Sophia-Antipolis	France	Valbonne	UNICE
Bureau de Recherches Géologiques et Minières	France	Orléans	BRGM
University of Science and Technology of China	China	Hefei	USTC
Institut de Radioprotection et de Sureté Nucléaire	France	Fontenay-aux-Roses	IRSN
Aristotle University of Thessaloniki	Greece	Thessaloniki	AUTH
Géodynamique et Structure	France	Bagneux	GdS

1.6 PROJECT ORGANIZATION

The first phase of E2VP was co-organized by:

- the Cashima project, funded by the French Alternative Energies and Atomic Energy Commission (CEA) and the Institute Laue Langevin (ILL);
- ISTERre (former LGIT);
- the Aristotle University of Thessaloniki (AUTH).

These three organizations brought the major contributions in different fields of tasks (logistical organization, scientific support and simulation results analysis, data and geomodel supply).

For phase 2 of E2VP, two incomers will also be considered as co-organizers for their major contribution in the preparation of both verification and validation tasks:

- the Comenius University of Bratislava (CUB);
- the ITSAK (Institute of Engineering Seismology and Earthquake Engineering of Greece).

The whole roadmap of E2VP-1 was articulated around periodic workshops for 2 to 3 days, and organized approximately every 6 months. A total of 5 workshops (kickoff, 3 intermediate and final) were held from May 2008 to June 2010. E2VP-2 will follow the same principle, starting with the Kickoff meeting that was organized in February 2012.

During these meetings, it is possible to deeply discuss on the results of previous computations and design the next ones. A couple of weeks before the meeting, it is asked to the different teams to upload their computations on a dedicated website. These results are analyzed, compared, *etc.* by ISTERre before the meetings in order to prepare the discussion. If it is determined during the workshop that further “iterations” (optimization) are required, updated computations may be scheduled within the few weeks that follow the workshop.

2 THE GEOLOGICAL MODEL OF THE MYGDONIAN BASIN

2.1 GEOLOGICAL CONTEXT OF THE EUROSEISTEST SITE

The Mygdonian basin is located in a seismically active zone, belonging to both Serbomacedonian massif and Circum Rodope zone. This basin can be subdivided into two different parts: the eastern part close to the Volvi Lake, striking E-W and the western part close to the Lagada Lake, striking NW-SE. The Euroseistest site is located at the center of the basin, between the two lakes.

The present-day structure of the basin (see Figure 3a) is composed of three structural units, from shallower to deeper unit: (1) the Mygdonian system, (2) the ProMygdonian system and (3) the Paleozoic basement (Manakou, 2007). The Mygdonian and ProMygdonian systems are two sedimentary units with thickness variation of 140 meters, for the eastern part (close to the Volvi Lake) to 400 meters, for the western part (close to the Lagada Lake). The Mygdonian system is composed of fluvial-lacustrine, deltaic, lacustrine, lagoonal and estuarine deposits (Psilovikos, 1977; Sotiriadis *et al.*, 1983), Pleistocene to Holocene age (Quaternary). The ProMygdonian system is composed of conglomerates, sandstones, silt-sand sediments and red-beds (Raptakis *et al.*, 2005), Tertiary age. These two sedimentary units underlie the Paleozoic basement, composed of gneiss, amphibolites, two-mica schist and marble intrusions. These structural units are affected by a complex fault system. In the entire basin, the faults are mostly striking NW-SE, excepted in the eastern part (Volvi Lake) where the faults strike E-W and N-S. The main features are the 12 km long Vasiloudi - Gerakarou - Nikomidino - Stivos fault system, running through the southern and western part of the basin (F-GNSP for the main fault system and F-VL & F-Sx for its two segments, see Figure 3a). This fault system presents a constant dip to the North (70° - 80°), reduced to about 35° with increasing depth.

The tectonic evolution of the Mygdonian basin is marked by two major tectonic events: (1) the N-S extension of the Aegean Sea and (2) the movement of the western end of the north Anatolian fault (Papazachos *et al.*, 1979). The basin structural units recorded a complex tectonic history (see Figure 3b): (1) during Miocene: N-S extension (E-W normal faults), (2) late Miocene: subsiding graben filled by Pro-Mygdonian deposits, (3) Quaternary: continuous subsidence (minor faults) with parallel Mygdonian deposits and recent sedimentary deposits (alluvial fans).

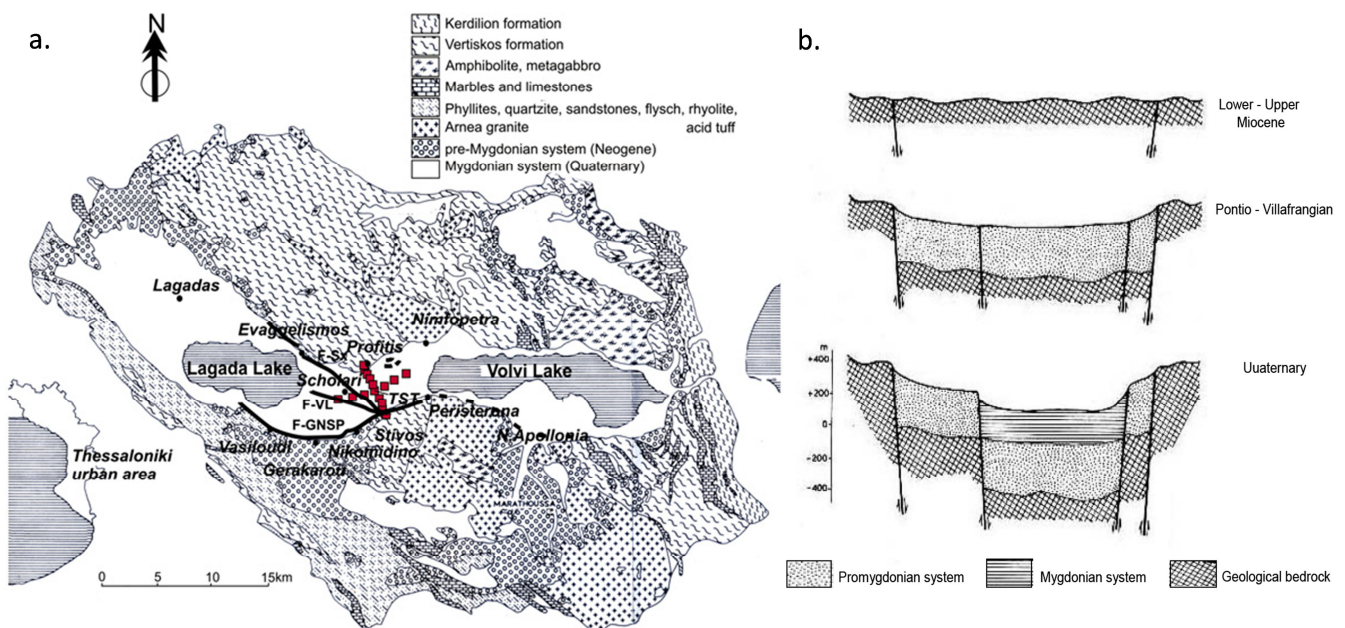


Figure 3: Geological map (a) and tectonic history (b) of the Mygdonian basin (Manakou *et al.*, 2010; Sotiriadis *et al.*, 1983).

2.2 GEOLOGICAL, GEOPHYSICAL AND GEOTECHNICAL CHARACTERIZATION

In the framework of the Euroseistest program, the Mygdonian basin has been characterized through the exploitation of data from many companies allowing the determination of the geometry and the soil properties within the main part of the Mygdonian basin 3D geometry (Manakou, 2007; Manakou *et al.*, 2010).

The geo-database is composed of:

- **geophysical data**, 1100 meters boreholes surveys (in situ SPT testing, 5 Down-Hole, 3 Cross-Hole) and surface seismic (20.5 km), electrical surveys (sounding, tomography) and array microtremor measurements;
- **geotechnical data**, surveys and tests (15 boreholes sampling, 20 CPT and laboratory test);
- **geological data**, boreholes geological descriptions. For data location, see Figure 4.

Using all these available data allowed to precise the bedrock depth and geometry of stratigraphic boundaries, V_P and V_S profiles of surface soil and deeper geological formations and finally, physical, mechanical and dynamic properties of soils formations.

2.3 GEOMETRIC MODEL CONSTRUCTION

The output of all these surveys is the construction of the detailed 2D Profitis – Stivos cross-section (Raptakis *et al.*, 2000; see Figure 5a) and finally the complete 3D structure of the whole basin (Manakou, 2007; see Figure 5b).

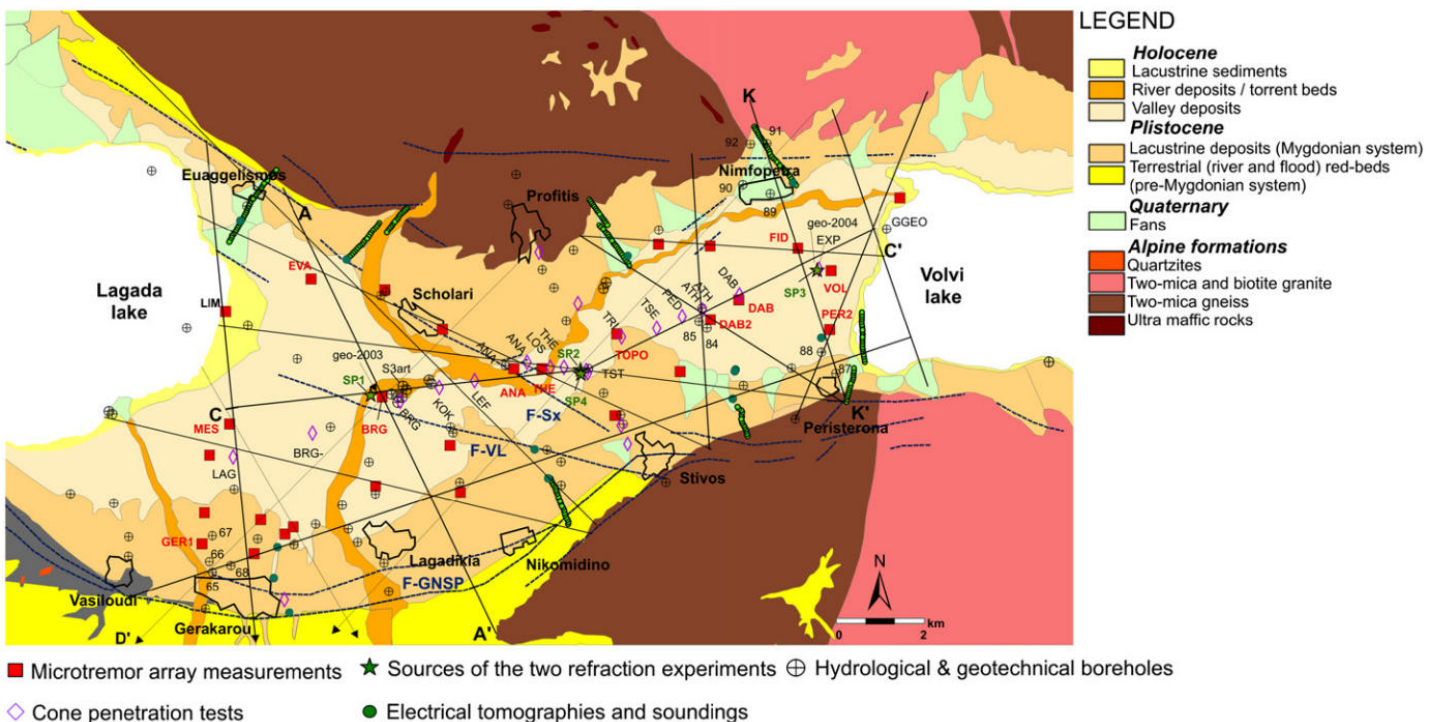


Figure 4: Map showing the location of the measurements used to build the Mygdonian basin 3D model.

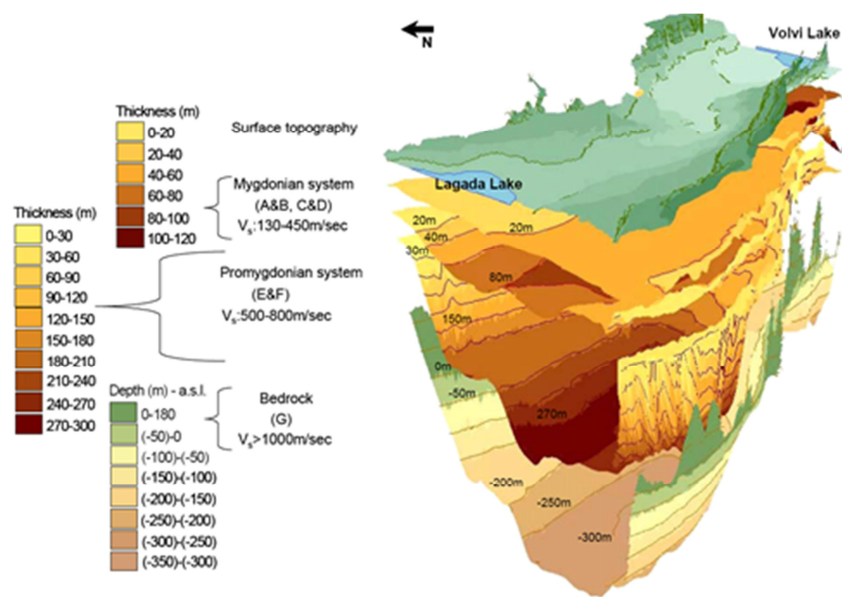
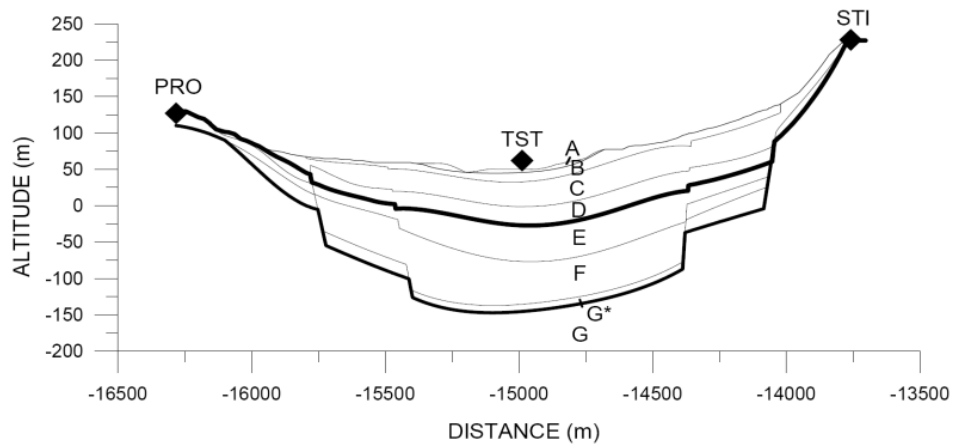


Figure 5: top) 2D - 7 layers model (Raptakis et al., 2000) and bottom) 3D - 3 layers model (Manakou, 2007) of the Mygdonian basin.

3 VERIFICATION OF THE ACCURACY OF THE 3D NUMERICAL METHODS

The verification part was designed in two separate parts: the first one was dedicated to the 3D, linear (visco-)elastic simulation, while the second was intended to compare non-linear codes with a 2D geometry. The present chapter addresses the first component, the second one is (briefly) addressed in the following chapter.

3.1 NUMERICAL METHODS

More than ten teams contribute to the verification of the 3D ground motion simulations by using a large variety of methods: the Finite-Difference Method (FDM), the Finite-Element Method (FEM), the Global Pseudospectral Method (PSM), the Spectral-Element Method (SEM), the Discontinuous Galerkin Method (DGM) and the Discrete-Element Method (DEM) (see Table 2).

Table 2: Applied 3D methods used by the participants of the E2VP. All are 2nd-order in time. GZB stands for Generalized Zener Body. ADE CFS-PML stands for auxiliary differential equations complex-frequency-shifted perfectly matched layer.

Team acronym	3D acronym	Method	Characterization	Attenuation	Absorbing boundary conditions
CUB	3D01	FDM	finite-difference, 4 th -order velocity-stress volume arithmetic and harmonic averages of density and moduli, respectively arbitrary discontinuous staggered grid	GZB 4 rel. mechanisms	CPML
UJF	3D02	SEM	spectral-element, Legendre 4 th -order polynomial Gauss-Lobatto-Legendre integration	GZB 3 rel. mechanisms	Lysmer & Kuhlemeyer
DPRI	3D03	FDM	finite-difference, 4 th -order velocity-stress non-uniform staggered grid	linear Q(f) f ₀ = 2 Hz	Clayton & Engquist A1 + Cerjan
OGS	3D04	PSM	Fourier pseudospectral, vertically stretching staggered grid	GZB 3 rel. mechanisms	CPML
NIED	3D05	FDM	finite-difference, 4 th -order velocity-stress discontinuous staggered grid	linear Q(f) f ₀ = 2 Hz	Clayton & Engquist A1 + Cerjan
LDG	3D06	DEM-SEM	hybrid discrete-element – spectral-element, Voronoi particles (6 dof: 3 in translation, 3 in rotation), 2 nd -order	hysteretic damping	Lysmer & Kuhlemeyer
CMU	3D07	FEM	finite-element, tri-linear elements octree-based discontinuous mesh	Rayleigh att. in the bulk	Stacey
POLIMI	3D08	SEM	spectral-element, Legendre 3 th or 4 th -order polynomial Gauss-Lobatto-Legendre integration	Rayleigh att. in the bulk	Stacey
UNICE	3D09	DGM	discontinuous Galerkin, 2 nd -order polynomial	<i>n.a.</i>	CPML
BRGM	3D11	SEM	spectral-element, Legendre 4 th -order polynomial Gauss-Lobatto-Legendre integration	Memory variables with 8 relaxation mechanisms (Liu & Archuleta, 2006)	paraxial P1 approximation (Stacey, 1988)
USTC	3D12	FDM	finite-difference, 4 th -order velocity-stress curvilinear discontinuous grid	<i>n.a.</i>	ADE CFS-PML

3.2 MODEL AND SOURCE CONFIGURATIONS

The numerical simulations by different methods are compared for a sequence of structural basin models ranging from the simplest up to the most complex. The models include laterally homogeneous sediments with a vertical gradient, 3 irregular homogenous sediment layers, and 3 irregular constant-gradient layers. Elastic and viscoelastic rheologies as well as low and large V_P/V_S ratios are also considered.

The first model (hereafter referred to as model A) is made of homogeneous layers with laterally varying thickness (see Figure 2) and is detailed in Table 3. The letters A-F in the definition of the model refer to the 6 sedimentary units used in the 2D model of Raptakis *et al.* (2000), which have been grouped into three main units in the E2VP 3D model. The second model (B) is a globally continuous model obtained by piecewise linear variations within the original three-layer model (see Table 4). Note that model B is only a very crude smoothed version of model A, no effort has been done yet to define a physically acceptable homogenization of model A.

Other models have been considered in the E2VP, for example a laterally homogeneous model with a vertical gradient, but will not be discussed here. Outside the basin, the regional 1D velocity model of Papazachos (1998) is used (see Figure 6).

Table 3: Mechanical properties of model A. Each layer has homogeneous properties but laterally varying thickness.

Layer	V_S (m/s)	V_P (m/s)	ρ (kg/m ³)	Q_S	Q_K
A+B	200	1500	2100	20	∞
C+D	350	1800	2200	35	∞
E+F	650	2500	2200	65	∞
Bedrock	2600	4500	2600	260	∞

Table 4: Mechanical properties of model B which is heterogeneous with no discontinuities within the sediments.

Layer	V_S (m/s)	V_P (m/s)	ρ (kg/m ³)	Q_S	Q_K
A+B	200-250	1500-1600	2100	20-25	∞
C+D	250-500	1600-2200	2100-2130	25-50	∞
E+F	500-900	2200-2800	2130-2250	50-90	∞
Bedrock	2600	4500	2600	260	∞

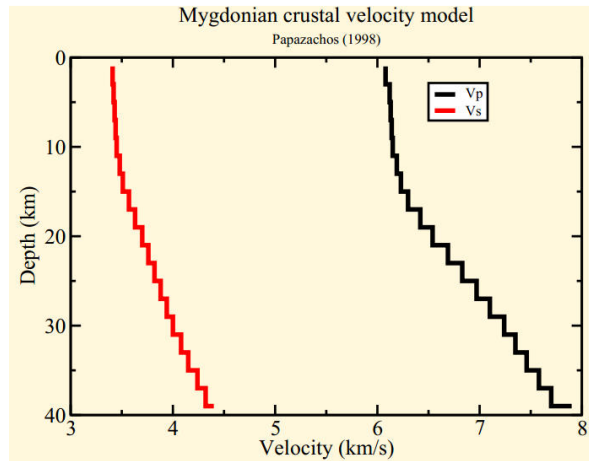


Figure 6: Regional 1D velocity model of the Mygdonian crustal structure (from Papazachos, 1998) considered as only depth-dependent with no lateral variation.

3.3 METHOD OF COMPARISON BETWEEN NUMERICAL PREDICTIONS

3D numerical predictions are compared using quantitative time-frequency envelope and phase goodness-of-fit criteria. Solutions are also compared with respect to model, wavefield and computational aspects of simulations.

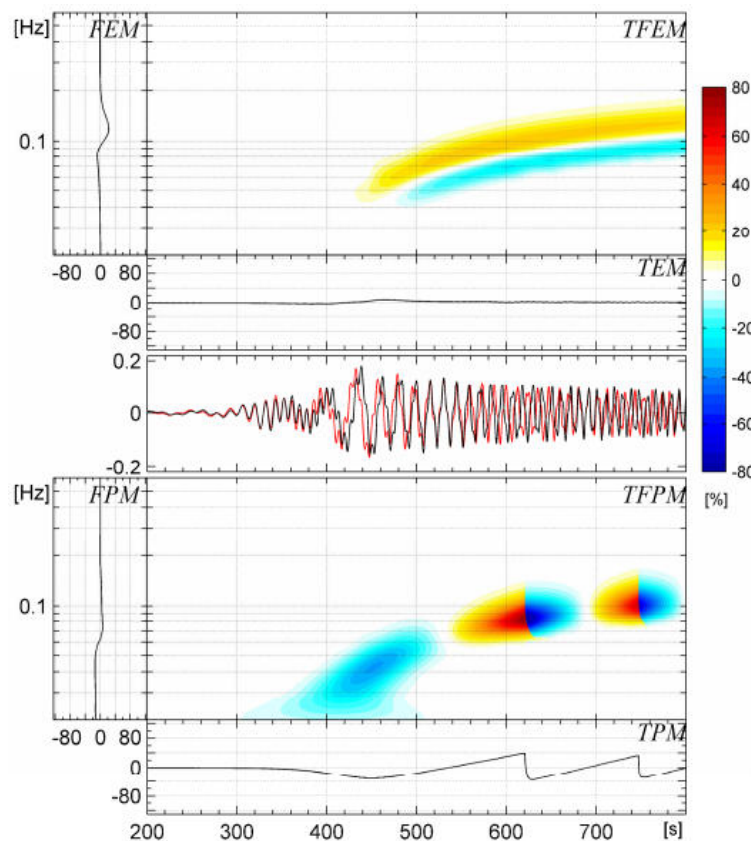


Figure 7: Example of computation of the Time-Frequency Envelope and Phase misfits between two signals (after Kristeková et al., 2006). TFEM and TPEM: time-frequency envelope and phase misfits, TPEM and TPPEM: time-dependent envelope and phase misfits, FPEM and TPPEM: frequency-dependent envelope and phase misfits.

In order to get a more global and quantitative picture of the differences between numerical predictions, we applied the time-frequency misfit and goodness-of-fit criteria proposed by Kristeková *et al.* (2009) and recalled in Figure 7 and Figure 8. From the time-frequency representation of two signals, an envelope and a phase misfits are computed, which are further averaged in time and frequency to give a single number. The misfit values are then converted into two envelope/phase goodness-of-fit (GOF) scores comprised between 0 (total misfit) and 10 (perfect fit) through the following non-linear scaling (see also Figure 8):

$$[1] \quad \text{GOF} = 10 \exp(-|\text{misfit}|).$$

In the validation part of E2VP, the synthetics are confronted to real data by comparing the values obtained on ten representative ground motion criteria: Arias duration, energy duration, Arias intensity, energy integral, PGA, PGV, PGD, response spectra, Fourier spectra and cross correlation (Anderson, 2004). The match between the observed records and synthetics is then quantitatively scored by computing the goodness-of-fit (GOF) scores for each ground motion criterion comprised between 0 (total misfit) and 10 (perfect fit) through the following non-linear scaling that is slightly different than the previous one (see also Figure 9):

$$[2] \quad \text{GOF} = 10 \exp(-\text{misfit}^2).$$

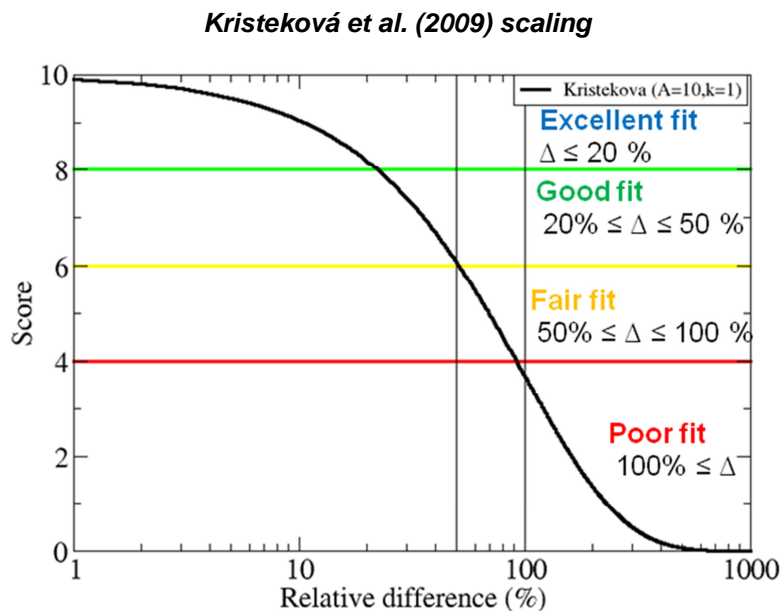


Figure 8: Non-linear scaling recommended by Kristeková *et al.* (2009) between the values of misfits and the values of goodness-of-fit (GOF) used in the verification part of the E2VP. Following Anderson (2004) and Kristeková *et al.* (2009), a cruder verbal scale (poor-fair-good-excellent) is also used.

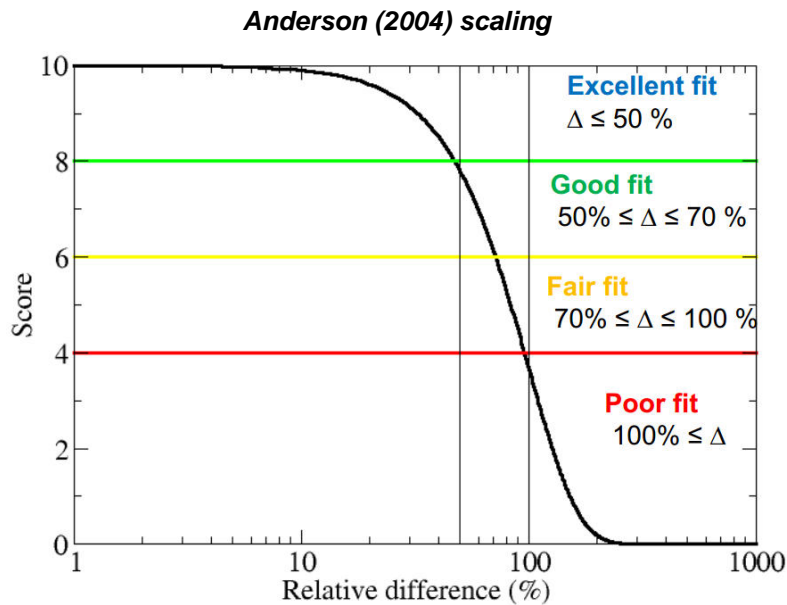


Figure 9: Non-linear scaling recommended by Anderson (2004) between the values of misfits and the values of goodness-of-fit (GOF) computed on representative ground motion criteria used in the validation part of the E2VP. Following Anderson (2004) and Kristeková et al. (2009), a cruder verbal scale (poor-fair-good-excellent) is also used.

3.4 SITE EFFECTS AND GROUND MOTION NUMERICAL PREDICTIONS IN THE MYGDONIAN BASIN

The comparative analysis presented hereafter identifies non-planar material interfaces, free surface and contact of the free surface with the interfaces as key factors affecting the accuracy of simulations, and, in particular, the generation and propagation of diffracted surface waves.

3.4.1 3D simulations of the ground motion caused by a virtual central event

In what follows, we compare different 3D numerical simulations of the ground motion in the Mygdonian basin models A and B, caused by a virtual M1.3 event, approximated by a double-couple point-source located 5 km beneath the TST central site (see Figure 10). For each source-model configuration, the teams were required to compute 30 seconds of ground motion at 288 receivers (yellow triangles in Figure 10).

3.4.2 Visco-elastic simulations in model A

Figure 11 shows the peak ground velocity maps computed by four teams for the three-layer model A, when intrinsic attenuation is included (this case is referred to as '12b' in the E2VP). All maps show similar distributions of peak values, the largest being located on the northern side of the basin where the sediment cover is the shallowest and the slope of the basin edge varies most. The time-series of ground velocity at the central site TST computed by 7 teams are shown in Figure 12. Note the good agreement between most of the predictions for early arrivals (less than 6 s), especially on the vertical component, and the (sometimes large) differences both in phase and amplitude seen on late arrivals. Some of those differences, in particular in amplitude, can be attributed to the fact that two teams (3D03, 3D05) imposed a linear dependence of the quality factor on frequency, instead of the required constant (see Table 2).

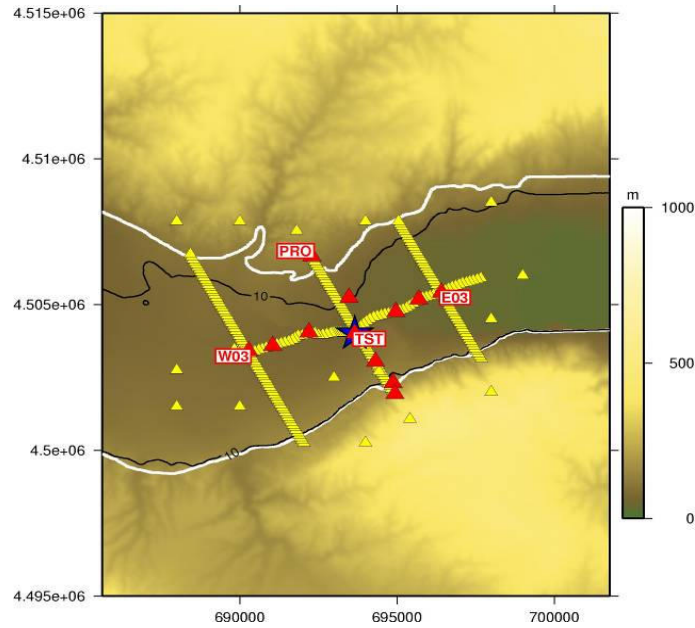


Figure 10: Detailed view of the Euroseistest accelerometric network (red triangles) and additional receivers (yellow triangles) used to compare 3D numerical solutions. The white line denotes the basin edge and the black line is the location where the sediment thickness equals 10m. The blue star is the epicenter of a virtual seismic event considered in the 3D numerical simulations.

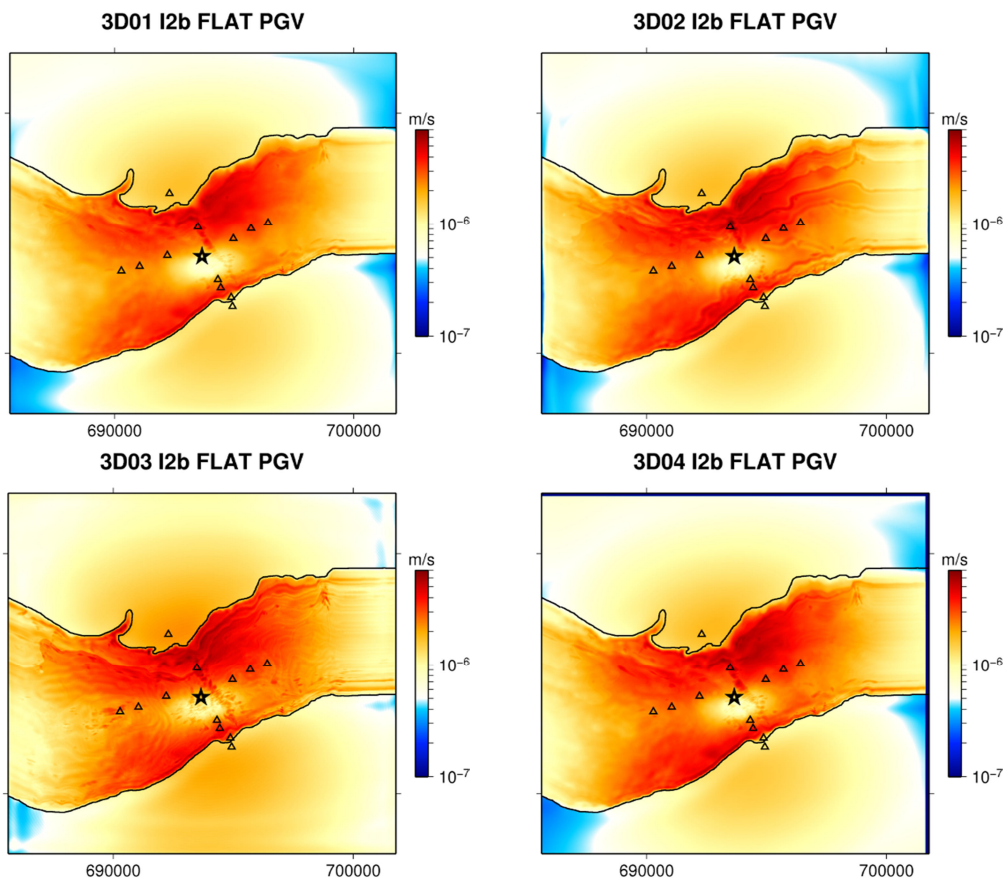


Figure 11: Maps of peak ground velocity obtained by four different teams for the E2VP case '12b' which considers a viscoelastic rheology in the three-layer model A of the Mygdonian basin. The triangles denote the positions of the Euroseistest array and the star is the epicenter of the point-source used for verification purposes. Note the similarities in the displayed maps, and the asymmetries between the northern and southern edges, the largest peak values being obtained where the slope of the basin edge is the most gentle.

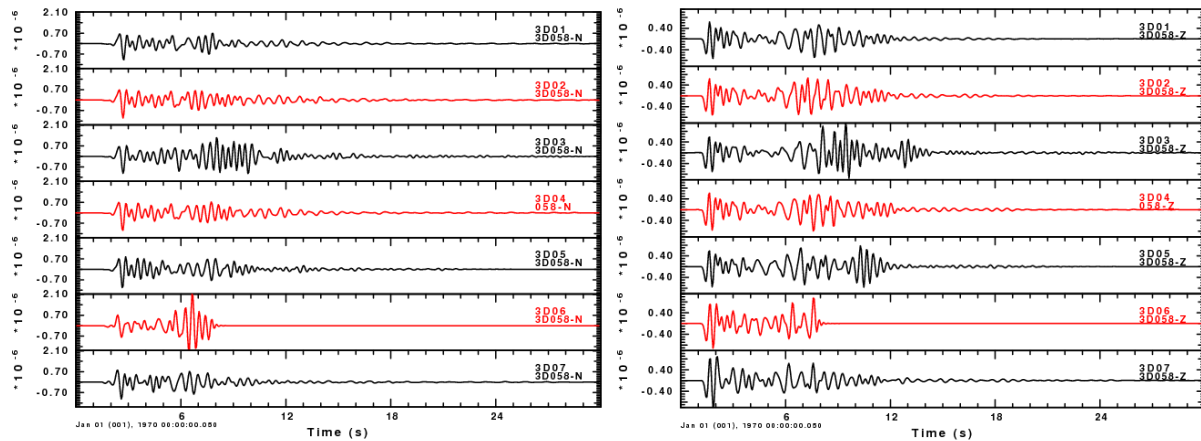


Figure 12: N-S (left) and vertical (right) components of ground velocity at TST computed by 7 different teams for the I2b case. Most of the predictions are very consistent for the first 6 seconds, before the arrival of late phases, among which surface waves diffracted off the valley edges. Some predictions are very close (3D01, 3D02, 3D04) for the whole time window. Note that teams 3D03 and 3D05 did not implement the imposed constant-Q visco-elastic rheology, and that team 3D07 used a maximum V_P/V_S ratio of 3.

Figure 13 shows the average of the phase and amplitude GOF values computed at the 288 receivers. Each colored dot corresponds to a weighted average over the three components of ground velocity in the frequency range of the simulation [0-4 Hz]. These maps are very useful to track differences between predictions, which can be further investigated by inspecting individual (phase or amplitude) GOF maps in separate frequency bands. Figure 13 shows that the results obtained by teams 3D01, 3D02 and 3D04 are the most similar, with mean GOF values comprised between 7.4 and 8.0. The larger misfit seen between 3D01 and 3D03 is partly due to differences in implementing attenuation. Not shown are the GOF maps for the other predictions which are all lower than the ones presented here, for reasons specific to each team: 3D05 did not implement the imposed visco-elastic rheology (the level of GOF between 3D01 and 3D05 is similar to the one between 3D03 and 3D01), 3D06 is still working on the development of its code, and 3D07 implemented a different attenuation mechanism and imposed a maximum V_P/V_S ratio of 3 due to limitations of computational resources.

3.4.3 Elastic simulations in model A

To cancel the effect of different implementations of attenuation in the misfits seen at late times, we have considered a case, referred to as 'I2c', with a pure elastic rheology. The PGV maps (computed by 5 teams) and the time series of ground velocity at TST (computed by 8 teams) are shown in Figure 14 and Figure 15, respectively. The I2c case, although completely non-physical, represents a numerical challenge since late arrivals, mainly very dispersive surface waves, are now dominating the time series. They also affect the maps of peak values with the presence of 'stripes'; their locations are very consistently reproduced by the different teams (see Figure 14). Those peculiar features are caused by spatially localized surface wave packets diffracted off the basin edges and propagating towards the center of the basin without being attenuated. Figure 16 shows the maps of GOF between the predictions of teams 3D01, 3D02, 3D04 and 3D09. The overall level of fit is generally lower than for the 'I2b' (attenuating) case, except for 3D03. The first impression that the two predictions from 3D01 and 3D03 (finite-difference) are the closest does not resist a further analysis of GOF maps in different frequency bands: it is rather seen that a reasonable fit (with global values around 7) is obtained between 3D01, 3D02, 3D04 and 3D09 for frequencies lower than 2 Hz, whereas the level of fit between 3D01 and 3D03 does not increase with decreasing frequency. Nonetheless, the higher part of the spectrum (above 2 Hz) appears extremely difficult to simulate consistently.

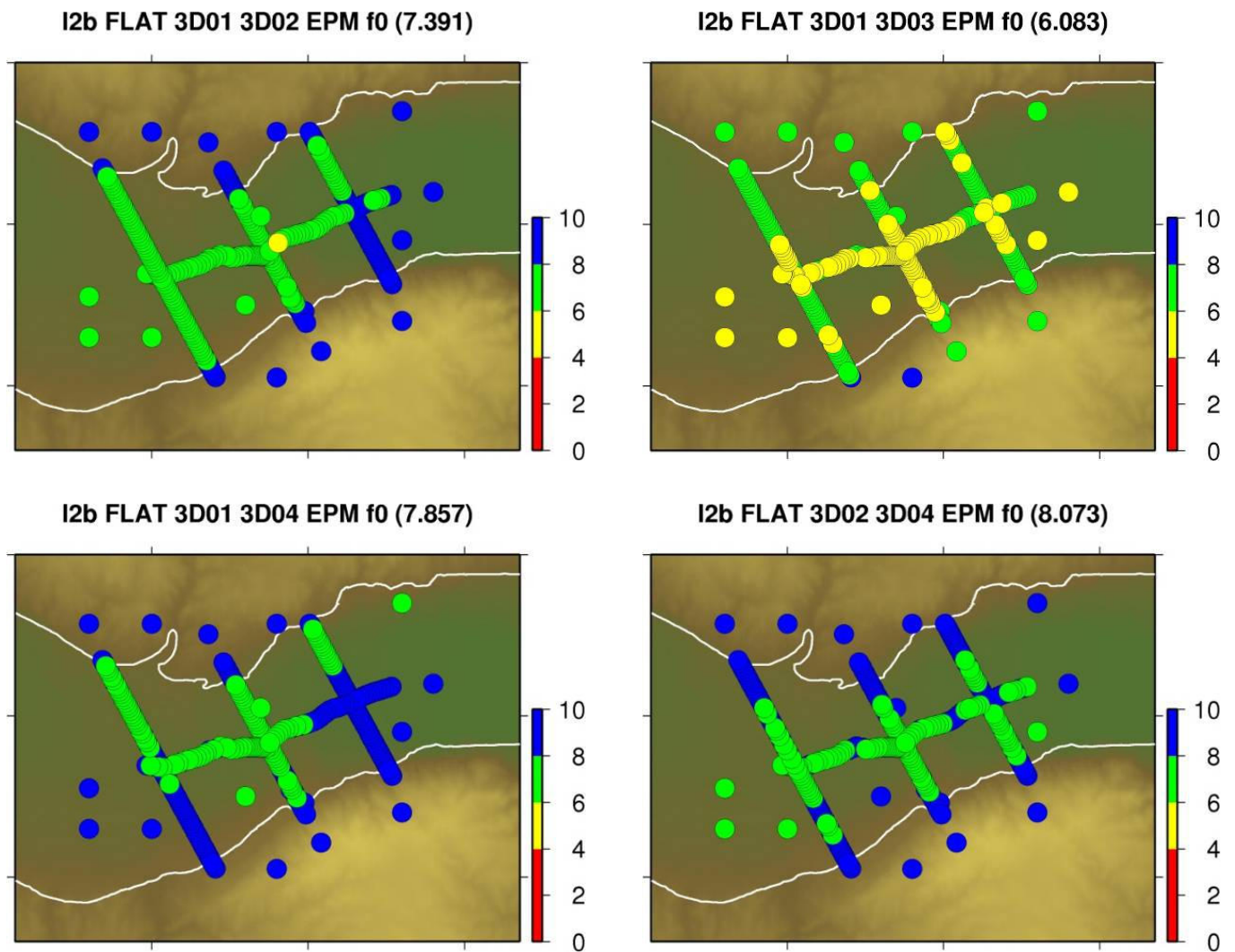


Figure 13: Maps of GOF (goodness-of-fit) computed for 4 different predictions (by teams 3D01, 3D02, 3D03, 3D04) of the E2VP case 'I2b' which considers a visco-elastic rheology in the three-layer model A of the Mygdonian basin. Each dot corresponds to the average of the amplitude and phase misfits computed for the three components of ground velocity in the whole frequency range [0-4 Hz], and translated in terms of goodness-of-fit to get a number between 0 and 10 (perfect fit). The global average computed for the 288 receivers is given in the title of each image. The first prediction 3D01 has been used as a reference for the first three maps (top left, top right and bottom left) but changing the reference does not change the overall conclusion as can be seen in the bottom right map. The fit is generally found to be excellent at rock sites and to decrease inside the basin. Note the good to excellent level of fit between the three predictions by teams 3D01, 3D02 and 3D04.

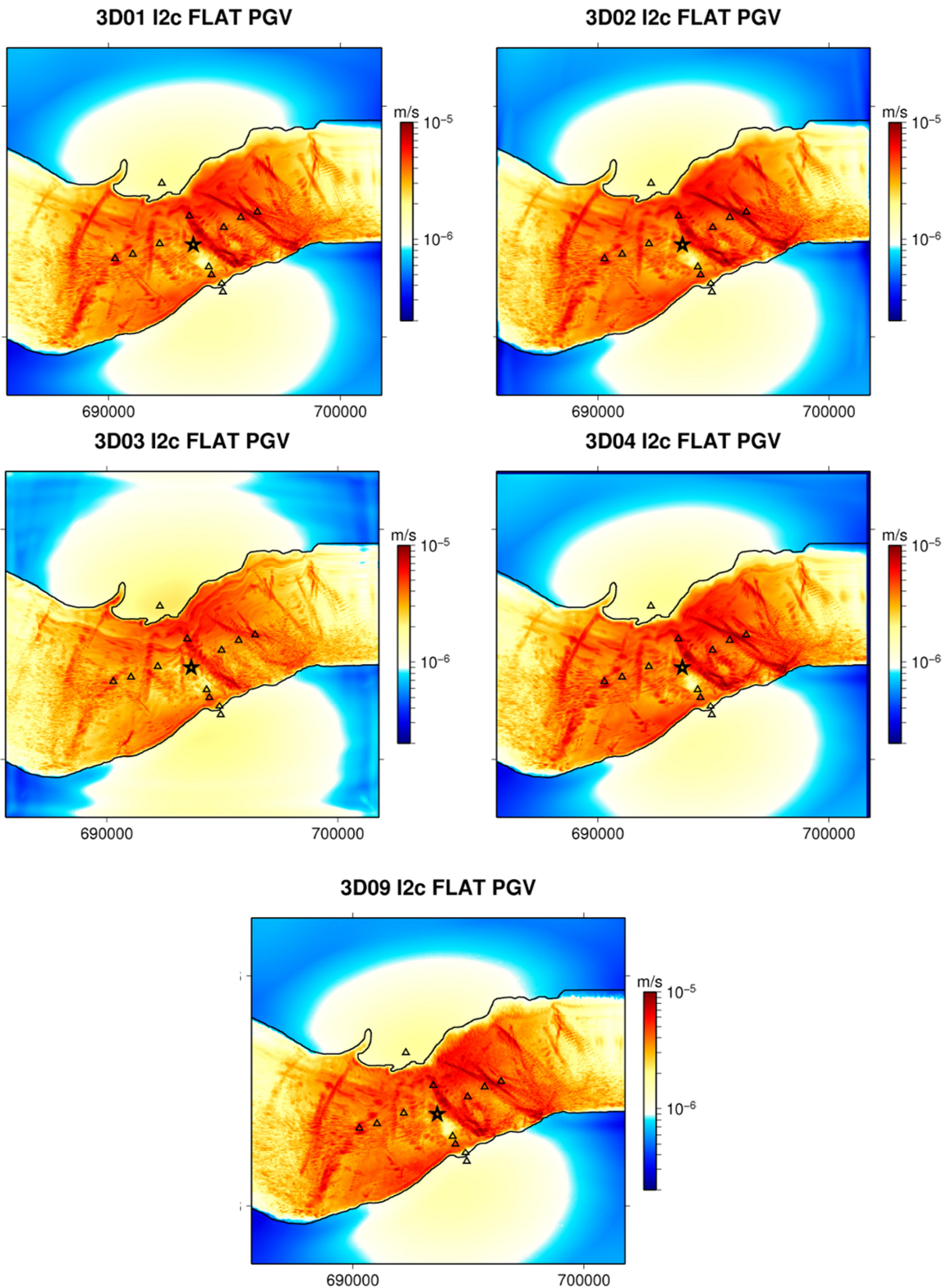


Figure 14: Maps of peak ground velocity obtained by five different teams for the E2VP case 'I2c', which considers a purely elastic rheology in the three-layer model A of the Mygdonian basin. The triangles denote the positions of the Euroseistest array and the star is the epicenter of the point-source used for verification purposes. Note the presence of "stripes" which correspond to late interferences with surface waves diffracted off the edges and propagating towards the basin without being attenuated.

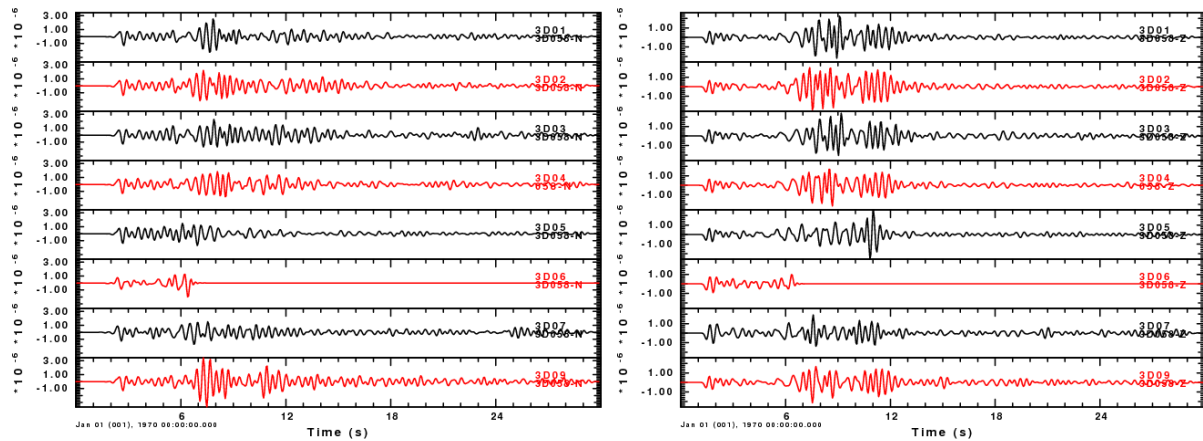


Figure 15: N-S (left) and vertical (right) components of ground velocity at TST computed by eight different teams for the I2c case. Note the large differences (in phase and amplitude) for late arrivals (after 6 seconds), corresponding partly to surface waves diffracted off the valley edges and travelling towards the center of the basin without being attenuated.

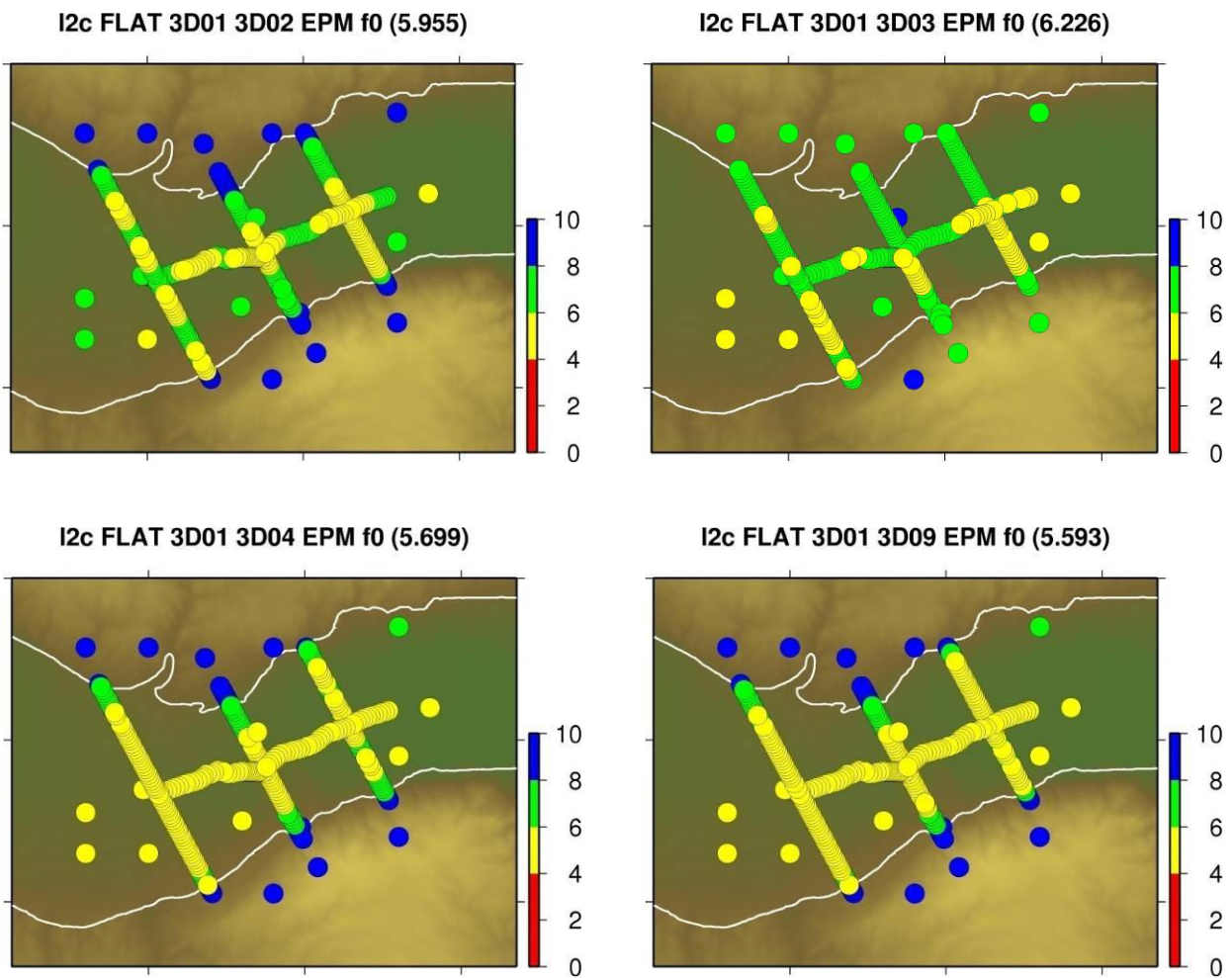


Figure 16: Maps of GOF (godness-of-fit) computed for 5 different predictions (by teams 3D01, 3D02, 3D03, 3D04, 3D09) of the E2VP case 'I2c' which considers a purely elastic rheology in the three-layer model A of the Mygdonian basin. The first prediction 3D01 has been used as a reference for all maps but changing the reference does not affect the overall conclusion. Note the general decrease of fit between the predictions, mainly due to large differences in high-frequency late arrivals, which are undamped compared to the visco-elastic case I2b. The misfits are larger in phase than in amplitude (not shown here).

3.4.4 Elastic simulations in model B

Among the ingredients which make the previous cases ('I2b' and 'I2c') challenging for numerical simulation is the fact that model A contains discontinuities in the mechanical parameters. In the E2VP, we also considered a few smooth models, laterally homogeneous or heterogeneous, which only contain first-order discontinuities (*i.e.* globally continuous, piecewise linear models).

Figure 17 shows the time-series of ground velocity at the central station TST, computed in the continuous, laterally heterogeneous model B defined in Table 4, assuming a purely elastic rheology (this case is referred to as 'IV2' in E2VP). The similarity of the different predictions, including late arrivals, is striking. The GOF maps with respect to the results obtained by team 3D01 are shown in Figure 18. They clearly show that the level of agreement between most of the predictions is very good, with global average scores reaching values above 8. Note that the prediction by team 3D03 is the farthest from the result of team 3D01, although both teams use different variants of the Finite-Difference Method.

3.4.5 Conclusions of the 3D verification exercise

The analysis and comparison of numerical predictions for the different models within the verification part of the E2VP confirms that, in general, the available numerical-simulation methods are not yet in a "press-button" mode: in most cases, iterations are needed to improve the agreement. However, a major achievement is that an encouraging similarity could be obtained among various simulations up to 4 Hz despite the relative complexity of models.

A detailed analysis allowed identifying the main sources of differences between teams and schemes, and the key elements for a reasonably accurate simulation of ground motion in complex sites: proper method and proper implementation are needed to correctly account for

- continuous and discontinuous material heterogeneity,
- large Poisson's ratios,
- attenuation,
- non-reflecting boundary and free-surface conditions.

This new exercise confirms that some important methodological questions remain to be addressed, understood and answered in order to improve the robustness of numerical codes and to extend their application field. This has led to several additional tests on "canonical cases" undertaken at the end of E2VP-1 (see next section 3.5), and highlights the necessity of pursuing the development of traditional and new numerical schemes in view of their application to complex realistic models.

However, the very good agreement obtained up to 4 Hz with very constraining goodness-of-fit criteria (*i.e.*, imposing very similar waveforms requires very similar frequency and phase contents) legitimates a wise and careful use of the numerical approach for predicting ground motion, at least in the linear, low-to-intermediate frequency range, and thus allows to investigate the validation issue by comparing the simulation results to the actual observations (chapter 0).

Finally the agreement between synthetics is also expressed in terms of goodness-of-fit on a selection of ground motion criteria representative of realistic data. We use the ten criteria defined by Anderson (2004): Arias duration, energy duration, Arias intensity, energy integral, PGA, PGV, PGD, response spectra, Fourier spectra and cross correlation. A goodness-of-fit score between synthetics is computed for each of these criteria following the scaling described in Figure 9. This scaling recommended by Anderson (2004) means that a difference of 50% on a criterion corresponds to a GOF score of 8/10 (while the scaling used previously was more severe, see the details in part 3.3).

Some Anderson goodness-of-fit scores are given in Table 5 and Table 6 quantifying the agreement between the results from team 3D01 with other teams simulating two different events: a virtual central event in the 3-layers visco-elastic model A (Table 5) and a real event located northeastward of the receivers in the same model (Table 6). In general the agreement on these ground motion criteria is really excellent.

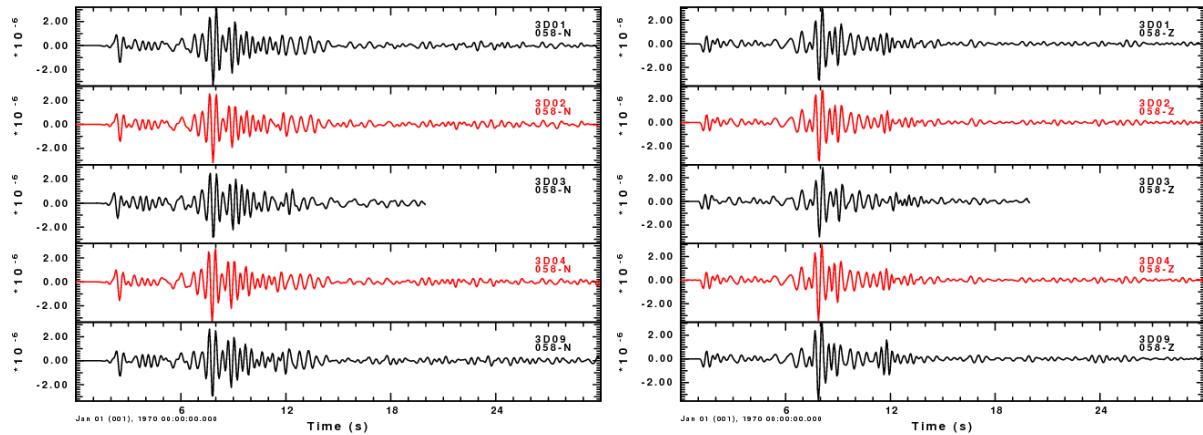


Figure 17: N-S (left) and vertical (right) components of ground velocity at TST computed by five different teams for the IV2 case which considers a purely elastic rheology in the smooth heterogeneous model B of the Mygdonian basin. Note the excellent agreement between the predictions even for surface wave packets arriving at late times.

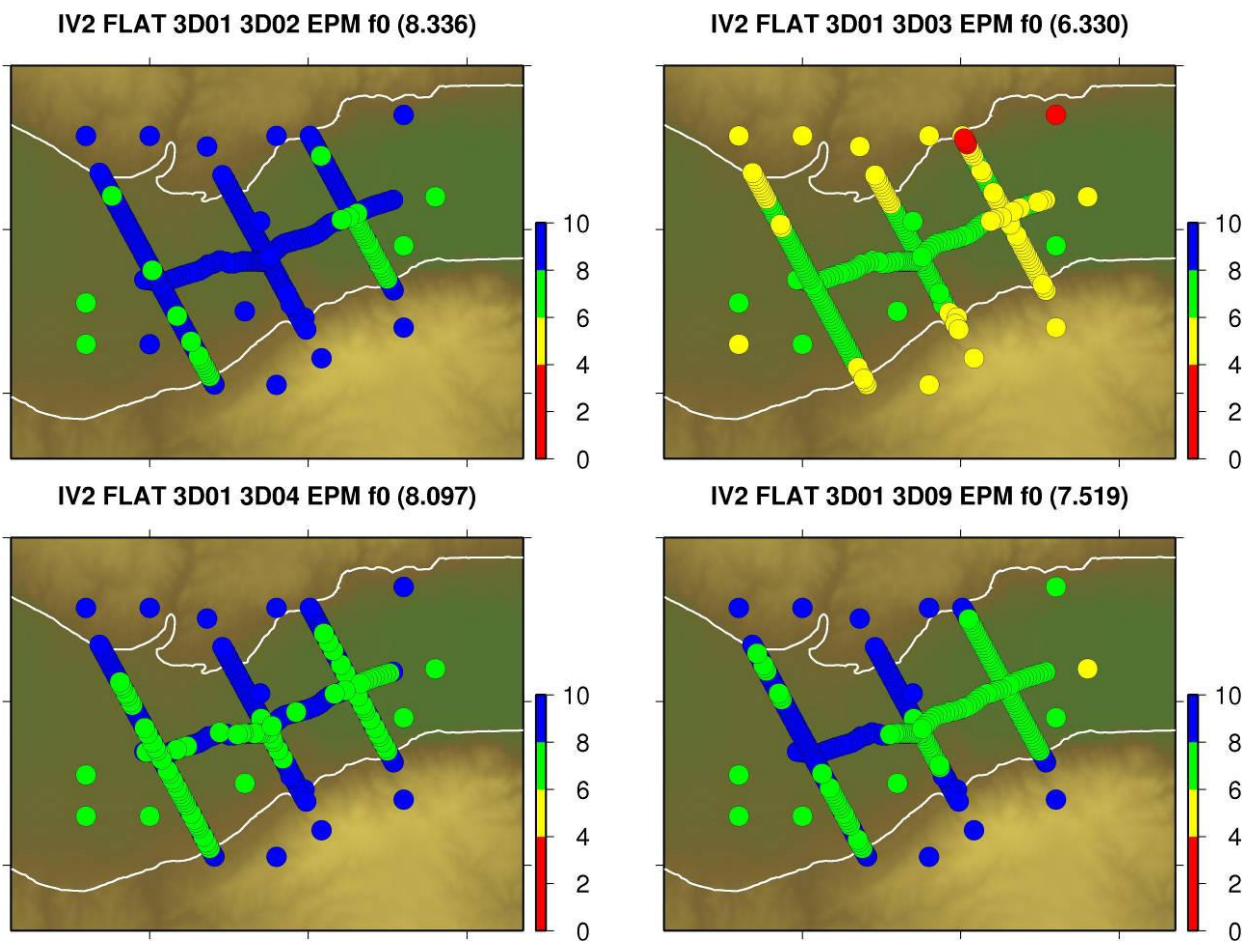


Figure 18: Maps of GOF (goodness-of-fit) computed for 5 different predictions (by teams 3D01, 3D02, 3D03, 3D04, 3D09) of the E2VP case 'IV2' which considers a purely elastic rheology in the smooth laterally heterogeneous model B of the Mygdonian basin. The first prediction 3D01 has been used as a reference for all maps. Note the very good level of fit between predictions by teams 3D01, 3D02, 3D04 and 3D09, even larger than when intrinsic damping is considered in the three-layer model A.

Table 5: Anderson goodness-of-fit scores between synthetics computed by team 3D01 and the other teams (3D02, 3D03, 3D04, 3D05, 3D06, 3D07 and 3D11) on 4 representative ground motion criteria (Arias intensity, energy duration, PGA and response spectra) for the visco-elastic simulation of a central virtual event in model A (see Table 3 and Figure 11) calculated at 5 different sites: TST0 (central soil site), TST5 (rock site, downhole, 197 m bellow TST0), E03 (soil site), W03 (soil site) and STE (rock site). The scores are averaged on the two horizontal components of ground motion. The average Anderson score (Anderson, 2004) is also given in the last column. The score and color scaling is described in part 3.3.

3D01 vs 3D02

site	Arias intensity	energy duration	PGA	response spectra	average Anderson score
TST0	9.6	9.2	9.9	9.9	8.5
TST5	10.0	7.6	8.7	8.8	8.5
E03	9.2	9.6	9.9	10.0	9.3
W03	9.0	9.2	9.8	9.8	8.5
STE	9.8	9.4	9.9	10.0	9.8

3D01 vs 3D03

TST0	0.1	5.9	4.3	6.7	3.9
TST5	-	-	-	-	-
E03	5.4	7.6	10.0	9.9	7.6
W03	7.6	8.1	9.8	9.4	7.8
STE	4.1	8.9	8.8	9.5	8.1

3D01 vs 3D04

TST0	9.0	8.8	9.7	9.8	9.0
TST5	9.9	7.1	9.8	9.8	8.9
E03	7.9	7.2	9.8	9.8	8.5
W03	6.2	9.1	9.3	9.5	8.4
STE	9.7	6.0	9.7	9.9	8.8

Table 5 (continued)

3D01 vs 3D05

TST0	3.9	8.9	6.7	8.2	6.4
TST5	5.0	5.7	10.0	9.8	7.3
E03	4.1	8.4	9.6	9.8	7.8
W03	4.9	8.3	5.9	8.3	5.9
STE	9.9	8.6	10.0	10.0	9.4

3D01 vs 3D06

TST0	4.5	5.8	3.1	6.6	4.8
TST5	7.2	6.6	9.9	9.8	7.6
E03	8.7	7.7	9.6	9.6	7.9
W03	9.9	5.7	9.7	9.2	7.5
STE	9.7	7.9	9.9	9.9	8.7

3D01 vs 3D07

TST0	9.1	8.3	9.9	9.5	8.2
TST5	9.7	8.1	9.9	9.9	8.5
E03	7.6	8.2	9.9	9.9	8.3
W03	6.6	8.4	8.7	9.4	7.7
STE	8.9	7.3	9.8	9.9	8.4

3D01 vs 3D11

TST0	9.6	8.0	10.0	9.1	8.3
TST5	-	-	-	-	-
E03	7.8	7.6	9.9	9.9	8.5
W03	10.0	8.6	9.9	9.9	8.8
STE	9.9	6.0	9.9	10.0	8.8

Table 6: Anderson goodness-of-fit scores between synthetics computed by team 3D01 and the other teams (3D02, 3D03, 3D04, and 3D05) on 4 representative ground motion criteria (Arias intensity, energy duration, PGA and response spectra) for the visco-elastic simulation of a real event in model A (see Table 3) calculated at 5 different sites: TST0 (central soil site), TST5 (rock site, downhole, 197 m below TST0), E03 (soil site), W03 (soil site) and STE (rock site). The simulated event is the largest recorded event #4 presented in Table 13 and Figure 41. The scores are averaged on the two horizontal components of ground motion. The average Anderson score (Anderson, 2004) is also given in the last column. The score and color scaling is described in part 3.3.

3D01 vs 3D02

site	Arias intensity	energy duration	PGA	response spectra	average Anderson score
TST0	9.9	9.2	9.8	9.8	9.2
TST5	10.0	8.2	9.9	9.8	9.2
E03	9.8	9.8	10.0	10.0	9.6
W03	8.3	8.9	9.3	9.7	8.6
STE	10.0	9.6	10.0	10.0	9.8

3D01 vs 3D03

TST0	6.5	7.5	9.8	8.8	7.4
TST5	5.1	5.9	9.0	7.2	6.7
E03	9.9	9.3	10.0	9.8	9.2
W03	4.5	7.8	8.2	7.7	6.6
STE	9.3	8.5	10.0	9.9	9.2

3D01 vs 3D04

TST0	9.6	8.9	10.0	9.9	9.0
TST5	9.9	9.4	10.0	10.0	9.6
E03	9.9	9.5	10.0	10.0	9.4
W03	9.0	8.9	9.9	9.9	8.8
STE	10.0	9.7	10.0	10.0	9.9

3D01 vs 3D05

TST0	6.4	9.1	9.6	9.7	8.4
TST5	9.8	7.9	9.9	9.7	9.0
E03	9.1	9.2	10.0	9.9	9.2
W03	9.5	7.5	9.9	7.6	8.1
STE	9.4	8.6	10.0	9.9	9.4

3.5 CANONICAL CASES

The original reason for performing additional simulations for a set of canonical models is to clarify the differences between solutions submitted by 3D teams for the Mygdonian basin model within the E2VP.

Five canonical cases are defined:

- 1) Homogeneous halfspace with a high V_P/V_S ratio = 7.5 (CAN1)
- 2) Layered halfspace, with 3 homogeneous layers (CAN2)
- 3) Layered halfspace, with 3 gradient layers (CAN3)
- 4) Canonical basin with different sides, 3 homogeneous layers (CAN4)
- 5) Canonical basin with different sides, 3 gradient layers (CAN5)

All computations should be accurate enough up to 4 Hz. The three layers represent the layering below the TST station in the 3D Mygdonian basin model I2c of the E2VP.

For the cases CAN1, CAN2 and CAN3, a reference solution is available and will help to correctly evaluate the precision of the 3D modeling. This reference is the Discrete WaveNumber solution computed with Hisada's method (Hisada, 1994) and/or Axitra (Coutant, 1990). To quantify the fit of the computed 3D solutions with the reference solution, the goodness-of-fit (GOF) scores from Time Frequency Misfit criteria (Kristeková *et al.*, 2009) are used. However for the cases CAN4 and CAN5, no reference solution is available.

3.5.1 Homogeneous halfspace with high V_P/V_S ratio (CAN1)

The purpose of this case is to assess the precision of 3D modeling in a homogeneous halfspace with $V_P/V_S = 7.5$.

The geometrical configuration of canonical case CAN1 is shown in Figure 19. The receivers are grouped into 4 profiles, called lines: two lines at the surface (the 'north surface line' and the 'diagonal surface line') and two vertical lines (the 'north vertical line' and the 'NE vertical line'). Receiver spacing is 500 m along the surface lines and 50 m along the vertical lines. The maximum epicentral distance is 5 km. The source is a double-couple point source at 25 m depth, with strike $\phi_S = 22.5^\circ$, dip $\delta = 90^\circ$, rake $\lambda = 0^\circ$ and seismic moment $M_0 = 10^{18}$ Nm (see Figure 19). The exact location of the source and receivers, the material properties, the focal mechanism, the seismic moment and the moment time history are strictly the same for all participants to ensure uniformity in any comparison. In addition the grid spacing is imposed to all participants to be 10 m. This value corresponds to a sampling of the smallest S wavelength by 5 grid points.

The material properties of the homogeneous halfspace are the following: $V_P = 1500$ m/s, $V_S = 200$ m/s, $\rho = 2100$ kg/m³, $Q_P = \infty$, $Q_S = \infty$.

The computation should be accurate enough up to 4 Hz and the signal should last 30 seconds. The reference is the Discrete WaveNumber solution computed with Hisada's method and code (Hisada, 1994).

The description of the CAN1 was first available on 2011, May 5th. Up to now, 9 teams sent their 3D numerical solution for that case (see Table 7).

The east horizontal component along the same profile is shown in Figure 21. The north horizontal component that is very similar to the vertical component is not shown here. Note that the P wave is only seen at 500 m epicentral distance on the vertical and north components (its amplitude is very weak for such a large V_P/V_S ratio), that the non-dispersive Rayleigh wave is only seen on the vertical and north components, and that the east component is made of S wave only.

Figure 20 shows the comparison of vertical ground velocity along the north surface line (see Figure 19) computed by team 3D01 in red with the reference Discrete Wavenumber solution in black. The numbers at the right of each trace indicate the envelope and phase goodness-of-fit (GOF) scores over the frequency band [0.2 Hz, 4 Hz] with $A=10$ and $k=1$ (as defined in Kristeková *et al.*, 2009).

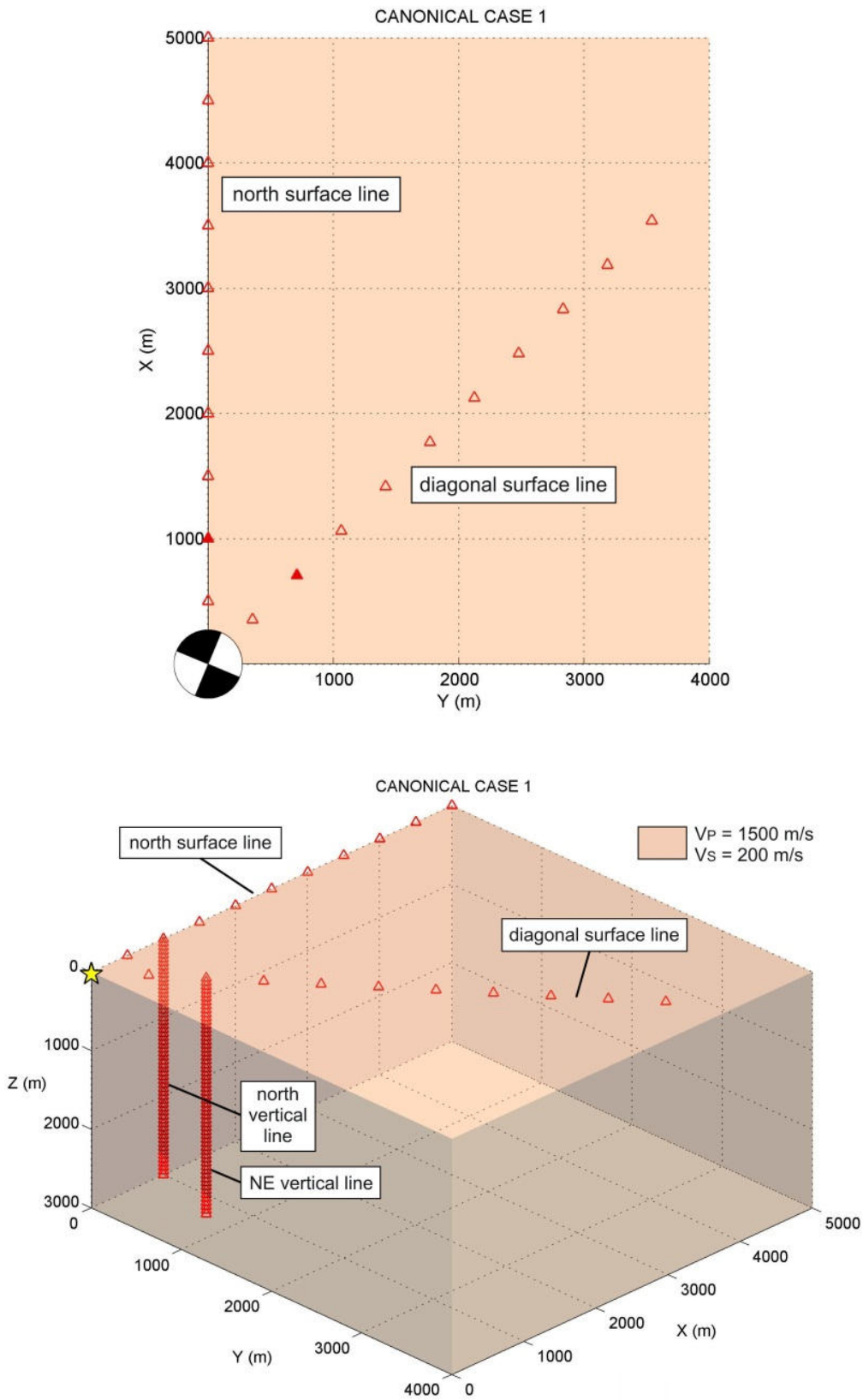


Figure 19: Surface (top) and 3D (bottom) view showing the position of the epicenter (beachball and yellow star) and of the 140 receivers (red triangles) for the CAN1 case. X points to the North, Y to the East and Z downward.

Table 7: Participating 3D teams to the CAN1.

3D acronym	Team acronym	Class of method
3D01	CUB	FDM
3D02	UJF	SEM
3D04	OGS	PSM
3D05	NIED	FDM
3D06	LDG	DEM-SEM
3D07	CMU	FEM
3D08	POLIMI	SEM
3D11	BRGM	SEM
3D12	USTC	FDM

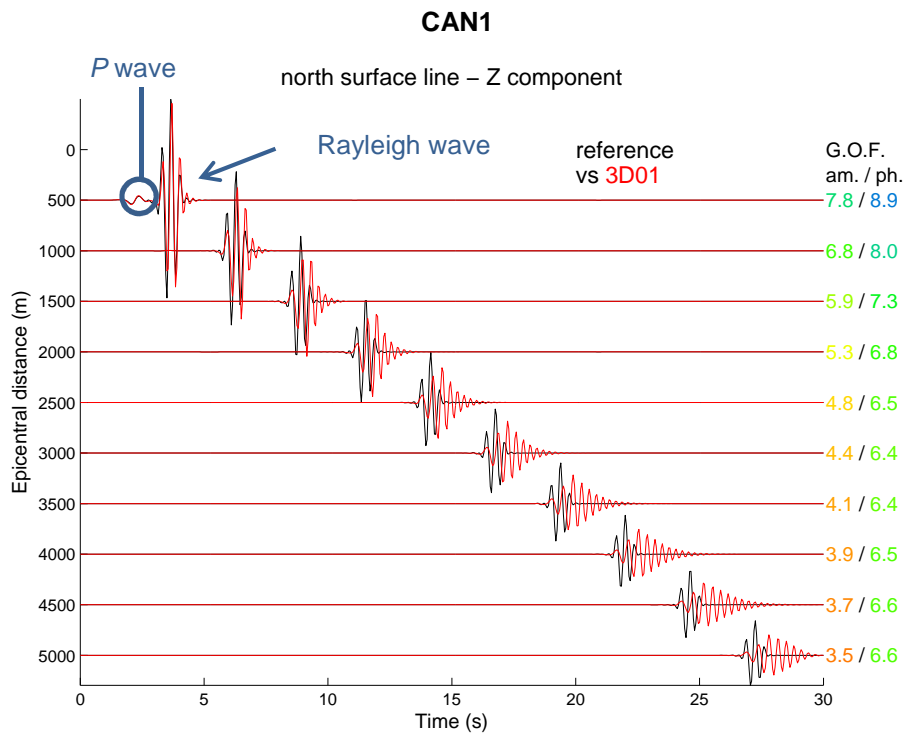


Figure 20: Vertical component of ground velocity for CAN1 along the north surface line (see Figure 19) computed by team 3D01 (in red) compared to the reference Discrete WaveNumber solution (in black). The amplitude (envelope) and phase goodness-of-fit (GOF) are displayed at the right of each trace.

For the particular example shown here, several observations are made:

- The GOF scores decrease with the epicentral distance because the errors are cumulative with the distance;
- The GOF scores for the S wave are excellent (see Figure 21);
- The misfit is the highest for the Rayleigh wave (see Figure 20).

The reference solution shows a non-dispersive Rayleigh wave, as it should be in a homogeneous halfspace, while the 3D01 solution shows a strong numerical dispersion of that same wave. This difference leads to the high misfit (low GOF) that is therefore observed only on the Rayleigh wave.

Those observations are valid for all computations (not shown here for the sake of clarity). While the body waves are often correctly estimated, the Rayleigh wave is affected by a numerical dispersion whose characteristics depend on the numerical method: this numerical dispersion can be either 'causal' (the high frequencies are slower than the low frequencies, see Figure 20) or 'acausal' (the high frequencies are faster than the low frequencies, see Figure 22 showing the vertical ground velocity along the north surface line computed by team 3D02).

Figure 23 shows the comparison of vertical and north ground velocity along the north vertical line (see Figure 19) computed by team 3D01 in red with the reference Discrete Wavenumber solution in black. The Rayleigh wave is seen on the shallowest receivers (< 200 m) of this vertical profile and is related to a systematic decrease of the GOF scores. At depth where the S wave is dominant, the GOF scores are excellent.

Figure 24 shows the vertical ground velocity computed by all teams for a selection of 4 receivers compared to the reference solution. It is clearly seen on all computations that the fit is better for the receivers closer to the source compared to the ones further away from the source. At 5000 m epicentral distance, the numerical dispersion significantly affects the Rayleigh wave, leading to important positive or negative delays compared to the reference solution. At such a distance, the fit is therefore better for the solutions that are the least affected by the numerical dispersion.

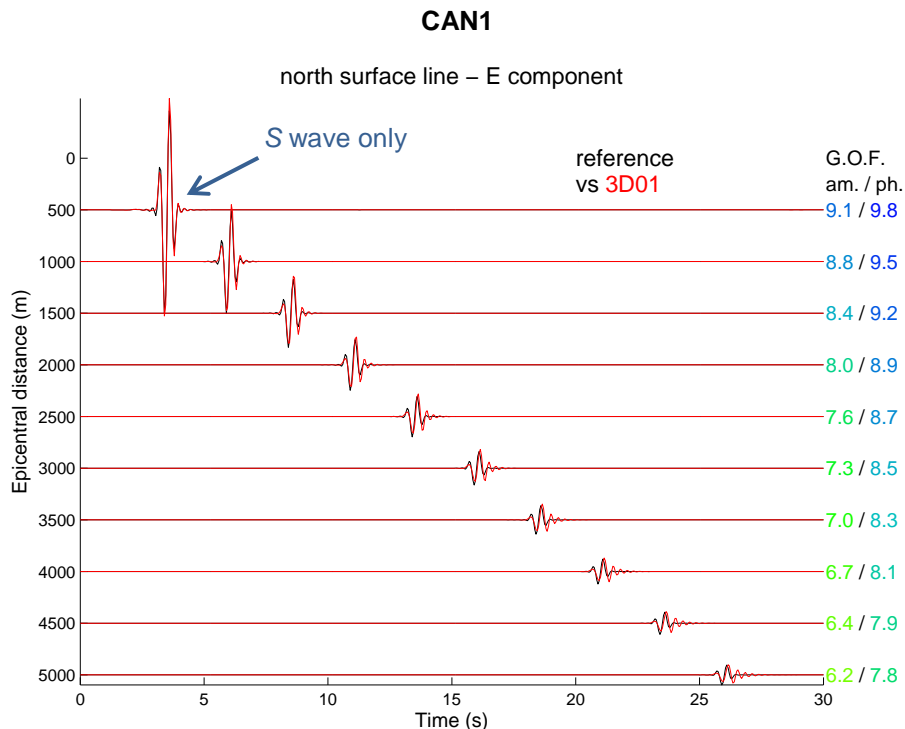


Figure 21: East component of ground velocity for CAN1 along the north surface line (see Figure 19) computed by team 3D01 (in red) compared to the reference Discrete WaveNumber solution (in black). The amplitude (envelope) and phase goodness-of-fit (GOF) are displayed at the right of each trace.

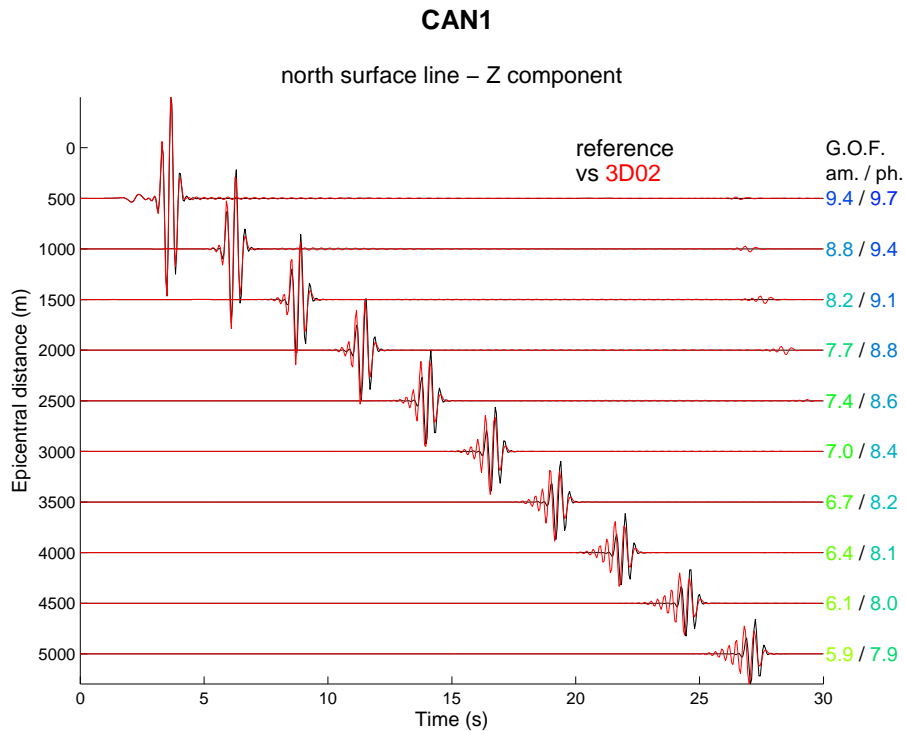


Figure 22: Vertical component of ground velocity for CAN1 along the north surface line (see Figure 19) computed by team 3D02 (in red) compared to the reference Discrete WaveNumber solution (in black). The amplitude (envelope) and phase goodness-of-fit (GOF) are displayed at the right of each trace.

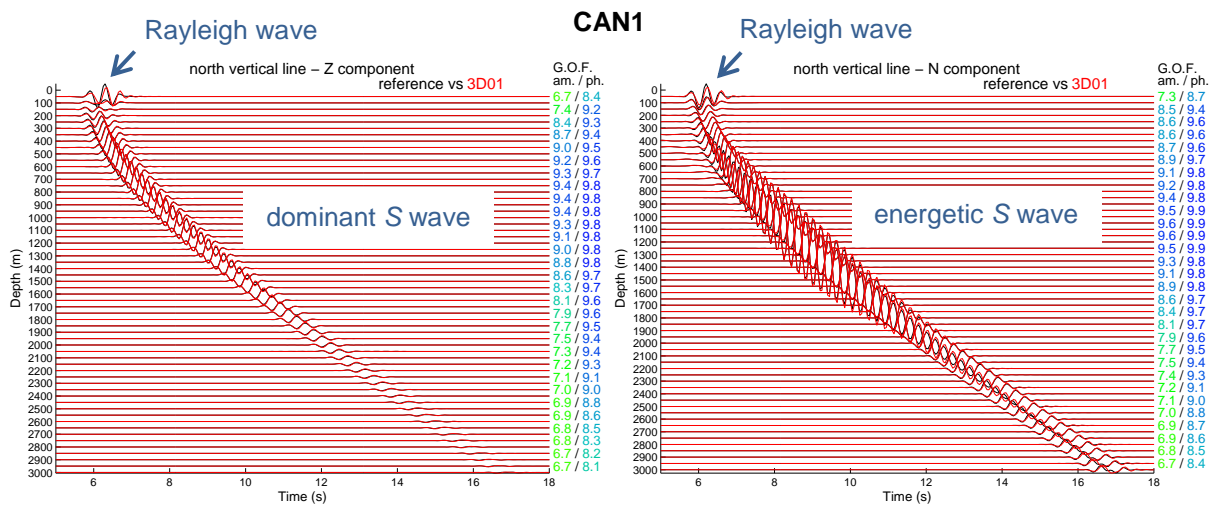


Figure 23: Vertical component (left) and north component (right) of ground velocity for CAN1 along the north vertical line (see Figure 19) computed by team 3D01 (in red) compared to the reference Discrete WaveNumber solution (in black). The amplitude (envelope) and phase goodness-of-fit (GOF) are displayed at the right of each trace.

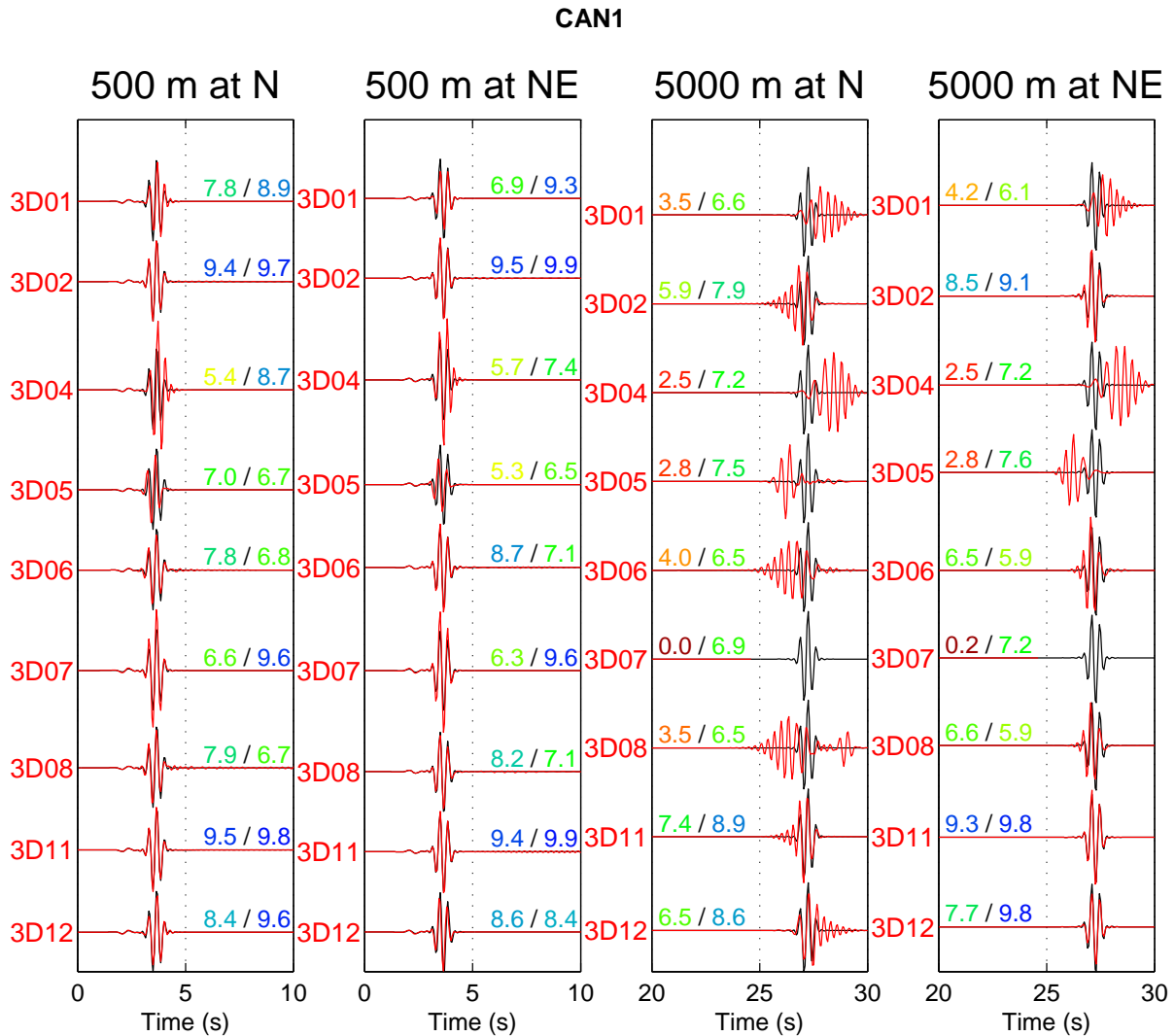


Figure 24: Vertical component of ground velocity for CAN1 computed by all teams (see Table 7) at 4 surface receivers: the two left columns show the ground velocity for the closest receivers to epicenter, the two right columns show the ground velocity for the furthest receivers to epicenter. The exact location of each receiver is mentioned at the top of each column. Each team solution (in red) is compared to the reference Discrete WaveNumber solution (in black). The amplitude (envelope) and phase goodness-of-fit (GOF) are displayed above each trace.

The numerical dispersion of the Rayleigh wave can be reduced, either by increasing the grid resolution (h-adaptivity), or by increasing the polynomial order for high-order methods, keeping the average grid spacing constant (p-adaptivity), as it is shown in Figure 25. The CAN1 should be computed using the same spatial discretization of the canonical model as the one of the Mygdonian basin model (see part 3.4). Most teams that participated in the first part of the verification exercise used a spatial discretization approximately equal to 10 m (depending on the numerical method) and that same value was therefore used for CAN1. From the results shown in Figure 25, it appears that the 10 m discretization is not sufficient to accurately model the ground motion in a large homogeneous volume with high V_P/V_S ratio, in which the surface waves propagate for several kilometers. On the opposite, the basin layer having such a high V_P/V_S ratio represents only a very small part of the total volume of the Mygdonian basin model, and thus the surface waves could not be so much affected. Four teams performed additional computations of CAN1 with a higher resolution (a lower spatial discretization for the FDM, a higher polynomial degree for the SEM) in order to better model the Rayleigh wave in the CAN1. It is clear that it helps to improve the accuracy of the surface wave modeling, which leads to a general improvement of the GOF scores (see Figure 25). Note also that increasing the grid resolution or the polynomial order also reduces the numerical anisotropy.

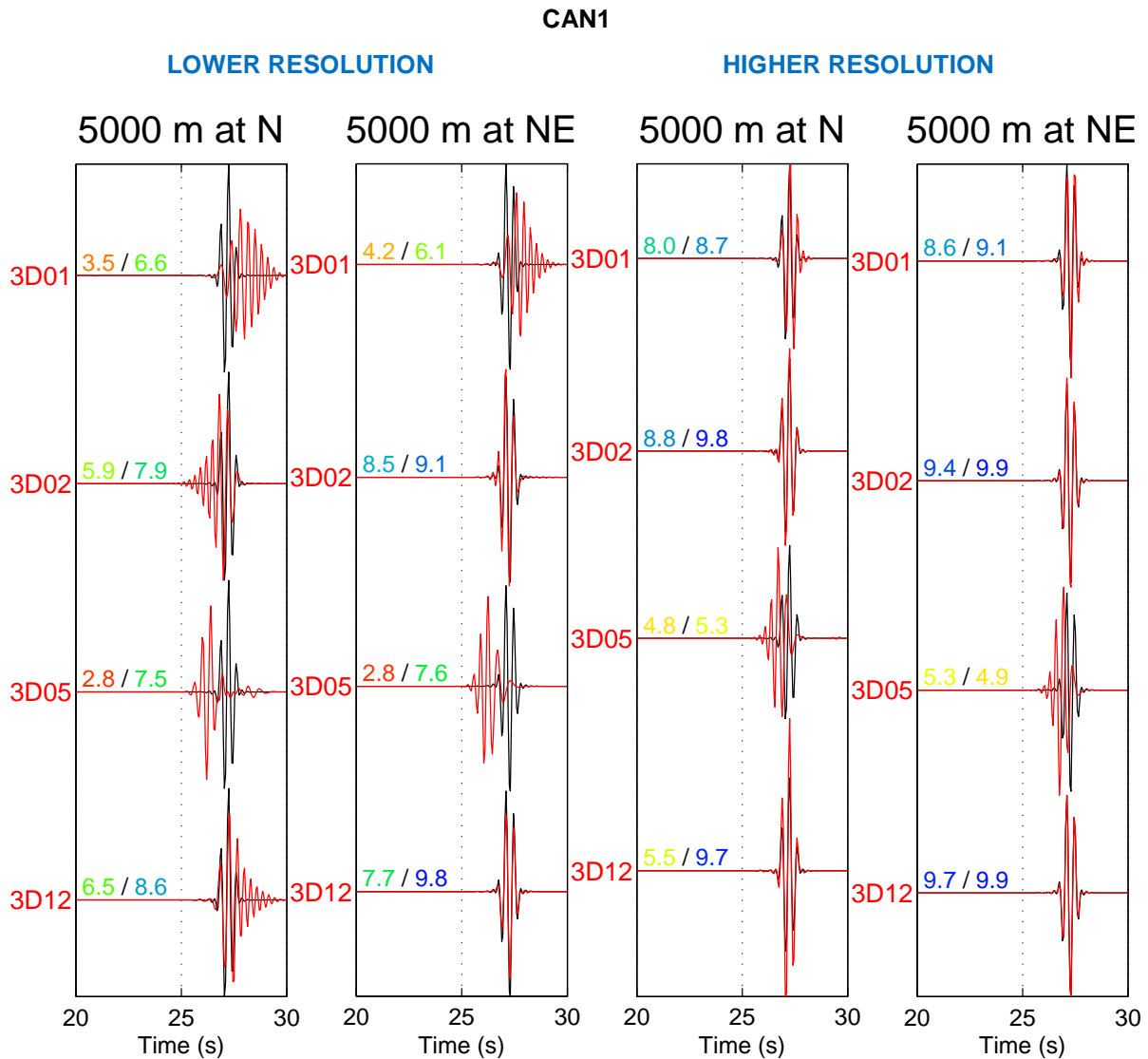


Figure 25: Vertical component of ground velocity for CAN1 computed by 4 teams (3D01, 3D02, 3D05 and 3D12) at 2 surface receivers located 5000 m away from the epicenter. The left columns show the ground velocity computed at a ‘lower’ resolution (FDM: spatial discretization = 10 m, SEM: polynomial degree 4, element size 40 m), the right columns show the ground velocity computed at a ‘higher’ resolution (FDM: spatial discretization = 5 m, SEM: polynomial degree 8, element size 80 m). Each team solution (in red) is compared to the reference Discrete WaveNumber solution (in black). The amplitude (envelope) and phase goodness-of-fit (GOF) are displayed above each trace.

The first canonical case helped us to quantify the accuracy of the simulated body and surface waves in a medium with large V_P/V_S ratio. It has been shown that the main source of numerical difficulty deals with the simulation of Rayleigh waves, for which an accurate implementation of the free-surface condition, as well as a moderate sensitivity to large Poisson's ratio, are required. Some additional studies have been started (and almost finished) to help separating those two effects: they include the quantification of accuracy in unbounded media with varying V_P/V_S ratios, and the quantification of accuracy for surface waves simulation in a medium with lower V_P/V_S ratio.

3.5.2 Layered halfspace (CAN2 and CAN3)

The purpose of these cases is to assess the precision of 3D modeling in a layered halfspace with 1) constant material properties in the layers and halfspace (CAN2), and 2) a vertical gradient of material properties in the layers (CAN3).

The geometrical configuration of canonical case CAN2 is shown in Figure 26. The configuration of CAN3 is exactly the same except for the material properties. The receivers are grouped into 4 profiles, called lines: two lines at the surface (the 'north surface line' and the 'diagonal surface line') and two vertical lines (the 'north vertical line' and the 'NE vertical line'). Receiver spacing is 100 m along the surface lines and 50 m along the vertical lines. The maximum epicentral distance is 5 km. For both CAN2 and CAN3, the wavefield is generated by a single vertical force at the free surface and by a double-couple point source at 3000 m depth, with strike $\Phi_S = 22.5^\circ$, dip $\delta = 90^\circ$, rake $\lambda = 0^\circ$ and seismic moment $M_0 = 10^{18}$ Nm. The exact location of the sources and receivers, the material properties, the focal mechanism, the seismic moment, the force time history and the moment time history are strictly the same for all participants to ensure uniformity in any comparison.

The material properties of the layers and halfspace are described in Table 8 for CAN2 and in Table 9 for CAN3.

The computation should be accurate enough up to 4 Hz and the signal should last 40 seconds. The reference is the Discrete WaveNumber solution computed with both Hisada's code (Hisada, 1994) and Axitra (Coutant, 1990).

As the three layers in CAN2 and CAN3 represent the layering below the TST station in the 3D Mygdonian basin model I2c, it is asked to all participants to keep the same spatial discretization for the CAN2 and CAN3 models as the one used originally at the TST site.

The description of the CAN2 and CAN3 was first available on 2011, October 14th. Up to now, 5 teams sent their 3D numerical solution for these two cases (see Table 10).

The two sources applied in CAN2 and CAN3 produce considerably different wavefields: the *P* and *S* waves are produced by the deep source while the surface waves are produced by the surface source.

The main observation of previous CAN1 is also valid for CAN2 and CAN3: the GOF scores for the body waves are excellent while the scores decrease for the Rayleigh wave (see Figure 27 for CAN2 and Figure 28 for CAN3).

The Rayleigh waveform is very different between the two cases (compare Figure 27 with Figure 28). The theoretical dispersion of the Rayleigh waves is more significant in CAN2 (homogeneous layers) than in CAN3 (gradient layers), for both the fundamental Rayleigh and the first harmonic, as it is shown in Figure 29. These differences in dispersion lead to considerably dissimilar waveforms between the two canonical cases. The GOF scores are slightly better on the less dispersive Rayleigh wave of CAN3 than on the strongly dispersive Rayleigh wave of CAN2.

These cases are critical to assess the accuracy of numerical simulation of body and (mainly) surface waves propagation in a stratified medium which combines layers with large Poisson ratio and a strong physical dispersion in the frequency band considered. It provides an opportunity to quantify the accuracy of the discrete representation of the model by first-order homogenization techniques (the averaging strategy proposed by Moczo *et al.*, 2002) used by teams 3D01, 3D04 and 3D12, or by polynomial interpolation (used in SEM when the physical discontinuities do not coincide with element boundaries, as it may happen in realistic cases).

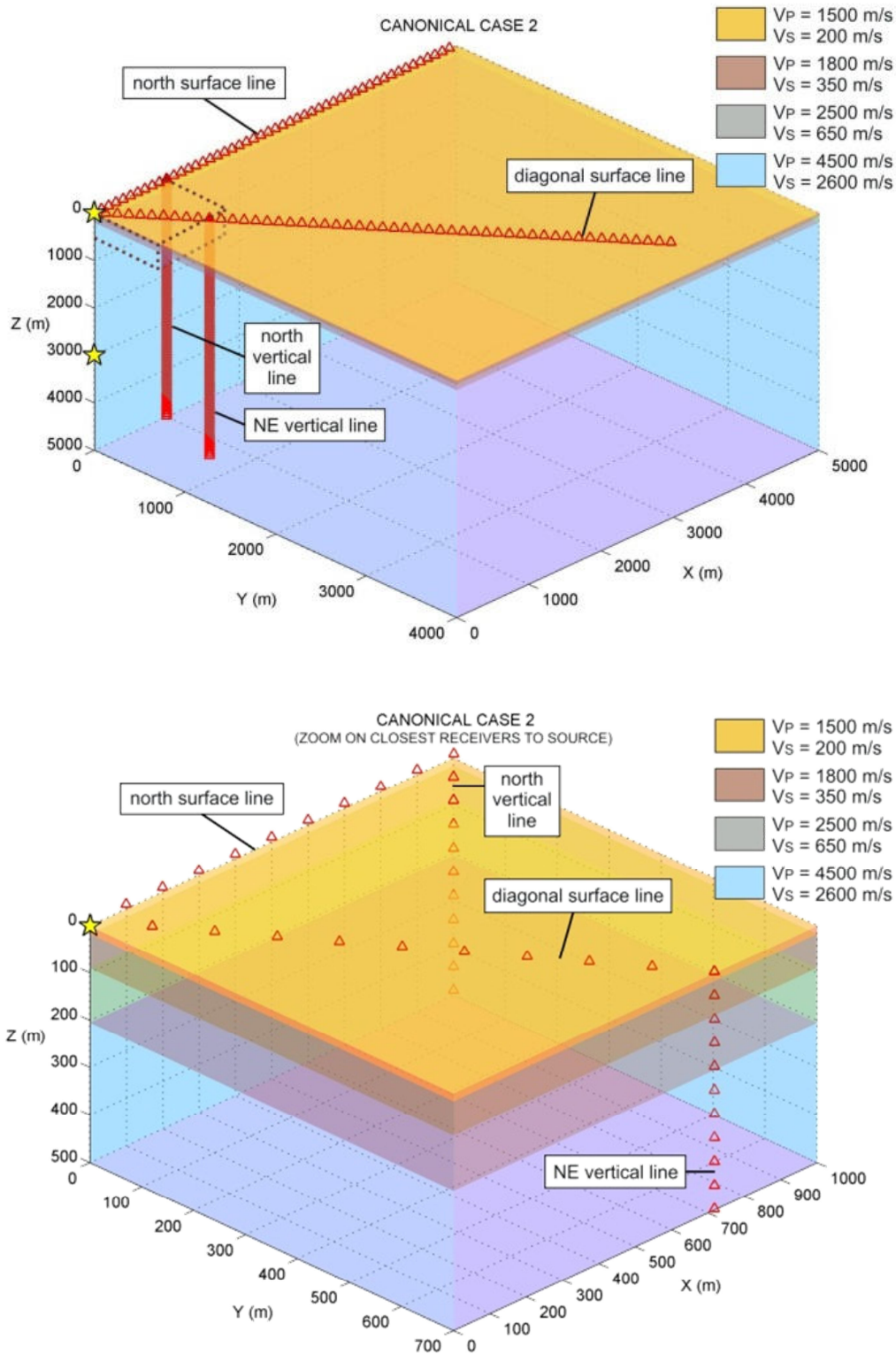


Figure 26: 3D large view (top) and 3D closed view (bottom) showing the position of the two hypocenters (yellow stars) and of the 302 receivers (red triangles) for the CAN2 case. The dotted black box on the left panel indicates the location of the zoom made on the right panel. X points to the North, Y to the East and Z downward.

Table 8: Material properties for the CAN2 model (3 homogeneous elastic horizontal layers over a homogeneous halfspace).

Thickness of the layer (m)	V_P (m/s)	V_S (m/s)	Density (kg/m^3)	Q_P	Q_S
17.3	1500	200	2100	∞	∞
72.5	1800	350	2100	∞	∞
115.6	2500	650	2200	∞	∞
∞	4500	2600	2600	∞	∞

Table 9: Material properties for the CAN3 model (3 vertically constant-gradient elastic horizontal layers over a homogeneous halfspace).

Thickness of the layer (m)	V_P (m/s)	V_S (m/s)	Density (kg/m^3)	Q_P	Q_S
17.3	1500-1600	200-250	2100	∞	∞
72.5	1600-2200	250-500	2100-2130	∞	∞
115.6	2200-2800	500-900	2130-2250	∞	∞
∞	4500	2600	2600	∞	∞

Table 10: Participating 3D teams to the CAN2 and CAN3.

3D acronym	Team acronym	Class of method
3D01	CUB	FDM
3D02	UJF	SEM
3D04	OGS	PSM
3D11	BRGM	SEM
3D12	USTC	FDM

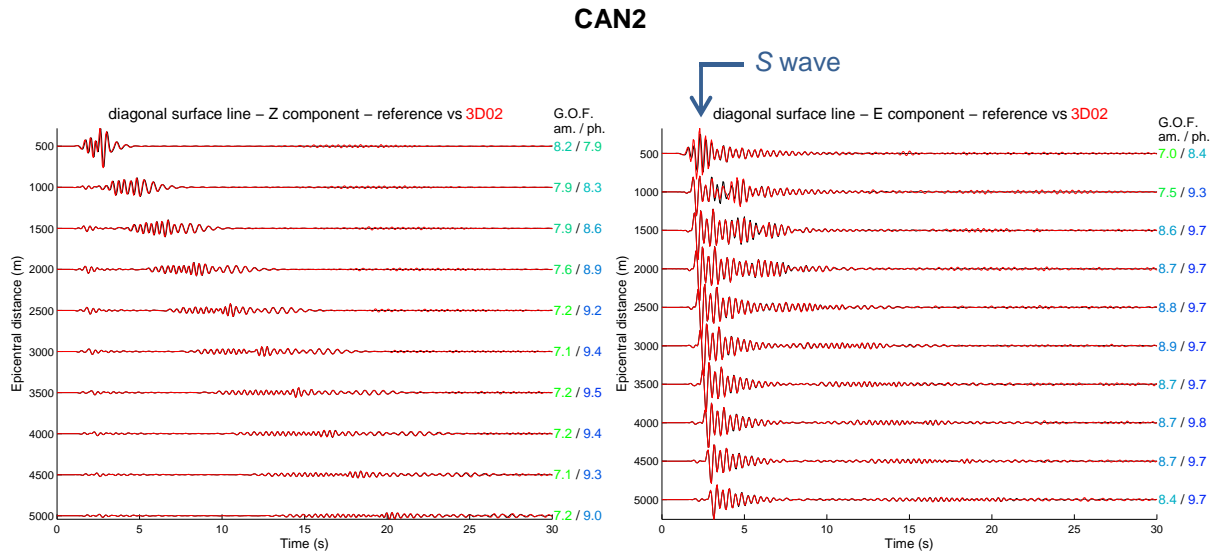


Figure 27: Vertical component (left) and east component (right) of ground velocity for CAN2 along the diagonal surface line (see Figure 26) computed by team 3D02 (in red) compared to the reference Discrete WaveNumber solution (in black). The amplitude (envelope) and phase goodness-of-fit (GOF) are displayed at the right of each trace.

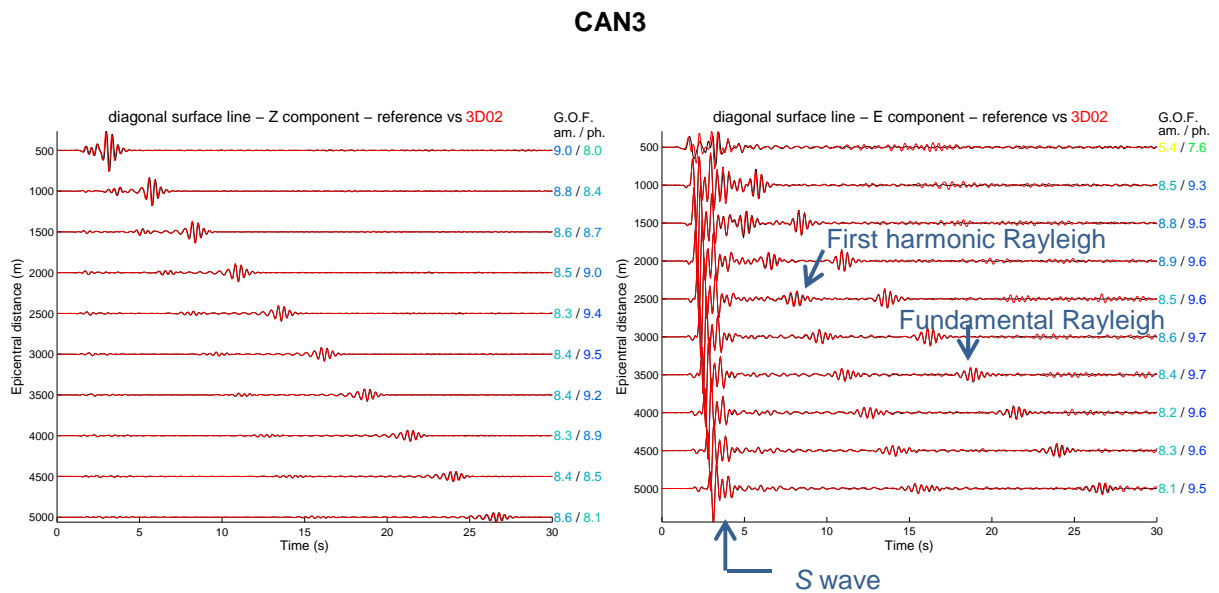


Figure 28: Vertical component (left) and east component (right) of ground velocity for CAN3 along the diagonal surface line (see Figure 26) computed by team 3D02 (in red) compared to the reference Discrete WaveNumber solution (in black). The amplitude (envelope) and phase goodness-of-fit (GOF) are displayed at the right of each trace.

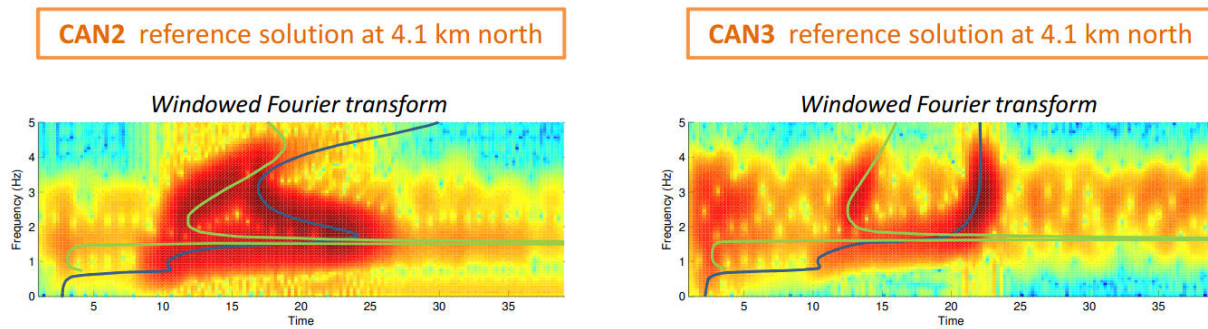


Figure 29: Theoretical dispersion of Rayleigh waves together with arrival times at 4.1 km (based on group velocity) for the fundamental Rayleigh (blue curve) and the first harmonic Rayleigh (green curve).

Figure 30 shows the vertical ground velocity computed along the diagonal surface line by teams 3D01, 3D02, 3D04, 3D11 and 3D12.

Although some solutions are still being iterated (for example 3D01 which has an amplitude problem in the wavefield generated by the surface force), the agreement between the numerical and reference solutions is in general quite good, as it can be seen by inspecting the values of goodness-of-fit in amplitude and phase. The two spectral element solutions (3D02 and 3D11) are very close, apart from late noisy arrivals due to a poor performance of absorbing boundary conditions. They are both close and consistent with the FD prediction of 3D12, which uses a grid size of 5 m, *i.e.* 50% to 100% smaller than for the other teams.

The fit on the Rayleigh wave after a few kilometers of propagation is found to be better than in the CAN1 case, confirming that the latter case was more demanding than required for simulations in the Mygdonian basin.

Note that UJF provided two solutions: 3D02, in which the physical discontinuities within the sedimentary layers are well represented (they coincide with elements boundaries), and 3D022 where the first discontinuity (at 17.3 m depth) is interpolated on the basis of high-order polynomials. The effect of the interpolation is dramatic on the accuracy of the simulated surface waves as can be seen in Figure 30.

The results for CAN3 are shown in Figure 31. Note that some solutions are still being iterated (3D01/CUB and 3D04/OGS which have both an amplitude problem in the wavefield generated by the surface force).

The fit to the reference solution is found to be similar or better than for the layered case CAN2. Note that the interpolated strategy in the SEM (3D022) proves to be very efficient in this smooth model.

This preliminary result seems to confirm what we already observed in the phase 1 of E2VP: the level of discrepancies between different numerical predictions of ground motion tends to decrease whenever the velocity model is smooth in the sediments.

CAN2

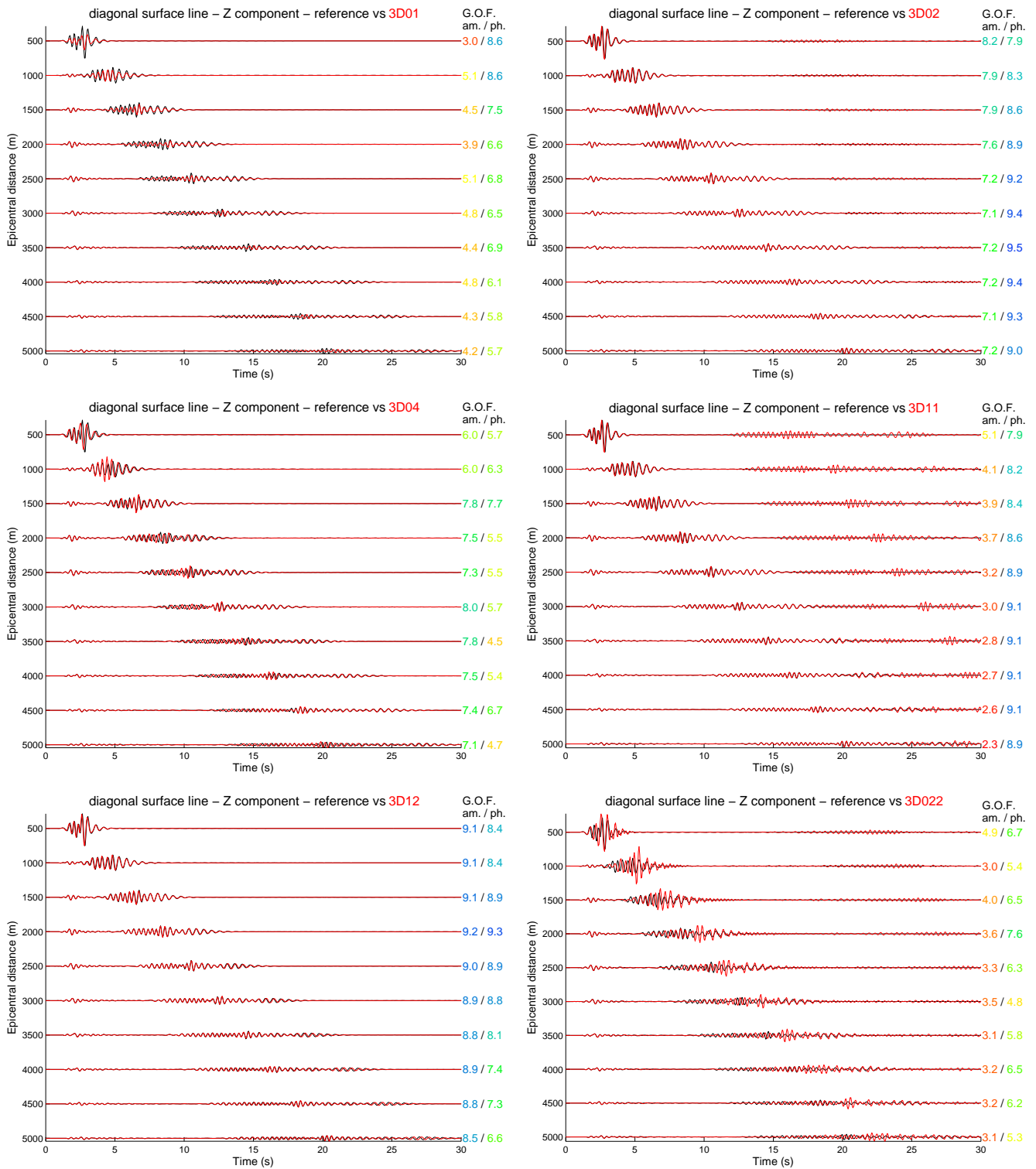


Figure 30: Vertical component of ground velocity for CAN2 along the diagonal surface line (see Figure 26) computed by teams (in red) 3D01, 3D02, 3D04, 3D11 and 3D12 compared to the reference Discrete WaveNumber solution (in black). The amplitude (envelope) and phase goodness-of-fit (GOF) are displayed at the right of each trace. The last panel shows the solution obtained by team 3D02 when the depth of the first sediment interface does not coincide with elements' edges (see text).

CAN3

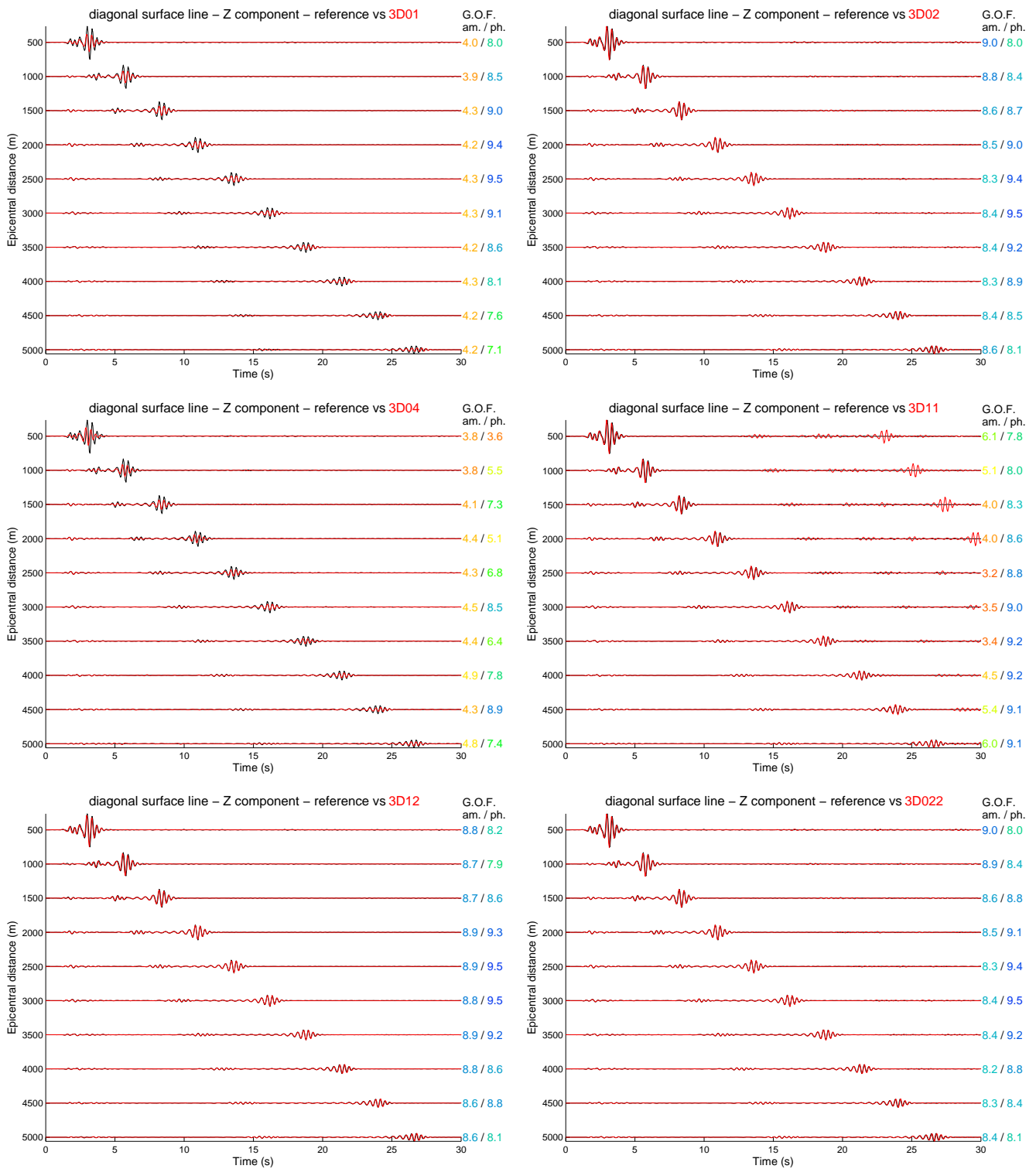


Figure 31: Vertical component of ground velocity for CAN3 along the diagonal surface line (see Figure 26) computed by teams (in red) 3D01, 3D02, 3D04, 3D11 and 3D12 compared to the reference Discrete WaveNumber solution (in black). The amplitude (envelope) and phase goodness-of-fit (GOF) are displayed at the right of each trace. The last panel shows the solution obtained by team 3D02 when the depth of the first sediment interface does not coincide with elements' edges (see text).

3.5.3 Canonical basin with different sides (CAN4 and CAN5)

The purpose of these cases is to assess the precision of 3D modeling in an asymmetrical basin with 1) homogeneous layers inside the basin (CAN4), and 2) vertical constant-gradient layers inside the basin (CAN5).

The geometrical configuration of canonical case CAN4 is shown in Figure 32. The configuration of CAN5 is exactly the same except for the material properties. The canonical basin has two different edges: a smooth slope at the North (see Figure 33), reflecting a simplified geometry of the northern edge of the Mygdonian basin, and a vertical artificial edge at the South. The receivers are grouped into 5 profiles, called lines: four lines at the surface (the 'NS1', 'NS2', 'NS3' and 'EW' surface lines) and one vertical line. Receiver spacing is 100 m at the surface of the basin, 10 m in the basin layers and 500 m outside the basin. For both CAN4 and CAN5, the source is a double-couple point source at 3000 m depth under the center of the basin, with strike $\Phi_s = 22.5^\circ$, dip $\delta = 90^\circ$, rake $\lambda = 0^\circ$ and seismic moment $M_0 = 10^{18}$ Nm. The exact location of the source and receivers, the geometry of the basin, the material properties, the focal mechanism, the seismic moment and the moment time history are strictly the same for all participants to ensure uniformity in any comparison.

The material properties of the layers and halfspace are the same between CAN2 and CAN4 (see Table 8), and the same between CAN3 and CAN5 (see Table 9).

The computation should be accurate enough up to 4 Hz and the signal should last 50 seconds. Unlike the previous cases, no reference solution is available for CAN4 and CAN5.

The description of the CAN4 and CAN5 was first available on 2011, November 7th. Up to now, 5 teams sent their 3D numerical solution for at least one of these two cases (see Table 11).

These cases are important to assess the accuracy of the generation process of the surface waves at the valley edges and their propagation towards the center of the valley. The fact that the two edges have a different slope makes it particularly representative of the difficulties encountered in practical situations. In particular, it is very demanding, and in practice not achieved, to explicitly implement the sediment-bedrock interface of the northern edge in a Spectral Element mesh, so there is a need to quantify the accuracy of the approximation done in such situation.

Figure 34 shows the *SH* seismic sections obtained by 5 teams for the CAN4 case along the easternmost surface profile. These sections are dominated by the Love waves generated at the northern edge, which propagate to the South and get reflected at the vertical southern edge (between 15 s and 25 s).

The overall agreement between the different predictions is satisfactory. A closer look at the time series of ground velocities at two particular receivers is shown in Figure 35: receiver 046 (right panel of the figure) stands 1 km away from the northern surface trace of the edge, and receiver 016 (left panel of the figure) stands 1 km away from the southern edge.

As it is seen for both receivers, the agreement on first arrivals is excellent, irrespectively of the implementation of the bedrock-sediment interface close to the edges.

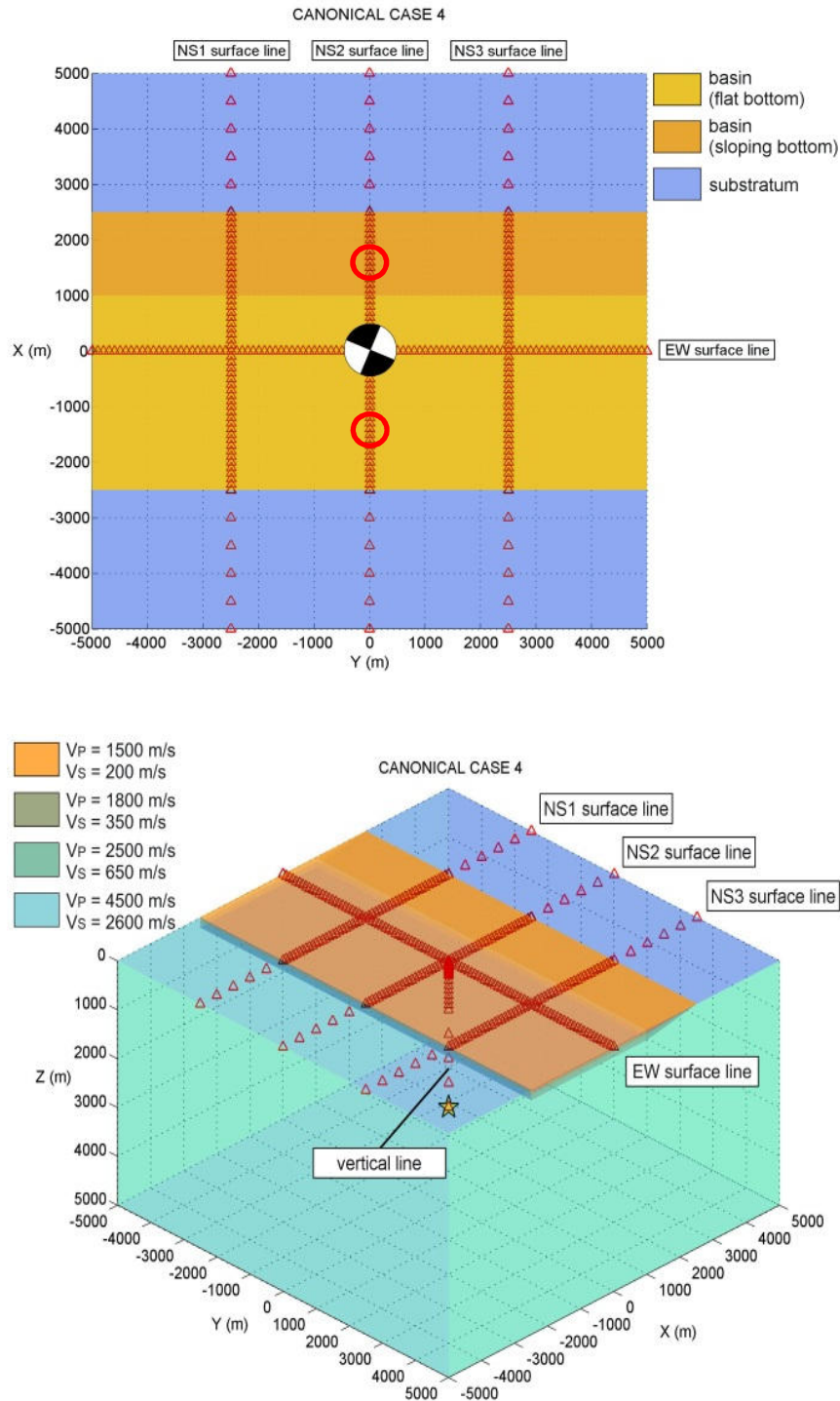


Figure 32: Surface (top) and 3D (bottom) view showing the position of the epicenter (beachball) and hypocenter (yellow star) and of the 326 receivers (red triangles) for the CAN4 case. X points to the North, Y to the East and Z downward. The red circles on the left panel indicate the position of two receivers where the computed ground motion is shown in Figure 35 and Figure 37.

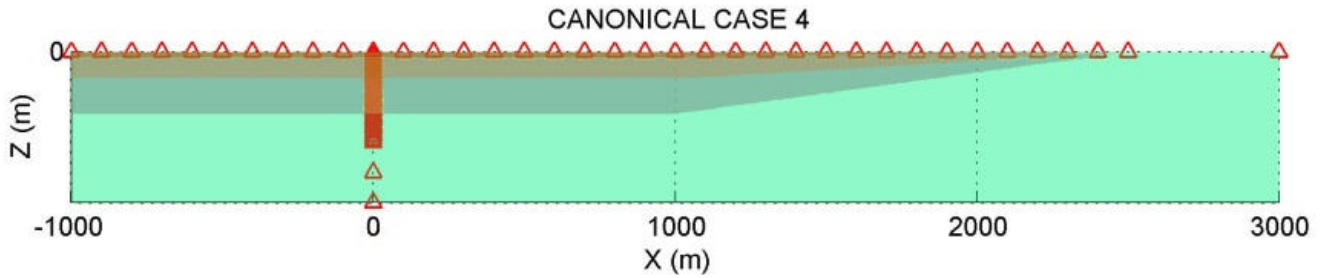


Figure 33: Profile view showing the geometry of the asymmetrical basin for the CAN4 case. This picture is a closed view on the first 500 m on the vertical and centered on the North edge of the basin.

Table 11: Participating 3D teams to the CAN4 and CAN5.

3D acronym	Team acronym	Class of method
3D01	CUB	FDM
3D02	UJF	SEM
3D04	OGS	PSM
3D11	BRGM	SEM
3D12	USTC	FDM

The Love surface wave generated at the northern edge seen around 5 s for the northernmost receiver (right panel of Figure 35) is quite consistently simulated by the five teams. A closer look shows that the 3D02 prediction is slightly different from the others, that the 3D01 and 3D04 predictions are quite close, and that the 3D11 and 3D12 predictions show a perfect match. This is consistent with the way the bedrock-sediment interface is implemented by the 5 teams: 3D02 uses a crude polynomial interpolation of the interface in the SEM, 3D01 and 3D04 use the volume averaging technique defined in Moczo *et al.* (2002) with a grid size of 10 m (reduced to 7 m for 3D04 in the vertical direction), 3D12 uses the same approximation but the grid size is 5 m, and 3D11 succeeded in generating a Spectral Element mesh that exactly follows the interface (this leads to a huge computational time since the stability condition for the explicit time scheme used is very severe).

The agreement at the southernmost receiver (left panel of Figure 35) is quite good, with noticeable differences seen on the Love wave trains generated at the northern edge (for times around 15 s and later). A closer inspection shows that 3D01 and 3D04 predictions are again very similar, so are the predictions of 3D02 and 3D11 obtained with the SEM. The prediction of 3D12 is globally closer to the ones by 3D01 and 3D04, with additional phase differences that are not well understood yet.

Note that the misfits and goodness-of-fit scores were not computed yet, as the predictions are not all completed.

The *SH* seismic sections obtained by four teams for the CAN5 case are shown in Figure 36. As in the previous case, the overall agreement is seen to be quite good, with the exception of the prediction by 3D11 which is under iteration and should be disregarded for the moment.

The time series of ground velocities obtained by the four teams at the two receivers considered previously (016 and 046) are shown in Figure 37. They show a remarkable agreement including for the late arrival of Love waves.

This is a confirmation that smooth models (at least in the sedimentary layers) are much easily handled by all numerical models. It also suggests that the approximation of strong contrasts in numerical models has to be carefully designed whenever surface waves are going to propagate along the approximated interfaces. For other type of waves (e.g. S wave), the approximation seems to be less critical even in the process of surface wave generation at valley edges.

CAN4

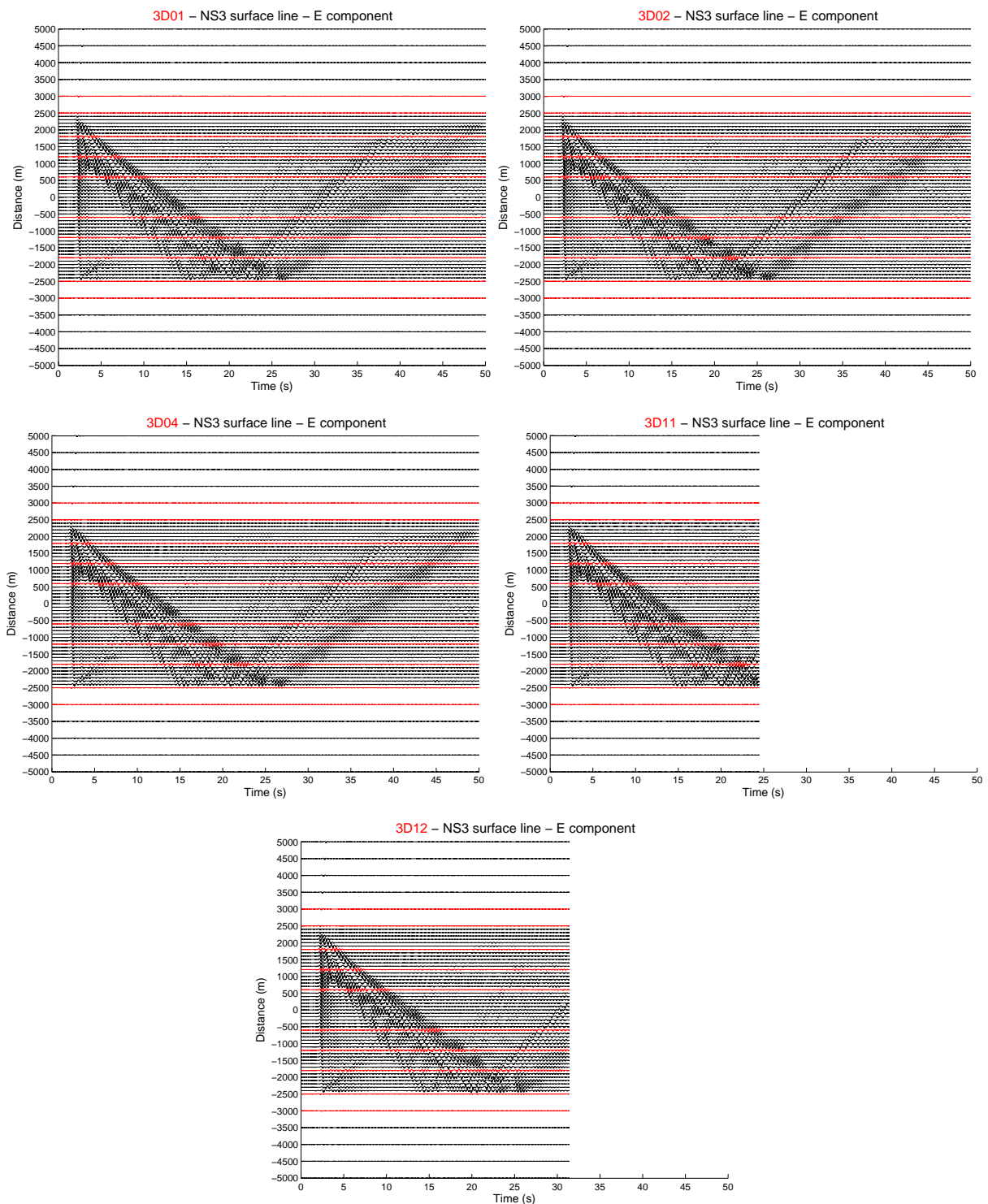


Figure 34: East component of ground velocity for CAN4 along the NS3 surface line (see Figure 32) computed by teams 3D01, 3D02, 3D04, 3D11 and 3D12.

CAN4

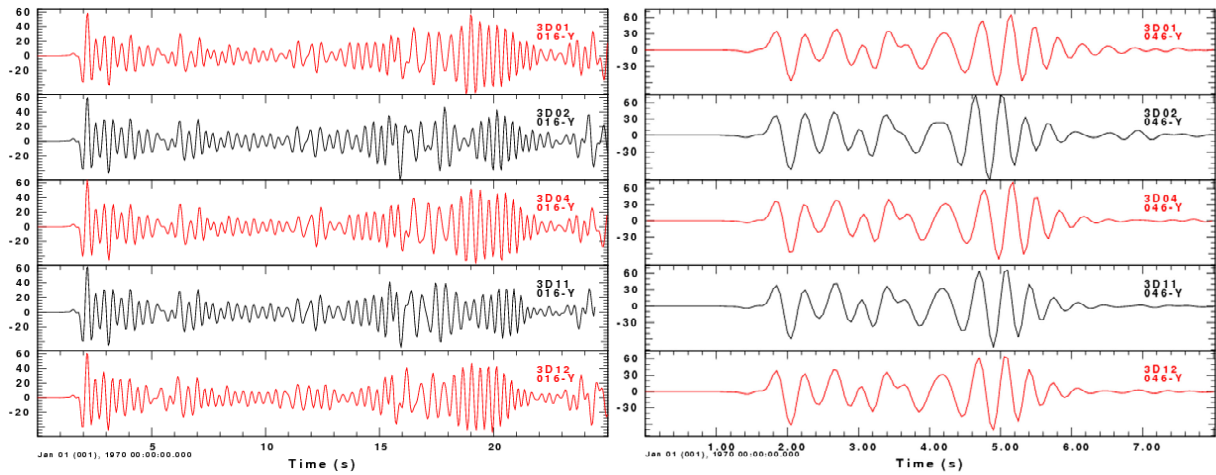


Figure 35: East component of ground velocity for CAN4 computed by teams 3D01, 3D02, 3D04, 3D11 and 3D12 at two receivers: 1500 m south of the epicenter (left) and 1500 m north of the epicenter (right). The location of the two receivers is shown as red circles in Figure 32.

CAN5

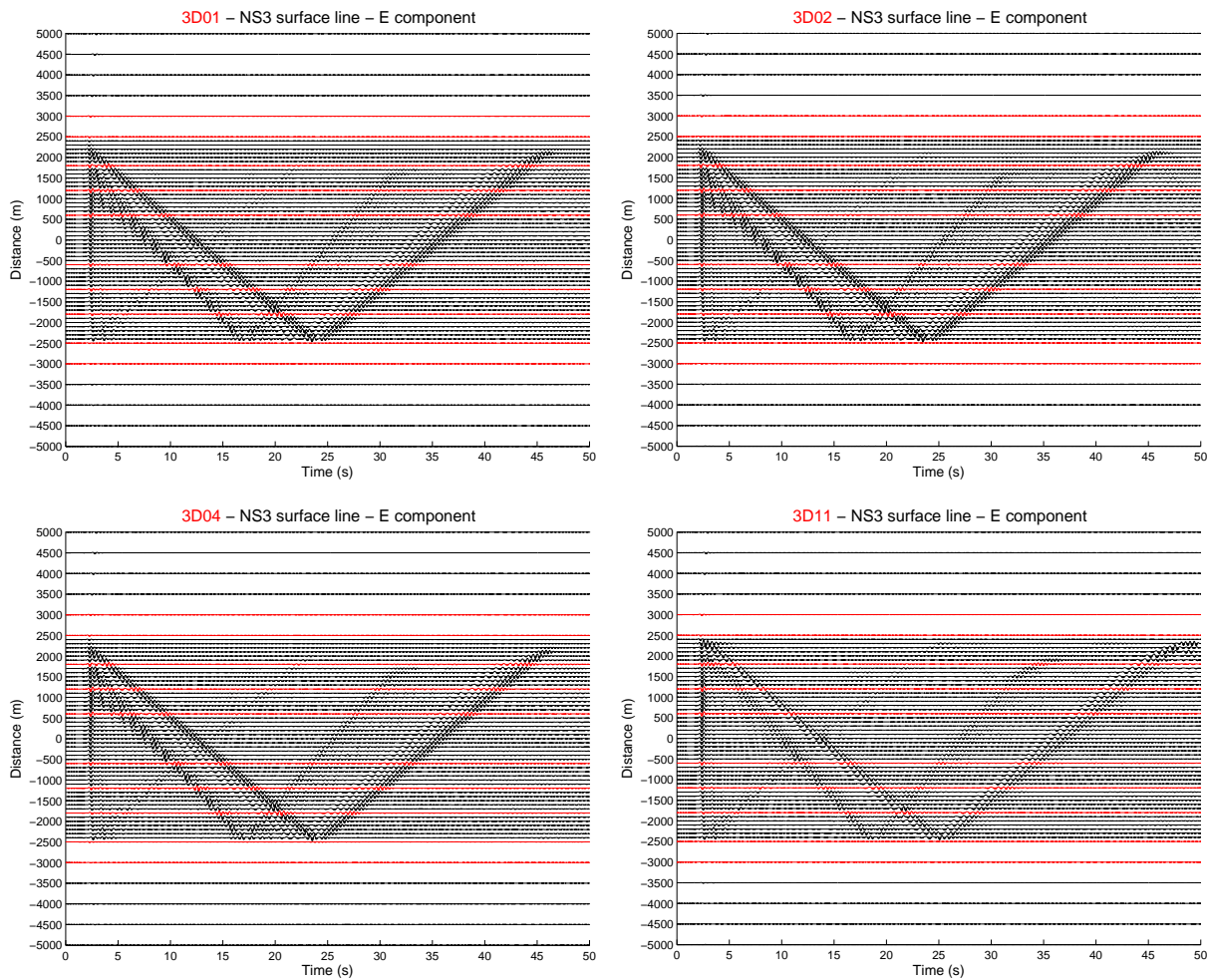


Figure 36: East component of ground velocity for CAN5 along the NS3 surface line (see Figure 32) computed by teams 3D01, 3D02, 3D04, and 3D11.

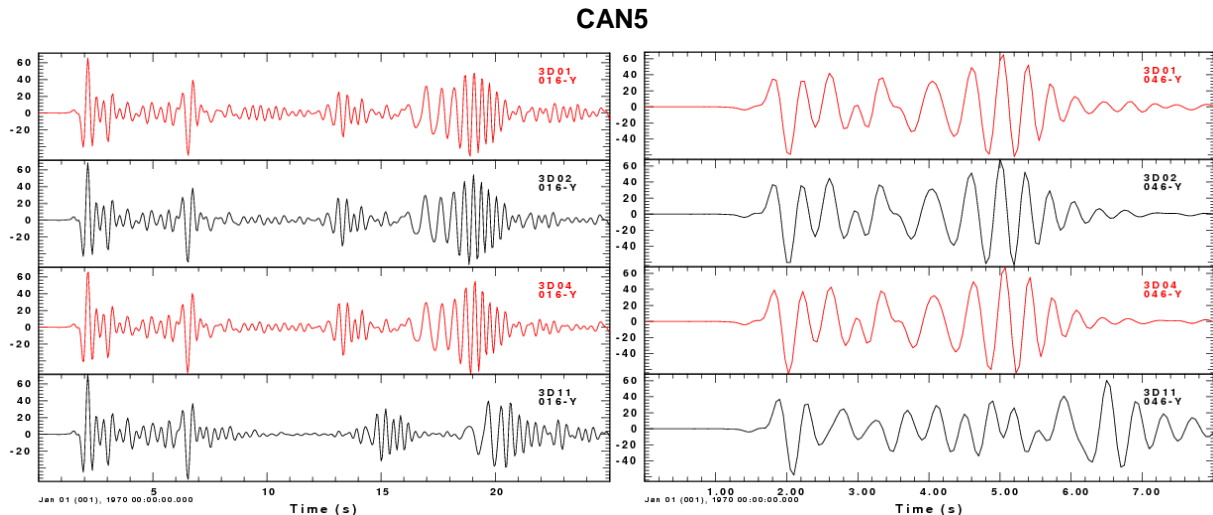


Figure 37: East component of ground velocity for CAN5 computed by teams 3D01, 3D02, 3D04, 3D11 and 3D12 at two receivers: 1500 m south of the epicenter (left) and 1500 m north of the epicenter (right). The location of the two receivers is shown as red circles in Figure 32.

4 2D VERIFICATION: LINEAR AND NONLINEAR CASES

The initial objective of this part was to compare the results of fully non-linear simulation tools within a 2D valley. In that aim, the central cross-section of the Mygdonian graben, along the Stivos-Profitis line was selected, with the most refined description including 7 different units (Figure 38). The request was to compute its NL response to a simple input signal of various amplitudes (from 0.05 to 0.25 g) carried by vertically incident plane S waves, and with a broad input spectrum up to 8 Hz. The comparison was to be performed on time histories and response spectra at receivers along the free surface, and on PGA profiles and stress-strain plots along vertical arrays. Four French teams had volunteered to participate with various codes (FEM, FDM, and DEM) in this exercise as indicated in Table 12.

The NL properties were provided in terms of "classical" degradation curves (shear modulus and damping versus strain, see Figure 38), for the various units. It turned out that the NL rheology built in some codes could not fulfill simultaneously shear modulus and damping curves, and a second set of NL properties was therefore derived on the basis of only the shear modulus degradation properties.

However, the first results proved to be very different from one team to another, and it was not clear whether this was due to the implementation of the NL behavior, or to the numerical scheme itself. It was thus decided to step back and to perform a comparison of the 2D response in the linear domain, with and without damping. Three additional teams could then participate to the linear part of this exercise, including FDM and SEM approaches.

Indeed, many iterations proved to be needed in order to try to reach an acceptable agreement and this part of the verification exercise could not be completed within the life time E2VP-1. The example results displayed in Figure 39 for the 2D linear case and Figure 40 for 2D NL case, witness the large discrepancies that still remained in NL computations, despite a relatively satisfactory agreement for the 2D linear case. Even though it could be completed, this exercise did bring some useful lessons that paved the way for the design of the NL component of the SIGMA/CASHIMA2 program. These main lessons can be summarized as follows:

- To the contrary of what could be hoped, 2D linear computations cannot yet be considered as "standard practice", since several iterations and cross-checks between different methods were

needed to reach a satisfactory agreement. *NL simulations involving 2D (and a fortiori 3D) geometries should always be first verified in the linear case by cross-checking with other techniques.*

- Results of NL computations with different codes having implemented the same $G-\zeta-\gamma$ curves exhibit a large variability even when the codes have been first verified in the linear domain. This variability can be seen very clearly not only on time histories, but also on engineering parameters such as response spectra (Figure 40), and on stress-strain plots and PGA/peak strain profiles versus depth (not shown). *This result emphasizes the need for further work to understand the origin of these discrepancies, especially as the NL codes used in this exercise are commonly used for engineering applications.*
- Some codes predict the onset of NL behavior at very low PGA levels (< 0.05 g), in relation with large damping in thick sediments, while some others exhibit significant nonlinearities only above 0.15 g for the same soil profile. *As these acceleration levels are only moderate, some validation of these codes could be obtained relatively easily with a limited number of carefully instrumented sites located in seismically active regions.*

Though somewhat disappointing, this 2D NL exercise allowed to reach some important practical conclusions, and was very helpful in designing the NL research component of the SIGMA-WP3/Cashima project:

- NL verification is a useful exercise that should definitely be performed again;
- it should be performed on the simplest possible cases (1D soil columns);
- it should be performed on already instrumented sites having recorded large acceleration levels;
- it should be associated with careful in-situ surveys and lab tests designed in tight connection with the needs of the rheological models implemented in the various NL codes;
- the required iterations and field surveys make it a time-consuming and expensive endeavor, which deserves significant funding.

Table 12: List of participants and methods for the 2D NL verification.

Partner	Numerical method	Label	Technical aspects	Attenuation model	Nonlinear rheology
BRGM	Finite Elements	FEM1	Triangular mesh	Kelvin-Voigt	Hujeux (1985)
GdS		FEM2	Triangular mesh	No	Prevost and Keane (1990)
IRSN	Finite Differences	FDM_RG2	Rotated staggered grid: order 2 in space and time	Day and Bradley (2001)	Iai et al. (1990) (combined with attenuation)
CUB		FDM_SG4	Staggered grid: order 2 in time and 4 in space	Kristek and Moczo (2003)	No
AUTH		FDM_SG4			No
UJF	Spectral Elements	SEM	Quadrangular mesh	Moczo et al. (2007)	No
CEA	Discrete Elements	DEM		Mariotti (2010)	Johnson and Rasolofosaon (1996)

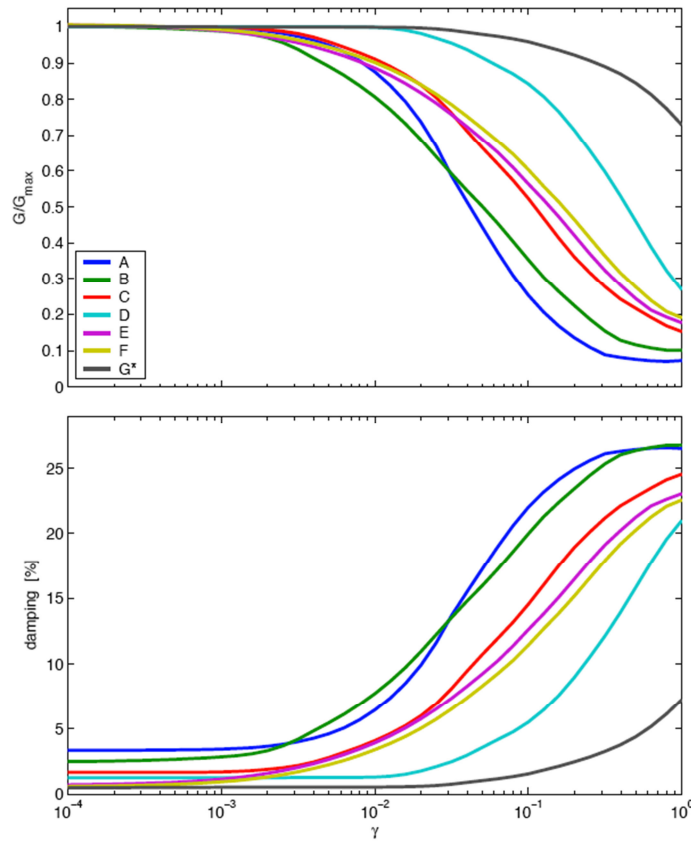


Figure 38: Geological cross-section (left), with different horizontal and vertical scales) and NL degradation curves (right; shear modulus on top, and damping on bottom) considered for the 2D, NL verification exercise. Each curve A to G* corresponds to one of the sedimentary layers of the cross-section (see the geometry on Figure 5). Underlying bedrock is considered fully linear.

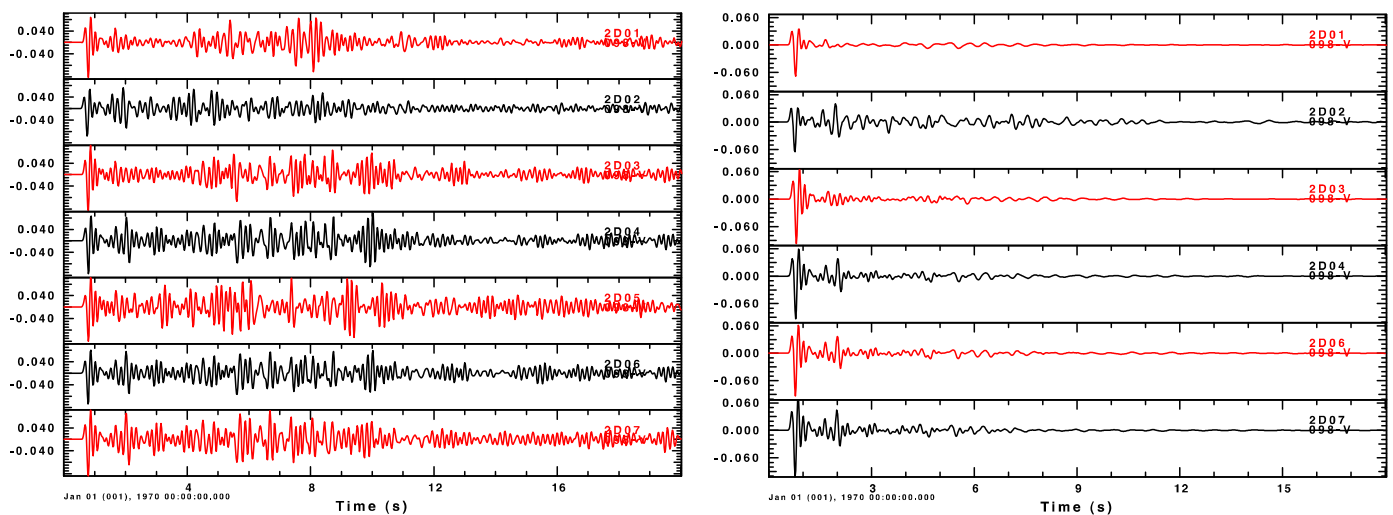


Figure 39: Example comparison of time histories (radial horizontal component) obtained for the 2D case in the linear domain, without damping (left, 7 teams) and with damping (right, 6 teams).

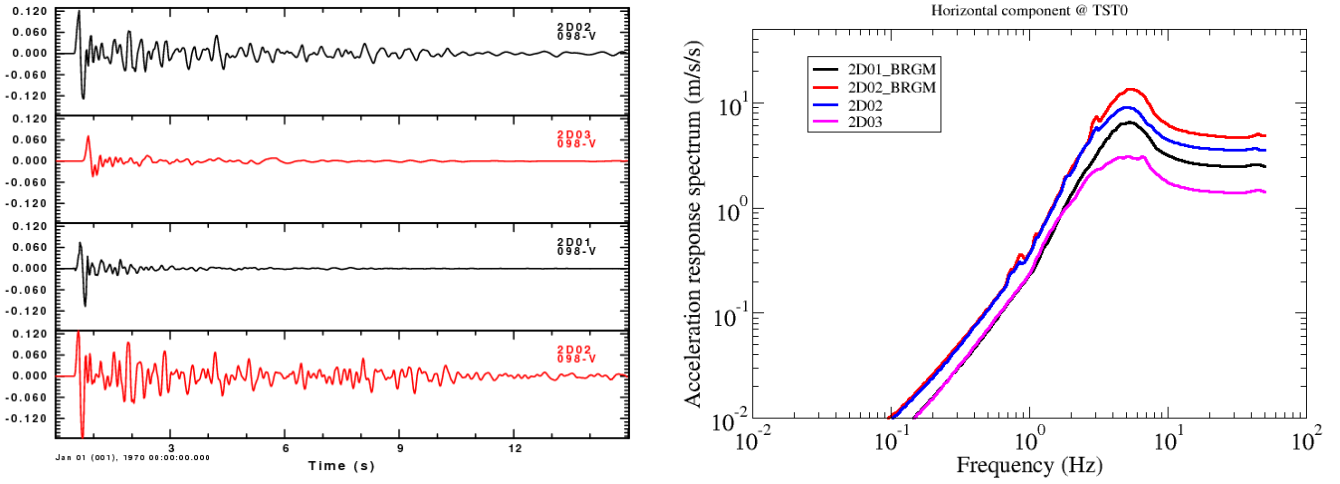


Figure 40: Example comparison of results obtained in 2D, NL case for the valley center. Left: time histories; Right: acceleration response spectra, for a simple input signal with a peak (rock outcrop) acceleration of 0.25 g.

5 VALIDATION OF THE NUMERICAL DATA FOR REALISTIC APPLICATIONS

5.1 COMPARISON WITH LOCAL EARTHQUAKE RECORDINGS FOR VALIDATION OF THE GROUND MOTION NUMERICAL PREDICTIONS

One of the validation steps consists in comparing numerical predictions with actual recordings up to 4 Hz. The exercise has been performed for 6 local, weak to moderate magnitude events, spanning various azimuths, depth and distances, and recorded by the local array of 19 surface and borehole accelerometers (see Figure 41 and Table 13).

In the following we only display the synthetics obtained by one of the numerical methods (SEM by team 3D02) since we have carefully checked in the verification phase of the project that they could be considered as a reference.

The synthetics are computed in the 3D anelastic layered model A of the Mygdonian basin (Figure 2 and Table 3). The simulations are accurate for frequencies up to 4 Hz and do not account for the surface topography.

The computed ground motion from the largest event (#4) is shown in Figure 42, illustrating the complex propagation of the seismic waves inside the Mygdonian basin. The recorded ground motion of this event (black curves) is compared with synthetics (red curves) at several stations: TST0 (surface soil site, Figure 43), TST5 (borehole, 197 m depth, Figure 44), E03 (soil site, Figure 45), W03 (soil site, Figure 46) and STE (rock site, Figure 47). Additional comparisons are available at other stations but are not shown here for the sake of clarity. For each site, velocity time histories, Fourier spectra and acceleration response spectra are displayed for the 3 components of ground motion.

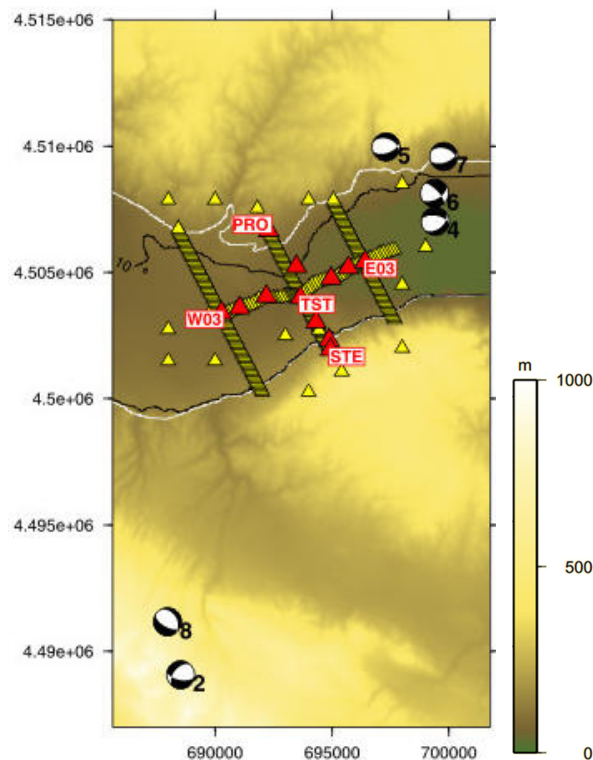


Figure 41: Detailed view of the Euroseistest accelerometric network (red triangles) that recorded 6 local events (beachballs with number ID). The additional virtual receivers (yellow triangles) were used in the 3D numerical simulations of these events. The white line denotes the basin edge and the black line is the location where the sediment thickness equals 10m.

Table 13: Magnitude, depth and focal mechanism of 6 selected real events (see locations on Figure 41) which recordings by the Euroseistest array were compared to numerical predictions.

Event ID	Magnitude	Depth	Strike	Dip	Rake
2	2.8	6.9 km	100°	60°	-50°
4	4.4	5.0 km	53°	43°	-127°
5	3.1	6.0 km	72°	55°	-113°
6	3.9	6.0 km	61°	55°	-115°
7	3.4	5.0 km	72°	55°	-113°
8	3.8	10.0 km	329°	34°	-64°

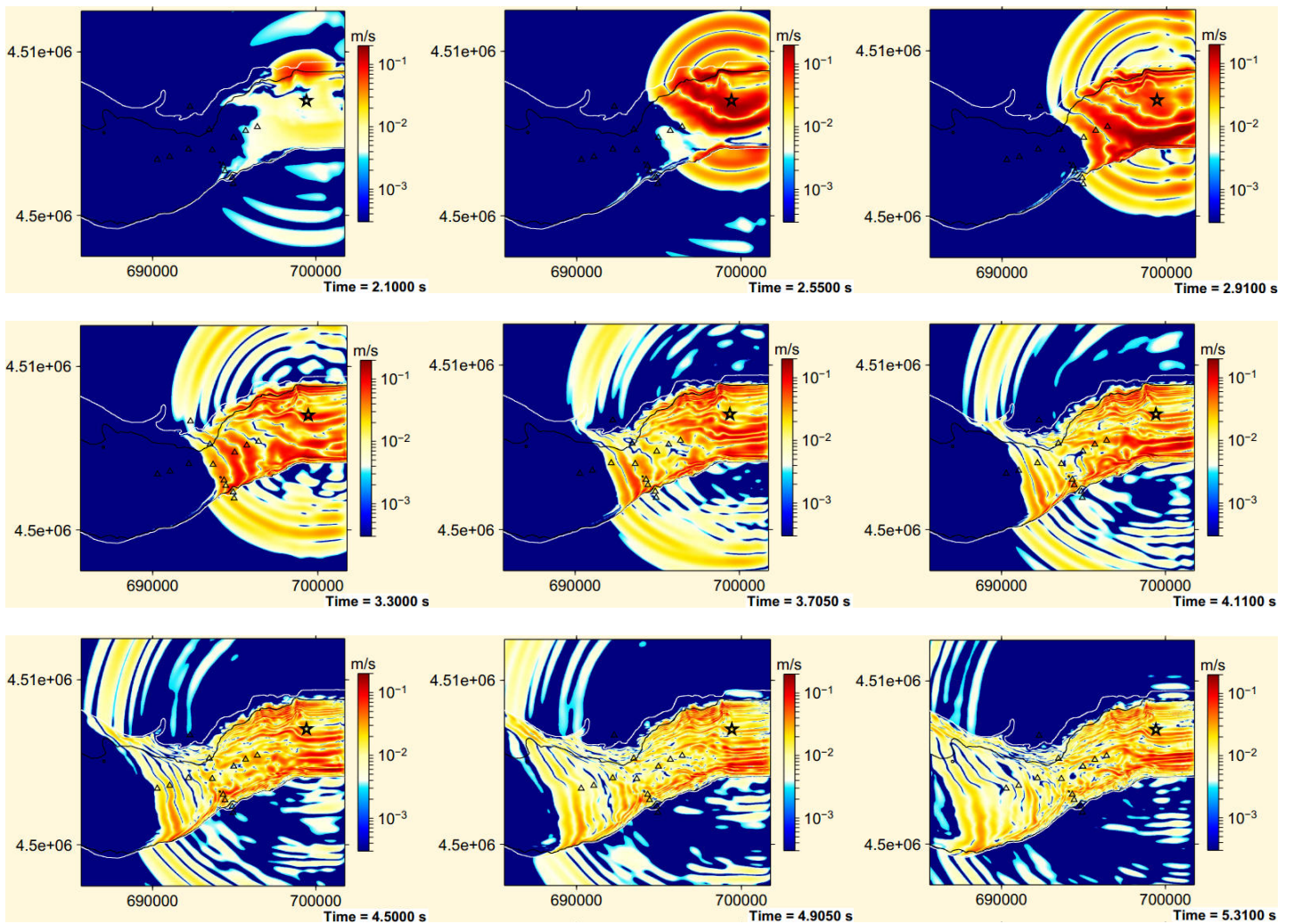


Figure 42: Time evolution of horizontal ground velocity computed for the Event #4.

TST0 – EVENT #4

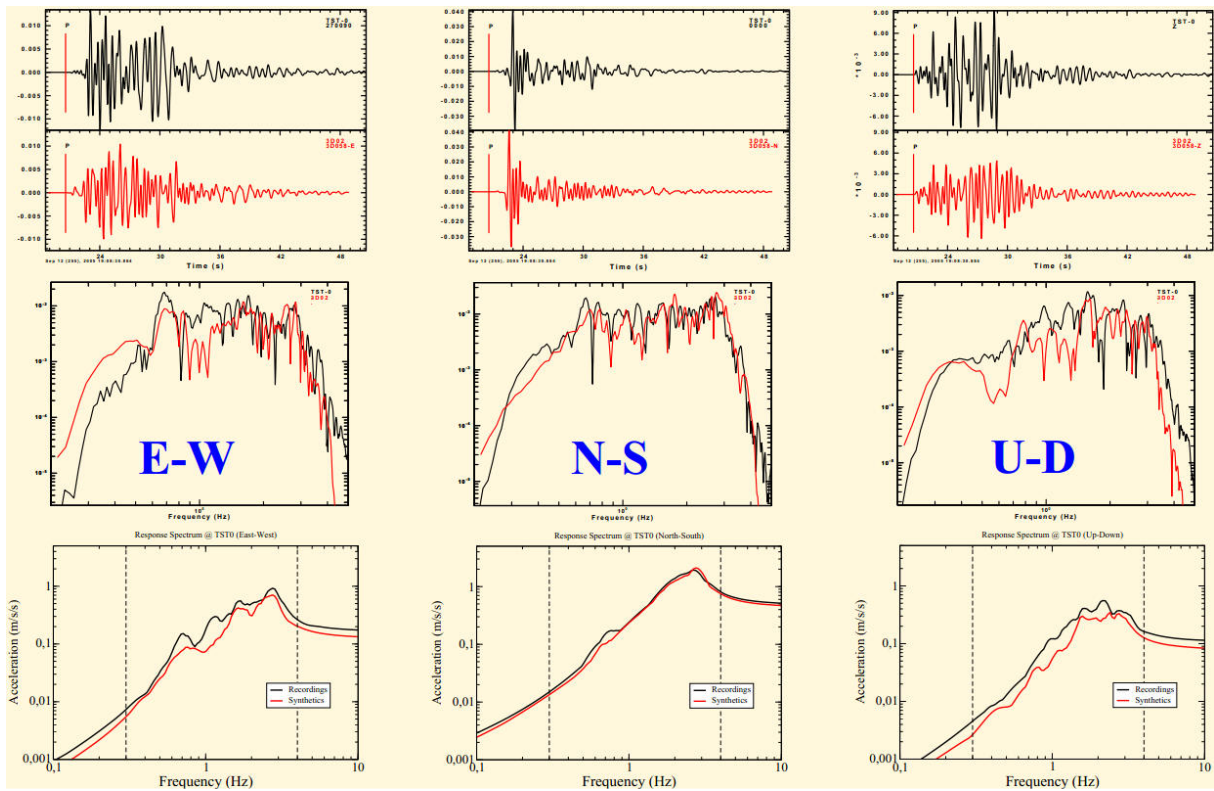


Figure 43: Comparison of recorded ground motion (black curves) with synthetics (red curves) at the station TST0. Time histories (top), Fourier spectra (middle) and acceleration response spectra (bottom) are displayed.

TST5 – EVENT #4

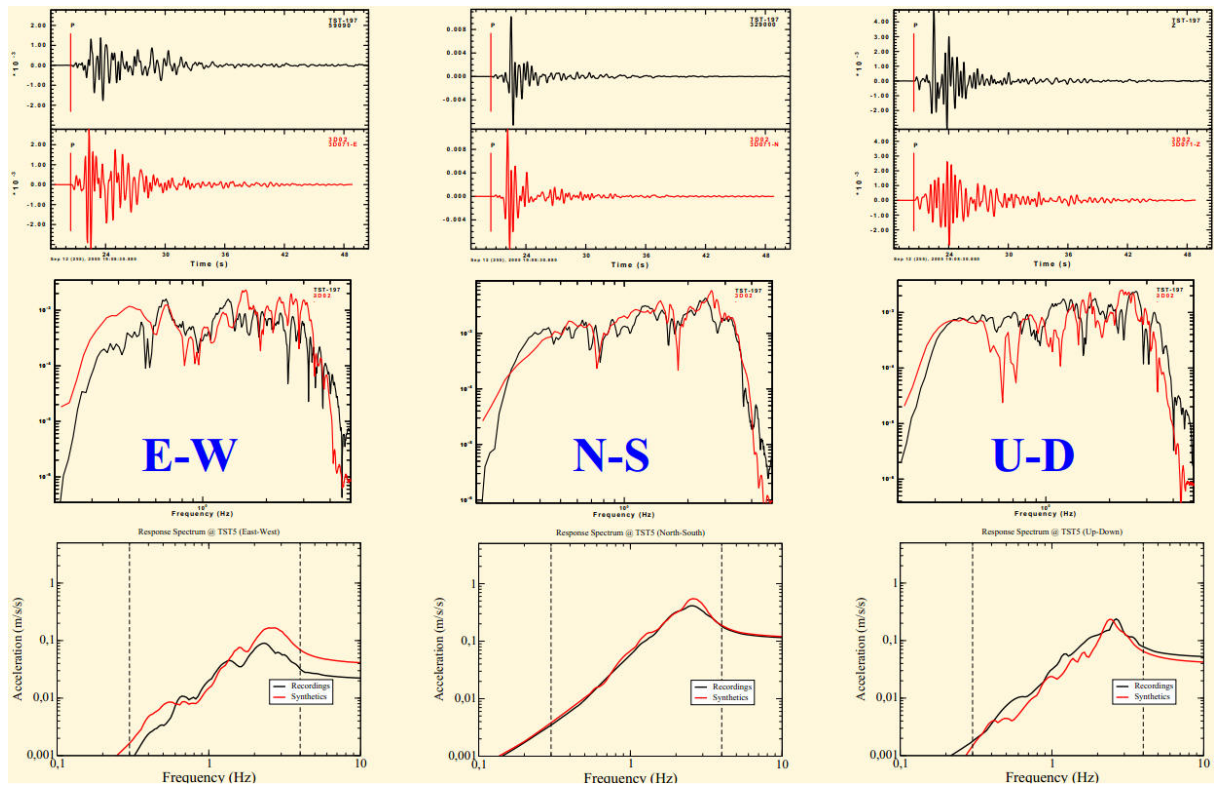


Figure 44: Comparison of recorded ground motion (black curves) with synthetics (red curves) at the station TST5. Time histories (top), Fourier spectra (middle) and acceleration response spectra (bottom) are displayed.

E03 – EVENT #4

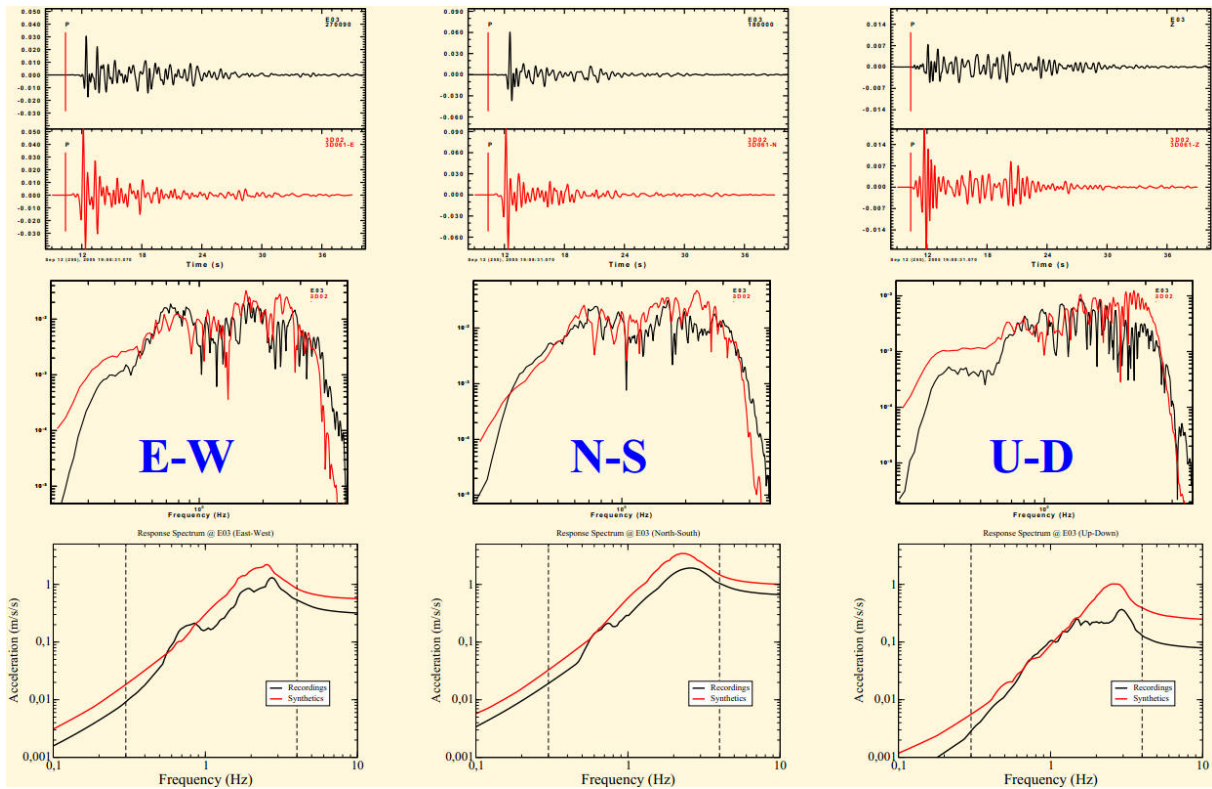


Figure 45: Comparison of recorded ground motion (black curves) with synthetics (red curves) at the station E03. Time histories (top), Fourier spectra (middle) and acceleration response spectra (bottom) are displayed.

W03 – EVENT #4

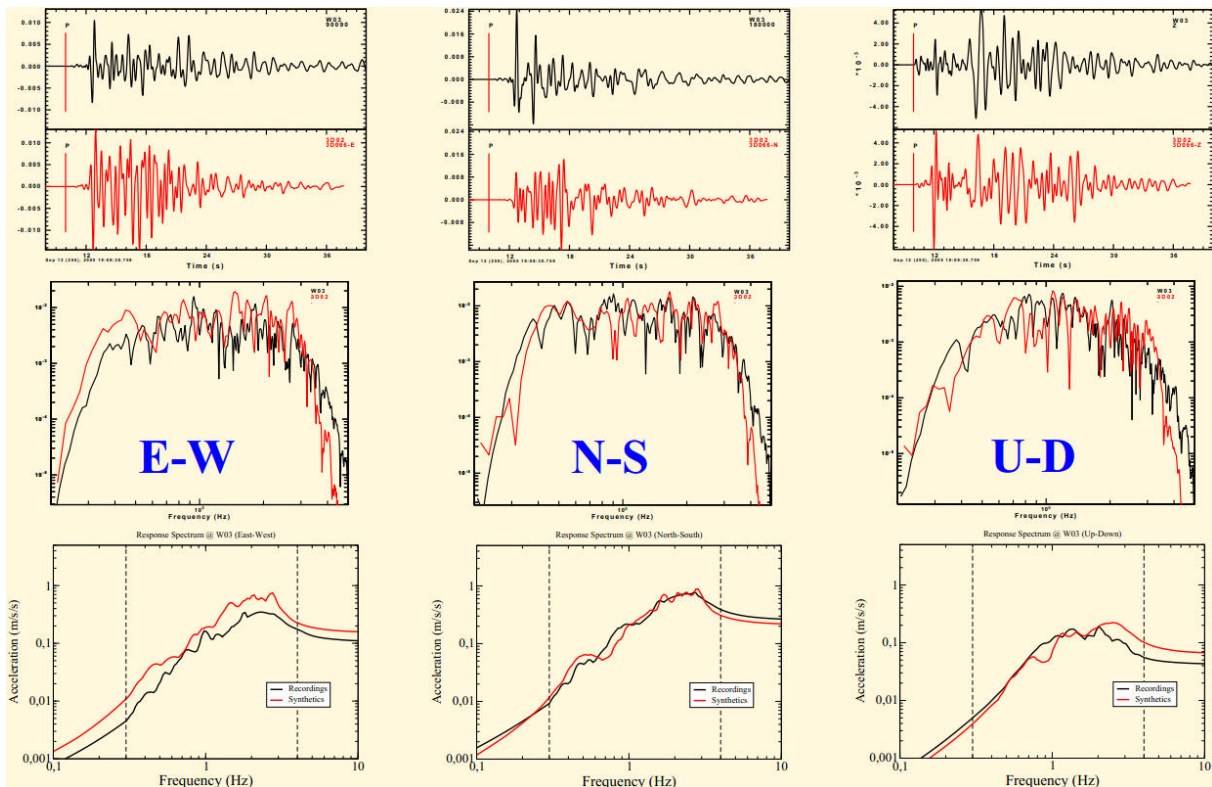


Figure 46: Comparison of recorded ground motion (black curves) with synthetics (red curves) at the station W03. Time histories (top), Fourier spectra (middle) and acceleration response spectra (bottom) are displayed.

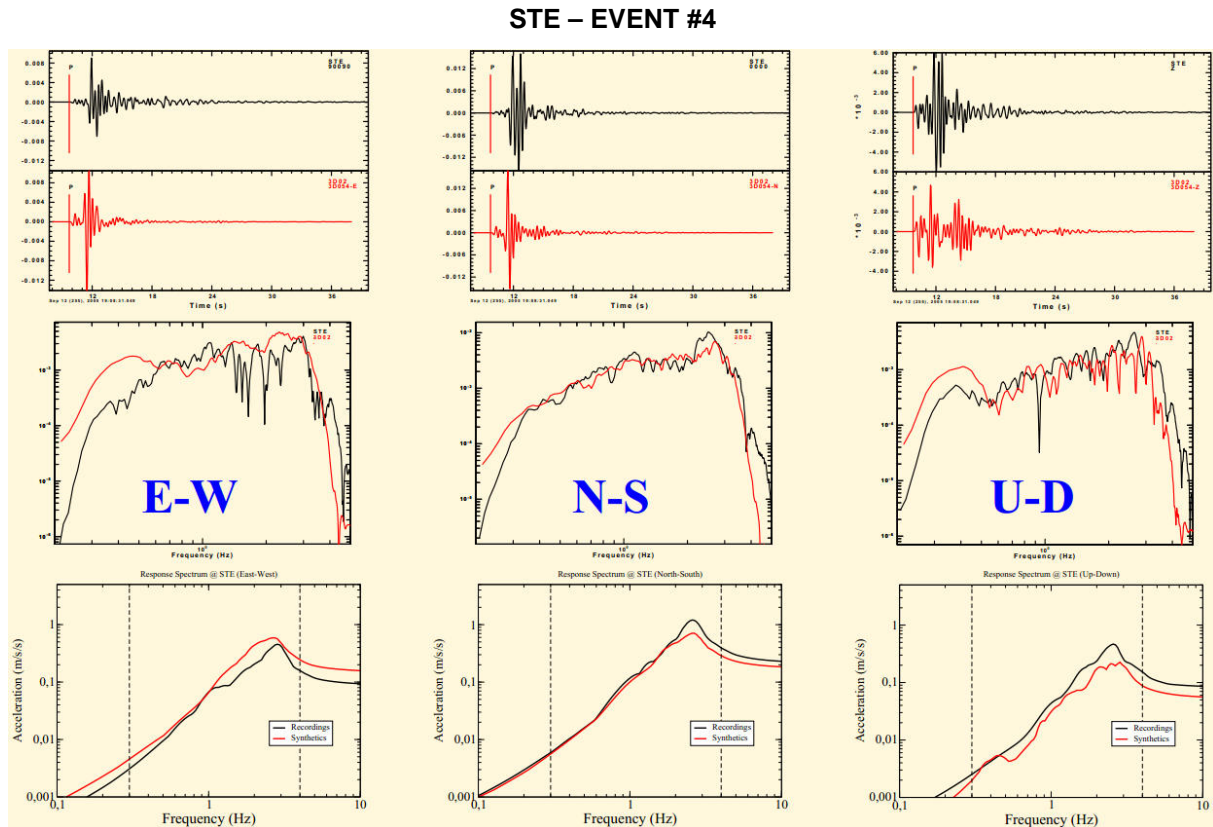


Figure 47: Comparison of recorded ground motion (black curves) with synthetics (red curves) at the station STE. Time histories (top), Fourier spectra (middle) and acceleration response spectra (bottom) are displayed.

In general, while the detailed waveforms do not match, the overall amplitude, duration, spectral shape and response spectra exhibit a relatively satisfactory agreement. The detailed waveforms are indeed very sensitive to the source parameters (hypocenter location and focal mechanism), to the shape of the sediment-basement interface and to the internal sediment layering.

The highest level of agreement is found on the NS component of the TST0 station (see Figure 43). The fit is excellent for the PGA, the acceleration response spectra and the energy duration. The same NS component of the TST5 borehole station, located 197 m beneath the TST0 station, also exhibits an excellent fit for the acceleration response spectra (see Figure 44).

The observed difference in envelope shape between the EW and NS components of TST0 is relatively well reproduced by the synthetics. The level of agreement is less satisfactory at the other sites, with the ground motion at E03 being entirely overestimated by the synthetics (see Figure 45). The fit at the rock sites (TST5, STE) is slightly better than at the soil sites (E03, W03), except at the central TST0 soil site that shows the best agreement between recordings and synthetics on the NS component of the ground motion.

The velocity structure of the Mygdonian basin is precisely best constrained along a central NS profile crossing TST0 (see part 1.3). This illustrates how strongly the accuracy of the ground motion numerical predictions is dependent of the geological structure knowledge at the site of interest.

The level of agreement is however found to be event-dependent, as a result of the combined uncertainties in the source parameters and in the basin structure. The best agreement is found indeed for the largest – and thus best known – event.

The comparisons with recorded data were performed for the other 5 events, located either to the East or to the South (see Figure 41). As the level of agreement is less satisfactory for these smaller events, we only show results for one of them in the following.

TST0 – EVENT #6

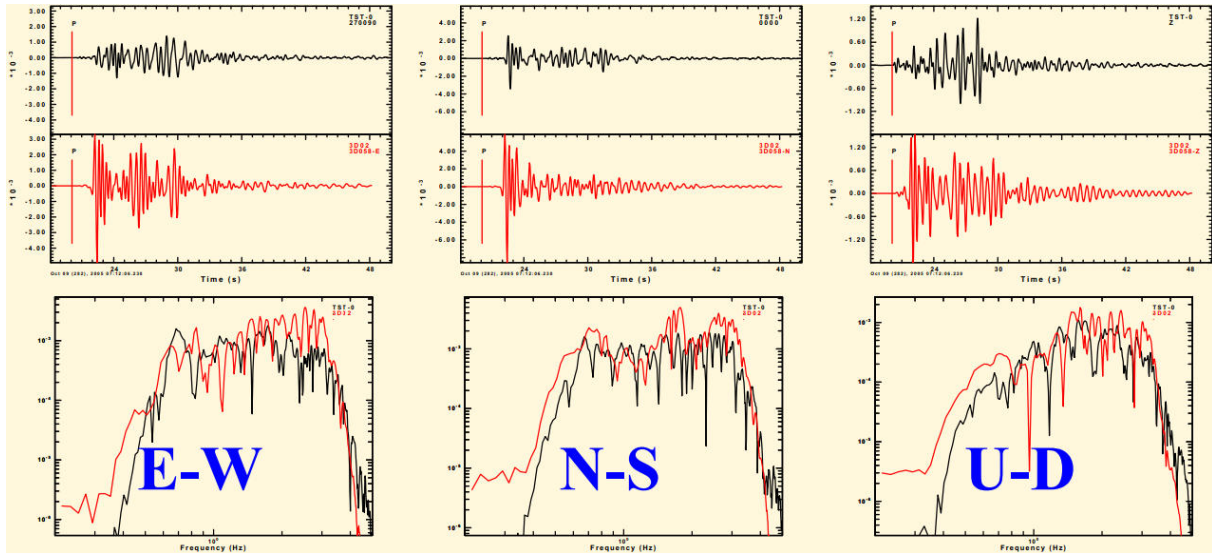


Figure 48: Comparison of recorded ground motion (black curves) with synthetics (red curves) at the station TST0 for event #6. Time histories (top) and Fourier spectra (bottom) are displayed.

TST5 – EVENT #6

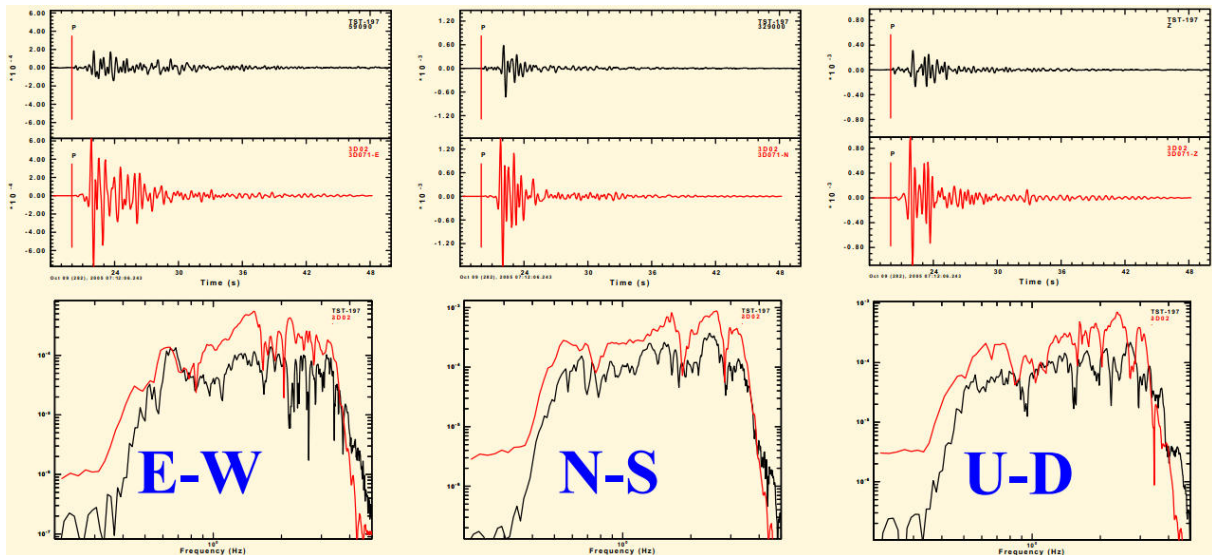


Figure 49: Comparison of recorded ground motion (black curves) with synthetics (red curves) at the station TST5 for event #6. Time histories (top) and Fourier spectra (bottom) are displayed.

Event #6 is located slightly deeper north of the Event #4, with a slightly lower magnitude and slightly different focal mechanism (larger strike-slip component). The comparison between recordings and synthetics is displayed only for TST0 (surface receiver, see Figure 48) and TST5 (downhole receiver, see Figure 49), for time histories (top) and Fourier spectra (bottom). While the surface motion exhibits comparable features (amplitude and duration), the downhole motion is overestimated. This might be due to some errors in the hypocenter location (especially its depth) and in the focal mechanism of the source. Some additional work is therefore required in order to improve the source description.

In order to remove (some of) the errors due to source parameter uncertainties, another comparison was based upon the Fourier transfer functions from the downhole sensor (TST5) to the surface sensor (TST0) at the central vertical array. The instrumental site-to-reference spectral ratios derived from the available recordings were compared with those derived from 1D and 3D synthetics (see Figure 50 and Figure 51). The best fit is obtained for 3D simulations, which do account for both the broad band amplification due to lateral reverberations and the scatter due to the sensitivity of the diffraction pattern to the source location. The theoretical 1D surface/downhole transfer function also overestimates the amplification at fundamental frequency, due to the systematic occurrence of destructive interferences at the sediment/basement interface at the fundamental frequency for vertically incident plane waves.

However, while the fundamental and overtones may be seen on each estimate, the amplification at intermediate frequencies, which proves to be large on observed SSR, witnesses further contribution of lateral reverberations and surface waves. There is a trend for underestimating the actual amplification in 3D simulations that could have several explanations: incorrect estimates of damping (too low Q values), incorrect internal sediment layering structure, mislocation of the buried pass just beneath the central profile, overestimation of hypocentral depth. Moreover, the increased standard deviation at intermediate frequencies for the observed SSR (when derived from many more events, see Figure 51) emphasizes the variability of the scattering/diffraction phenomena as a function of the source location. The derivation of the average synthetic SSR should thus take more events into account (6 events are definitely not sufficient).

A final comparison is based upon the ten ground motion criteria defined by Anderson (2004) to quantitatively score how well the synthetics match the statistical characteristics of the observed records: Arias duration, energy duration, Arias intensity, energy integral, PGA, PGV, PGD, response spectra, Fourier spectra and cross correlation. A goodness-of-fit score is computed for each of these criteria between recordings and synthetics following the scaling described in Figure 9. This scaling recommended by Anderson (2004) means that a difference of 50% on a criterion corresponds to a GOF score of 8/10 (while the scaling used in the verification part of E2VP was more severe, a difference of 50% corresponding to a score of 6/10).

The GOF scores on some representative ground motion criteria are given in Table 14 for all of the 6 selected local events shown in Figure 41 and simulated by team 3D02 in the Mygdonian basin model. Depending on the criterion, the event and the site, the scores are very variable. In general the best agreement between recordings and synthetics is unsurprisingly found at the TST0 site. The Figure 52 shows the map of the Anderson goodness-of-fit scores between recorded ground motion and synthetics computed by team 3D02 on response spectra for the 6 selected local events recorded at all available sites.

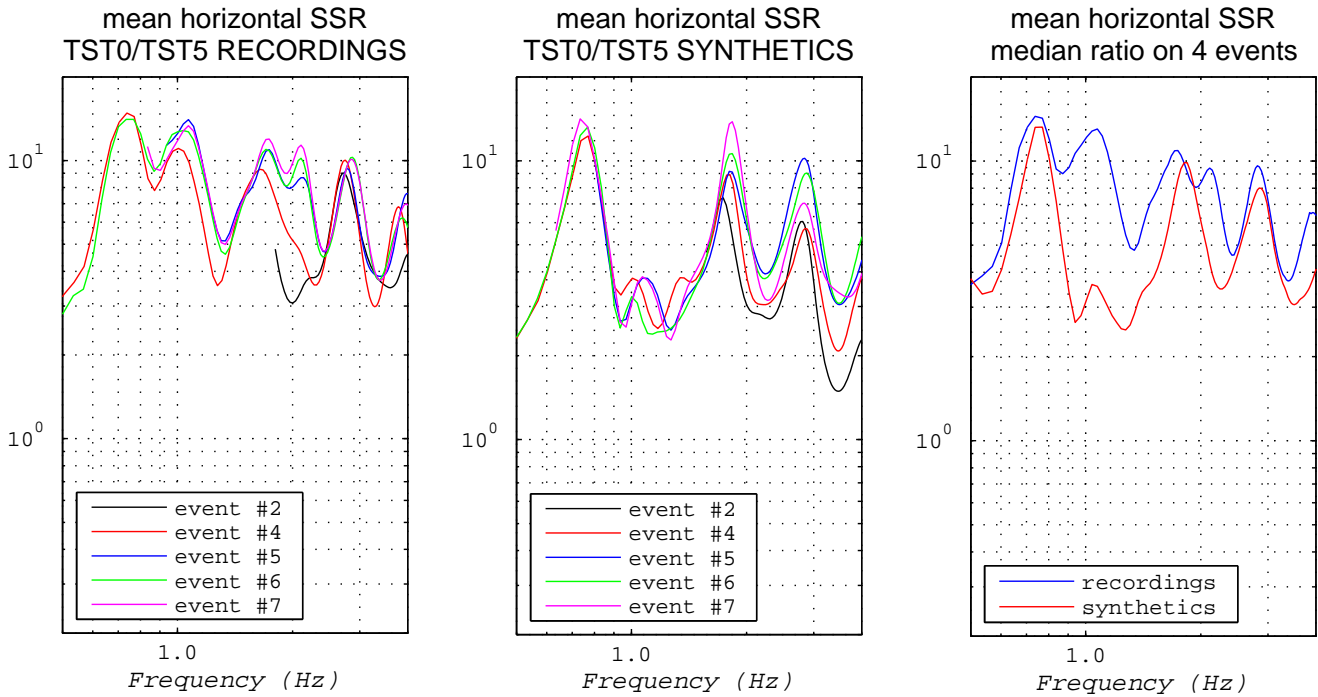


Figure 50: Standard spectral ratios of the mean horizontal component between stations TST0 (surface) and TST5 (borehole) for recordings (left) and synthetics (middle) of 5 local events (see Table 13). The event #8 was not recorded by TST5. The spectral ratios are plot only for frequencies where the signal-to-noise ratio is greater than 10. On the right panel, the median ratios for recordings (blue) and synthetics (red) are calculated on 4 events (#4, #5, #6 and #7). The event #2 is not included in the median ratio as its signal-to-noise ratio at TST is acceptable only above 2 Hz (this is both the furthest and lowest event).

Mean horizontal SSR TST0/TST5

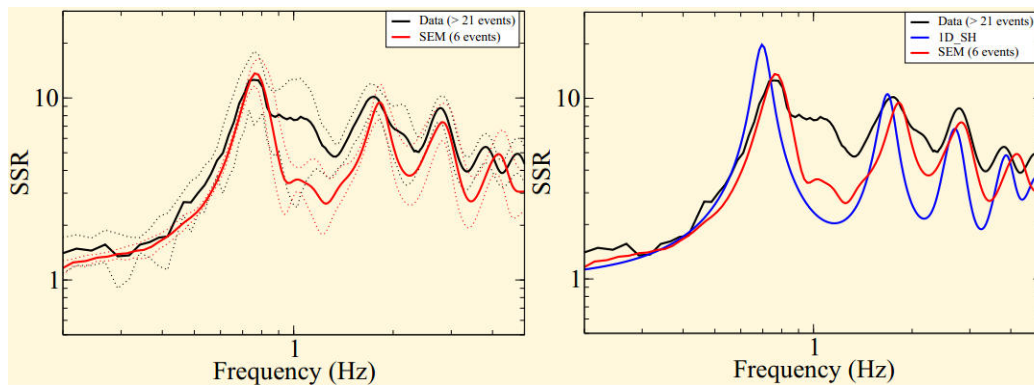


Figure 51: Standard spectral ratios of the mean horizontal component between stations TST0 (surface) and TST5 (borehole) for recordings (black curves), 3D synthetics (red curves) and 1D synthetics (blue curve). The left frame displays the average (plus/minus one standard deviation) spectral ratio derived from the available recordings (more than 21 events) and the synthetics (the 6 selected events), while the right frame compares these average SSR with the theoretical 1D SH transfer function.

Table 14: Anderson goodness-of-fit scores between recorded ground motion and synthetics computed by team 3D02 on 4 representative ground motion criteria (Arias intensity, energy duration, PGA and response spectra) for the 6 selected local events (see Figure 41 and Table 13) recorded at 5 different sites: TST0 (central soil site), TST5 (rock site, downhole, 197 m below TST0), E03 (soil site), W03 (soil site) and STE (rock site). The scores are averaged on the two horizontal components of ground motion. The average Anderson score (Anderson, 2004) is also given in the last column. The score and color scaling is described in part 3.3.

Event #2

site	Arias intensity	energy duration	PGA	response spectra	average Anderson score
TST0	8.8	7.7	9.3	7.4	7.5
TST5	2.5	8.1	6.8	5.7	5.6
E03	8.0	6.1	9.8	8.7	7.4
W03	3.4	7.3	7.0	7.4	5.6

Event #4

TST0	9.2	7.1	9.9	9.2	8.0
TST5	3.2	5.6	5.6	8.0	5.4
E03	0.7	5.2	4.3	3.9	4.0
W03	3.4	6.7	9.1	7.2	6.1
STE	5.1	3.1	7.8	7.3	5.6

Event #5

TST0	9.7	7.1	9.8	8.9	8.0
TST5	5.9	8.1	8.6	7.6	7.3
E03	9.1	7.1	9.3	7.2	7.2
W03	0.2	7.0	2.7	2.8	3.0
STE	0.0	6.1	0.7	2.0	2.3

Event #6

TST0	0.0	6.5	0.6	2.4	2.5
TST5	0.0	7.3	0.3	0.4	2.4
W03	0.0	6.8	2.5	2.4	2.8
STE	5.0	4.3	5.9	6.2	5.1

Event #7

TST0	1.0	7.2	5.2	5.2	4.3
TST5	0.0	7.8	2.0	2.0	2.9
W03	0.1	7.5	4.1	1.6	3.3
STE	6.8	4.8	9.1	8.2	6.6

Event #8

E03	8.7	6.4	4.4	5.1	4.4
W03	4.7	6.9	6.6	5.3	5.1
STE	5.9	6.7	9.4	7.0	7.0

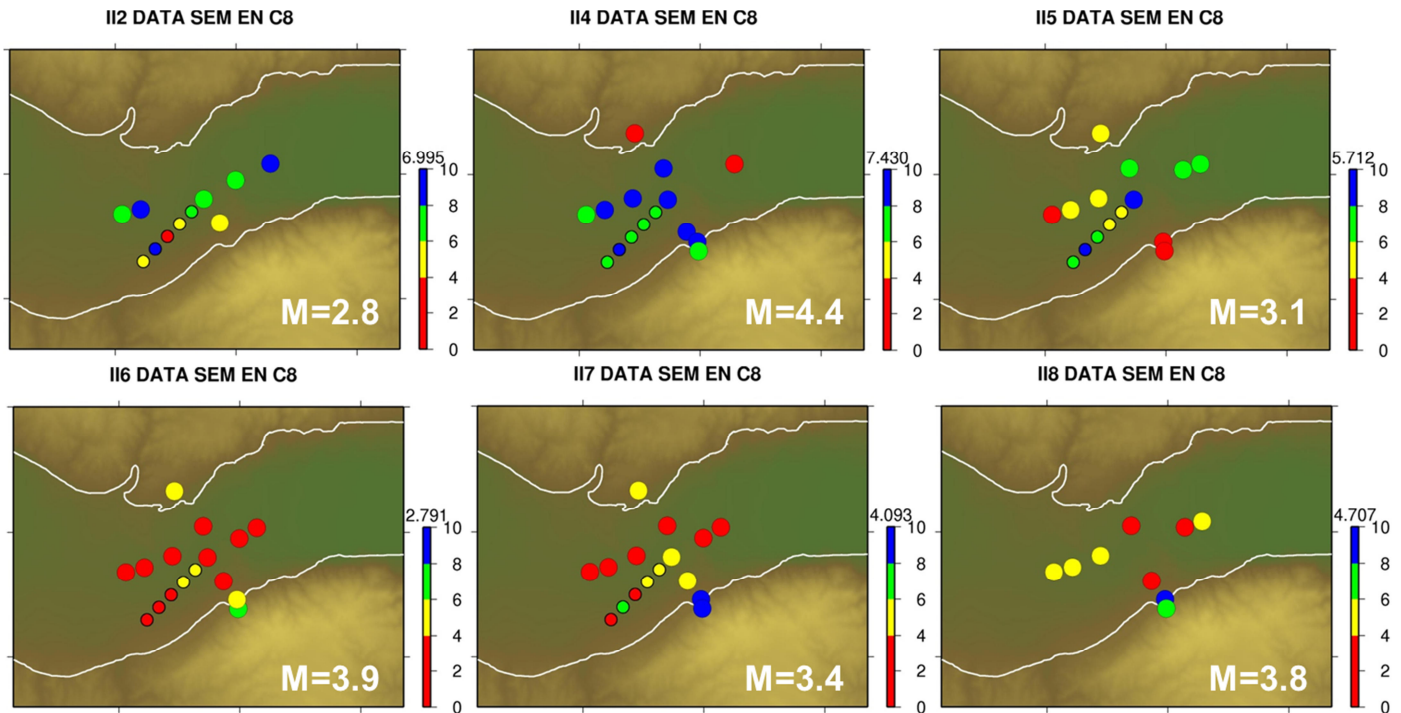


Figure 52: Map of the Anderson goodness-of-fit scores between recorded ground motion and synthetics computed by team 3D02 on response spectra for the 6 selected local events (see Figure 41 and Table 13) recorded at all available sites. The score and color scaling is described in part 3.3.

5.2 CONCLUSIONS OF VALIDATION

The validation exercise has certainly been handicapped by the relatively small number of well recorded local earthquakes and their small-to-moderate size, which impaired the precision of their localization (especially for the depth) and of their focal mechanism. However, several useful conclusions can be drawn from this limited set of comparisons:

- The smallest distance between data and simulations is significantly larger than the smallest distance between simulations (see Table 5, Table 6 and Table 14). For most events, the average validation scores are below 6/10, which means a discrepancy exceeding 70%. This emphasizes the fact that the verification phase was useful in correcting some bugs, and that the origin of the significantly lower "engineering score" of the validation part, even for the largest local event (#4), should be looked for in priority in the inadequacy of the model or of the source parameters.
 - This implies a thorough investigation of the sensitivity of validation scores on the source parameters and the details of model characteristics (geometry, mechanical properties).
 - It also implies to assess the present capabilities of geophysical and geotechnical surveys to provide the required details of the underground structure, not only for high frequencies and short wavelengths, but also for some still very badly known parameters such as material damping.
- While the prediction of the absolute motion should definitely be improved, including at rock sites, the gross characteristics of the amplification at valley center are well reproduced by the model, both in terms of spectral contents and signal duration, with a better – though still imperfect – agreement for 3D models. This is clearly an indication that a significant part of the discrepancies comes from uncertainties/errors in the source parameters (localization, focal mechanism). This is also a witness of the usefulness of vertical arrays for the validation of models.

- Finally, the small number of "candidate events" for validation is a typical situation of moderate/weak seismicity areas. Future validation events would certainly benefit from the possibility to include more distant events, which implies some "hybrid" numerical schemes coupling computations at different scales.

6 **SENSITIVITY STUDIES, 2D AND 3D CASES**

Several sensitivity studies were performed in order to determine the impact of variations in model geometry, damping and velocity model on the computed ground motion in the Mygdonian basin. Some of these studies were performed in 2D, others in 3D, and a few were performed both in 2D and 3D. Those sensitivity studies will help to understand the differences between recorded and synthetic waveforms. We will also estimate the impact of variations in model parameters through several ground motion criteria such as peak values, Arias intensity, response spectra, *etc.*

6.1 **SENSITIVITY TO MODEL GEOMETRY: EFFECT OF SURFACE TOPOGRAPHY**

In order to determine if the impact of the surface topography on the computed ground motion in the Mygdonian basin is so strong that it has to be taken into account in the simulations, two teams (one using 2D simulations and the other 3D simulations) computed the ground motion in the Mygdonian basin model with and without the surface topography.

The comparison of the 2D computations shows rather large changes in the waveforms that are considerably affected by the surface topography (see Figure 53). A slight deamplification due to topography is observed on the main horizontal component, while the secondary vertical component is amplified at the rock sites STE and PRO. They are indeed more affected by the topographic amplification as those two receivers are located on slightly elevated sites. However it is not clear whether an amplification or deamplification occurs at the central TST soil site where the vertical waveform is still significantly different.

The comparison of the 3D computations further illustrates how the effect of surface topography is limited inside the basin, except at the North edge and at the southern central part (see Figure 54). The PGV values are mainly affected outside the basin where the surface topography is important, but the effect remains limited in the central, quasi-flat part of the basin. This effect can punctually become significant inside the basin where the variation of basin thickness between the topographic and flat models is also important. Then the amplification/deamplification of the PGV values inside the basin is implicitly due to the difference of sediment thickness than to the direct effect of surface topography (or it is due to a combined effect of both sediment thickness and surface topography).

Both the 2D and 3D computations show that the effect of surface topography inside the quasi-flat Mygdonian basin is not significant for peak values but largely affects the waveforms. Nonetheless the effect of surface topography should certainly be taken into account for the definition of a reference rock site outside the basin.

Further analyses using spectral ratio at TST and further simulations with varying locations of the source (located under the central part of the basin in the shown examples) will be performed in order to detail the effect of surface topography inside the basin, as this effect is frequency-dependent and is also strongly sensitive to the orientation of the incident energy in relation to the topography.

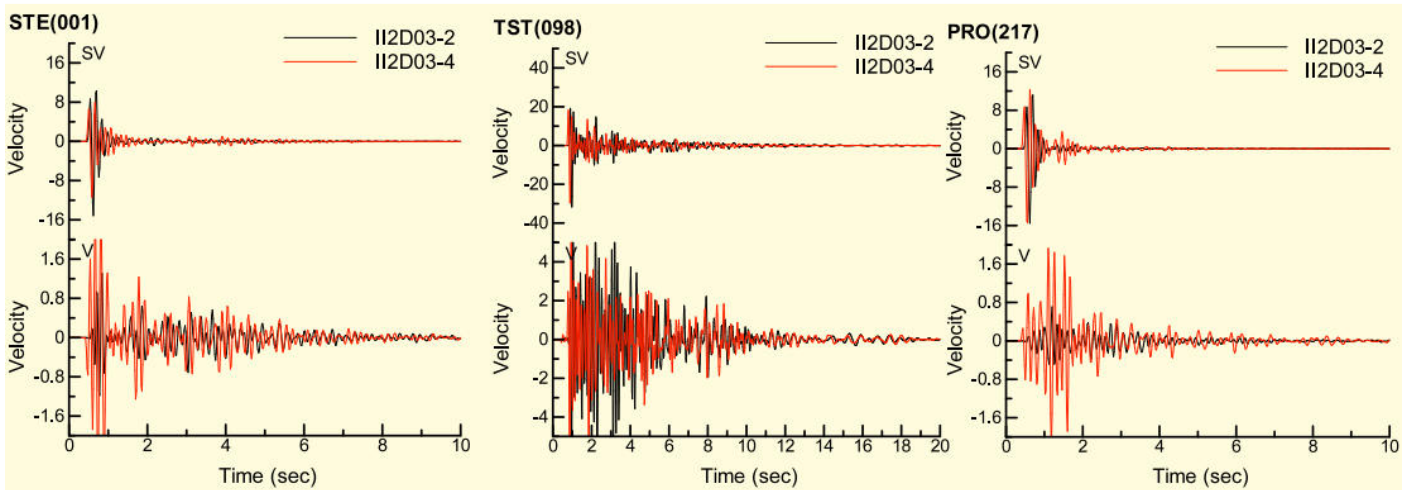


Figure 53: SV component (top) and vertical component (bottom) of ground velocity computed by team 2D03 on the Mygdonian basin model with topography (red waveforms) and without topography (black waveforms) at 3 receivers: STE (south of basin, rock site, left panel), TST (central soil site, middle panel) and PRO (north of basin, rock site, right panel).

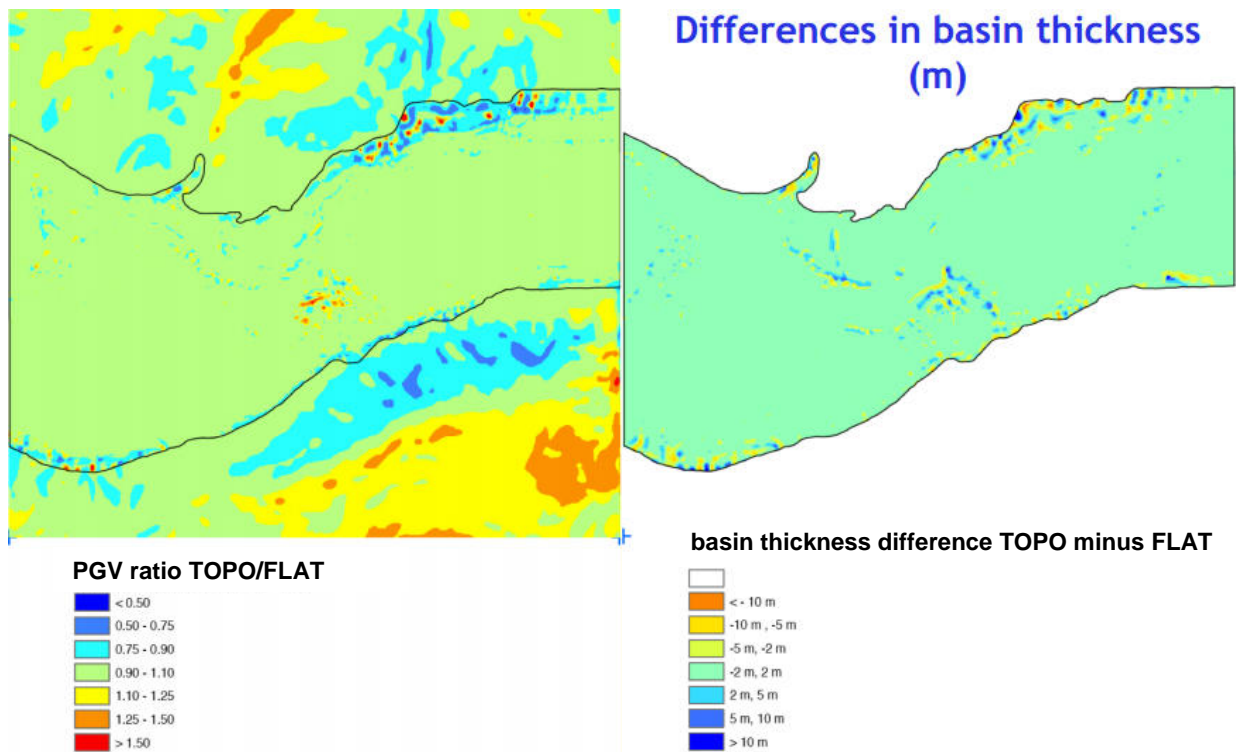


Figure 54: Map of PGV ratio (left) computed by team 3D02 (viscoelastic simulation) comparing values obtained with and without surface topography, and differences in basin thickness between the topographic and flat versions of the Mygdonian basin model (right).

6.2 SENSITIVITY TO DAMPING

The numerical simulation of the ground motion without attenuation is useful for the verification exercise as it preserves the whole complexity of the waveforms but the computed ground motion is unrealistic in this case. Thus, the following sensitivity study to damping will compare the impact of different values of damping on the computed ground motion, but will not tackle the case without attenuation.

The influence of f_0 for attenuation models with $Q(f) = Q(f_0).f/f_0$ on the computed ground motion is estimated from 3D calculations by team 3D05 in model A (see Table 3), with $f_0 = 1, 2,$ and 4 Hz. The sensitivity to damping is estimated from PGV maps and goodness-of-fit scores on several ground motion criteria.

This comparison using ground motion criteria is largely inspired from the Anderson's criteria to quantitatively measure the goodness-of-fit between two synthetic seismograms (Anderson, 2004). The present test and the followings were all analyzed using the ten Anderson's criteria (Arias duration, energy duration, Arias intensity, energy integral, PGA, PGV, PGD, response spectra, Fourier spectra and cross correlation) but only the most affected and/or representative criteria will be presented in this report. A goodness-of-fit score is given to each comparison of a criterion using a scaling slightly different than the GOF scaling recommended by Kristeková *et al.* (2009); while the GOF scaling used in the verification part of E2VP gives a score of 6/10 to a difference of 50% (see Figure 8), the Anderson GOF scaling used in the validation part of E2VP gives a higher score of 8/10 to a difference of 50% (Anderson, 2004, see Figure 9).

The PGV maps computed by team 3D05 using $Q(f) = Q(f_0).f/f_0$ with $f_0 = 1, 2,$ and 4 Hz are shown in Figure 55. When f_0 increases, the values of $Q(f)$ decrease. The differences between each case in Figure 55 are minor but the PGV map looks smoother for $f_0 = 4$ Hz compared to the other cases. This effect is however almost negligible.

The total energy of the signal is highly sensitive to the variation of attenuation (high differences on the Arias intensity, as shown in Figure 56) but other criteria are not so sensitive (cross correlation/waveforms, peak values).

A second study explores the influence of the scaling of Q_S with V_S on the computed ground motion based on 3D02 calculations in model B (see Table 4) where $Q_S = V_S/5, V_S/10,$ and $V_S/20$. The same observations can be made as in the previous study: the details of the PGV map become smoother when the value of Q_S decreases (see Figure 57). Again, the variation of attenuation mainly impacts the total energy of the signal while the other ground motion criteria are not so sensitive.

The differences on the computed ground motion obtained in this sensitivity test to damping are small before the differences obtained between recorded and synthetic waveforms. Therefore this sensitivity to damping is significant only if the simulated event is well defined and precisely located, and when the velocity model is well known.

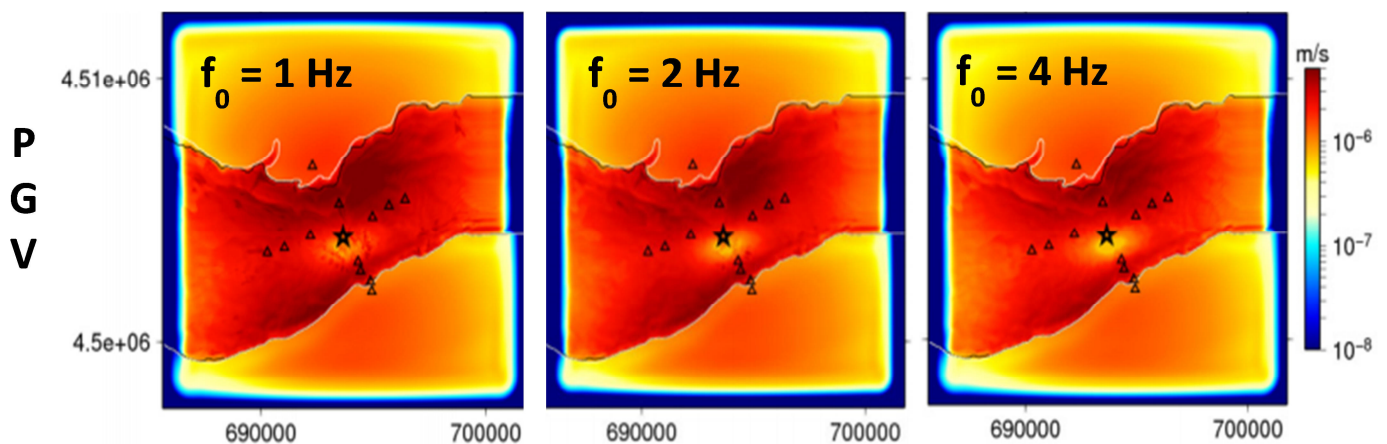


Figure 55: PGV maps computed by team 3D05 using $Q(f) = Q(f_0).f/f_0$ with $f_0 = 1, 2, 4$ Hz.

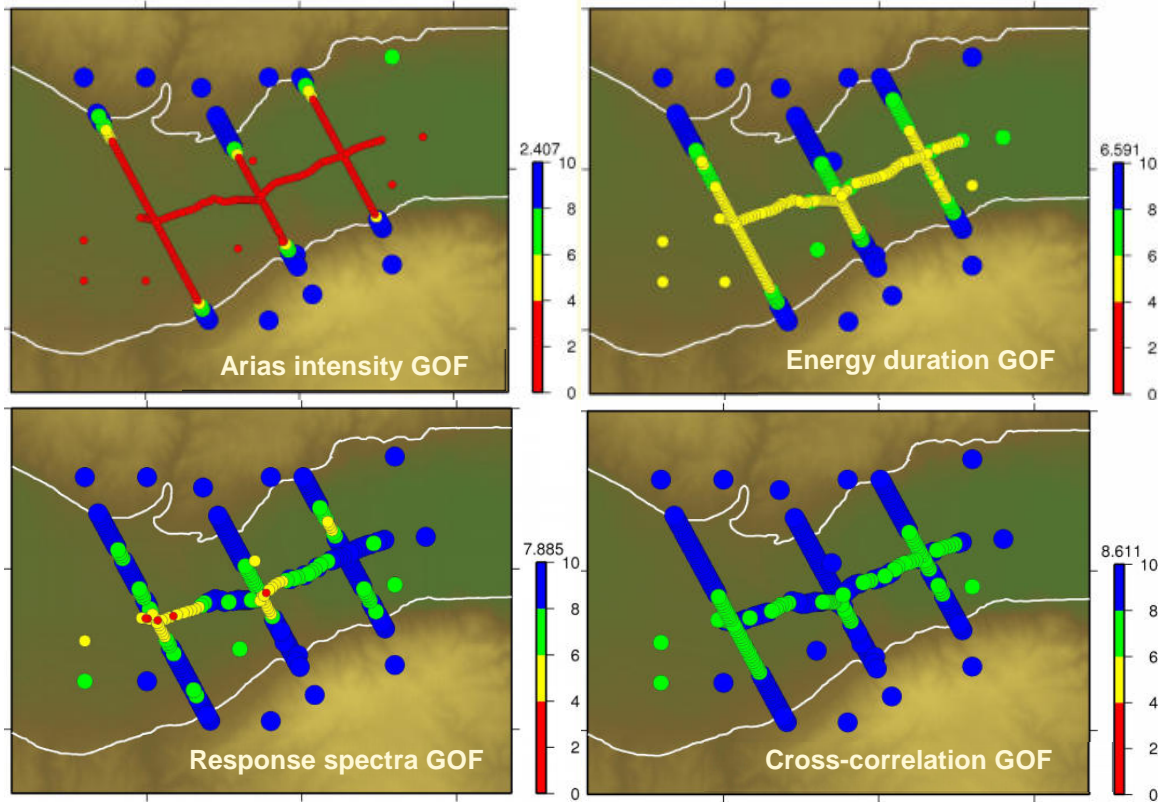


Figure 56: Maps of goodness-of-fit (GOF) between 3D05 computations using $Q(f) = Q(f_0) \cdot f/f_0$ with $f_0 = 1$ or 4 Hz, for Arias intensity, energy duration, response spectra and cross-correlation. Blue dots are for excellent fit ($GOF > 8$), green dots for good fit ($6 < GOF < 8$), yellow dots for fair fit ($4 < GOF < 6$) and red dots for poor fit ($GOF < 4$).

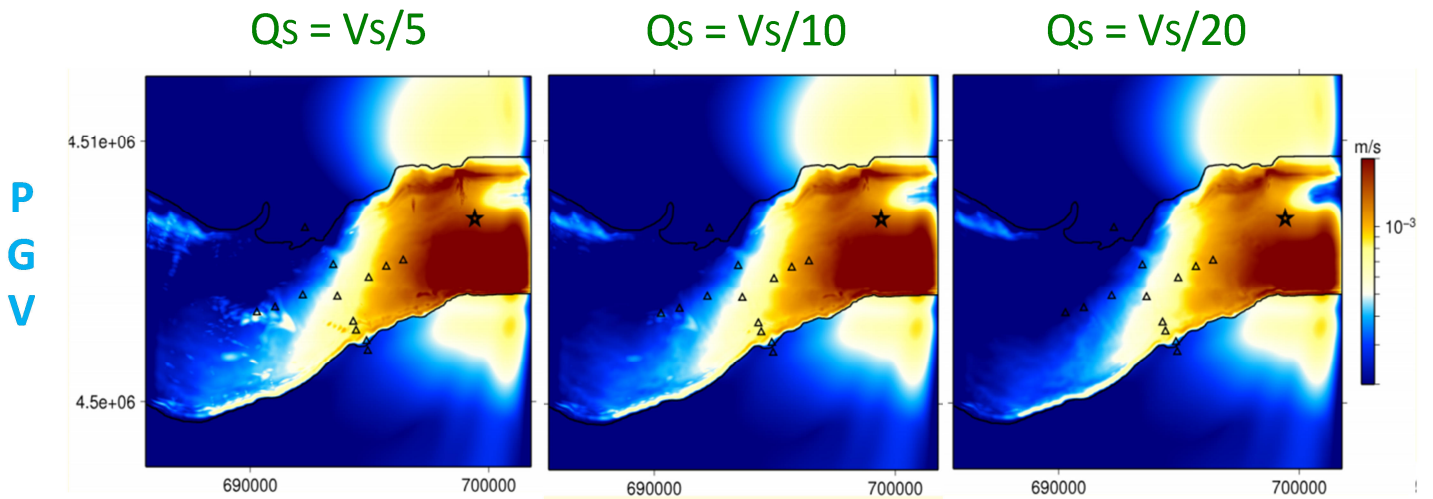


Figure 57: PGV maps computed by team 3D02 using $Q_s = V_s/5$, $V_s/10$ and $V_s/20$.

6.3 SENSITIVITY TO VELOCITY MODEL: EFFECT OF AN ALTERED SURFACE LAYER WITHIN ROCK

The sensitivity of the computed ground motion to the effect of an altered surface layer within rock is estimated from 2D calculations by team 2D03. This altered surface layer is included in the Mygdonian basin model by changing the material properties of the near-surface rock on each side of the basin. The material properties inside the altered surface layer from surface to 80 m depth become: $V_P = 1500\text{-}4500$ m/s, $V_S = 750\text{-}2600$ m/s, $\rho = 2250\text{-}2600$ kg/m³, $Q_S = 100$ and $Q_P = 200$. Bellow 80 m depth, the material properties of the unaltered bedrock stay the followings: $V_P = 4500$ m/s, $V_S = 2600$ m/s, $\rho = 2600$ kg/m³, $Q_S = \infty$ and $Q_P = \infty$.

As in the previous sensitivity study, the sensitivity of the computed ground motion to the effect of an altered surface layer within rock is assessed from the goodness-of-fit scores on the Anderson's ground motion criteria (Anderson, 2004). Some examples of the results are shown in Figure 58 and an average GOF score is calculated as the average of the ten individual GOF scores on the Anderson's criteria (see Figure 59).

The Figure 58 and the Figure 59 clearly show that the effect of an altered surface layer within rock is limited on the very edges of the basin and seen only at higher frequencies (where the effect is slightly more important on the vertical component). As the goodness-of-fit scores at the center of the basin are excellent between the two cases, it can be concluded that altering the near-surface material properties of the bedrock does not impact the ground motion inside the Mygdonian basin.

To improve the knowledge on the velocity model of the bedrock is therefore not a priority for progressing in the validation task of E2VP. Indeed the GOF scores in this sensitivity study are around 9/10 within the basin, while the GOF scores on the same ground motion criteria are around 6/10 when comparing synthetics with real recordings (see Table 14).

Yet this sensitivity is much stronger on the bedrock; the effect of an altered surface layer within rock should imperatively be taken into account for reference site issues.

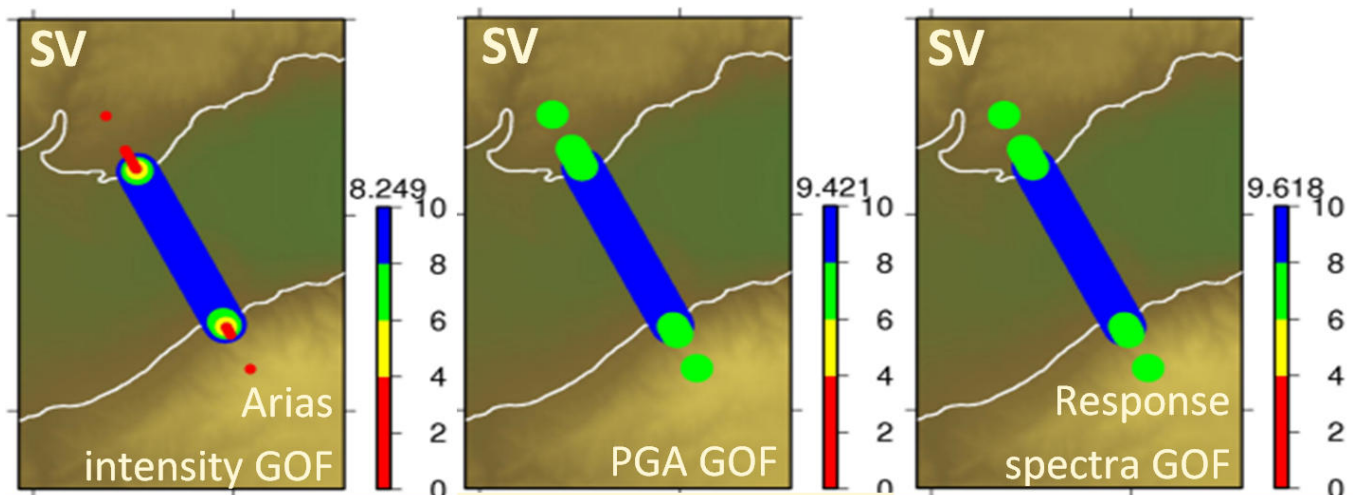


Figure 58: Maps of goodness-of-fit (GOF) scores on the SV component for Arias intensity (left), PGA (middle) and response spectra (right) comparing 2D computations by team 2D03 with and without an altered surface layer within rock. Blue dots are for excellent fit ($GOF > 8$), green dots for good fit ($6 < GOF < 8$), yellow dots for fair fit ($4 < GOF < 6$) and red dots for poor fit ($GOF < 4$). The number on top of the color scale is the mean GOF score of the corresponding map.

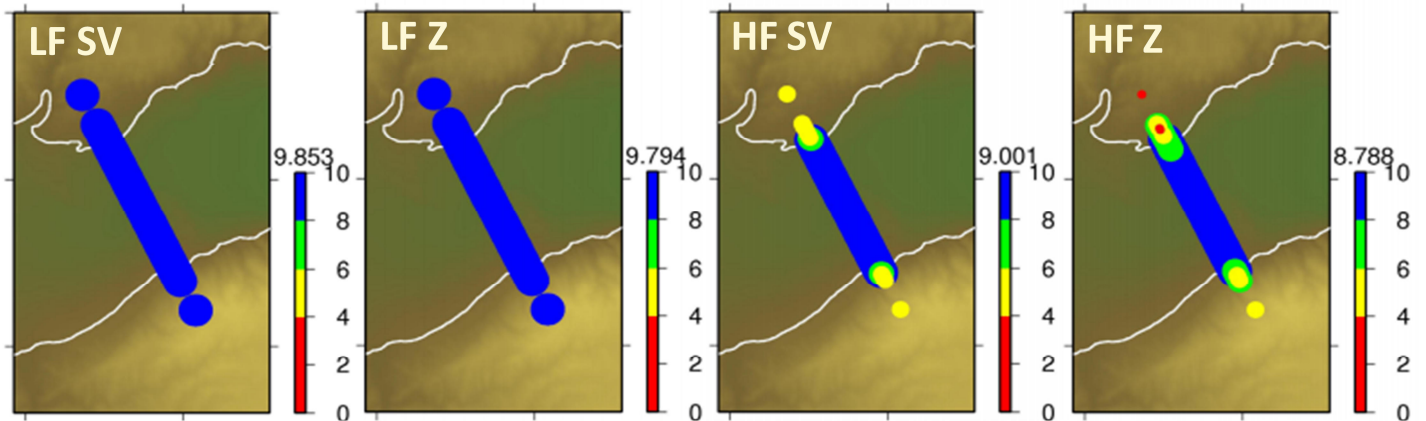


Figure 59: Maps of goodness-of-fit (GOF) average scores of the 10 Anderson's criteria (Anderson, 2004) on the SV component at low frequencies (first panel), on the vertical component at low frequencies (second panel), on the SV component at high frequencies (third panel), on the vertical component at high frequencies (fourth panel), comparing 2D computations by team 2D03 with and without an altered surface layer within rock. Blue dots are for excellent fit ($GOF > 8$), green dots for good fit ($6 < GOF < 8$), yellow dots for fair fit ($4 < GOF < 6$) and red dots for poor fit ($GOF < 4$). The number on top of the color scale is the mean GOF score of the corresponding map.

6.4 SENSITIVITY TO VELOCITY MODEL: IMPACT OF THE REPRESENTATION OF THE SEDIMENTS, LAYERING OR GRADIENT

The impact of the layering or gradient representations of the sediments on the ground motion in the basin was already partially explored in the elastic canonical cases (see part 3.5), where it was shown how different are the waveforms between the layering and gradient cases due to the strong differences in the physical dispersion of the surface waves.

This sensitivity to the representation of the velocity model was also estimated by comparing 3D visco-elastic simulations performed by team 3D02 in the layered and gradient models of the Mygdonian basin from a realistic event and by translating the differences in goodness-of-fit scores on the Anderson's criteria. The most representative results are shown in Figure 60. The PGD is almost insensitive to layering details, while the cross correlation (waveforms) and the total energy are very sensitive.

Another test was performed by team 2D03 in the elastic 2D gradient model of the Mygdonian basin, comparing the respective effects of laterally homogeneous gradients and laterally heterogeneous gradients in the sediments (see Figure 61). As in the previous sensitivity test, the PGD is much less affected than the cross correlation criterion. The vertical component of the ground motion is the most sensitive in the 2D case; while in the 3D case both horizontal and vertical components were equally sensitive.

Yet the effect of laterally homogeneous gradients strongly impacts the entire ground motion inside the basin as the Anderson GOF scores are all under 6/10 for all of the criteria. It is therefore not recommended to use laterally homogeneous gradients to represent the velocity model of the Mygdonian basin.

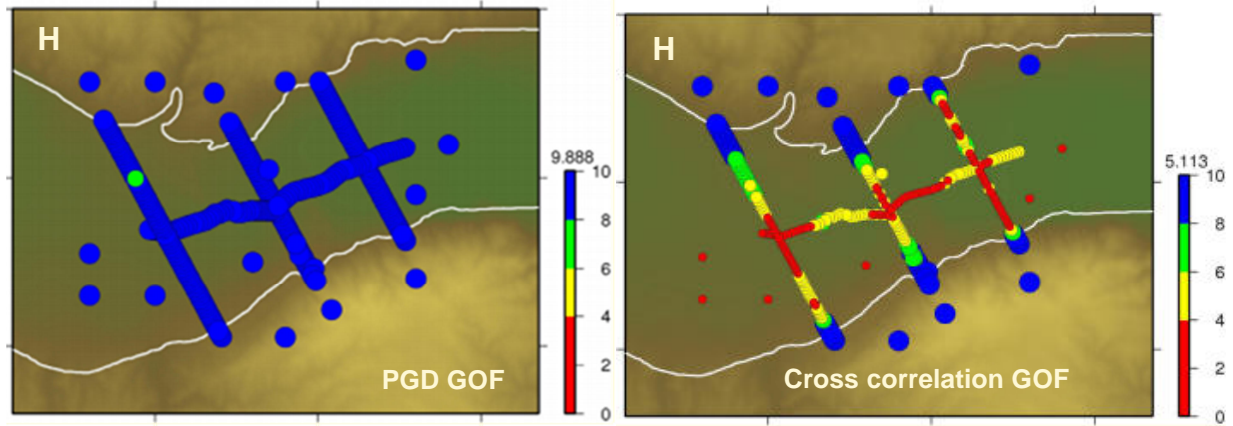


Figure 60: Maps of average goodness-of-fit (GOF) scores on the horizontal components for PGD (left) and cross correlation (right) comparing 3D visco-elastic computation by team 3D02 in the 3-layers model A (see Table 3) with the same computation in the gradient model B (see Table 4) of the Mygdonian basin. The source is the event #4 (see Table 13). Blue dots are for excellent fit ($GOF > 8$), green dots for good fit ($6 < GOF < 8$), yellow dots for fair fit ($4 < GOF < 6$) and red dots for poor fit ($GOF < 4$). The number on top of the color scale is the mean GOF score of the corresponding map.

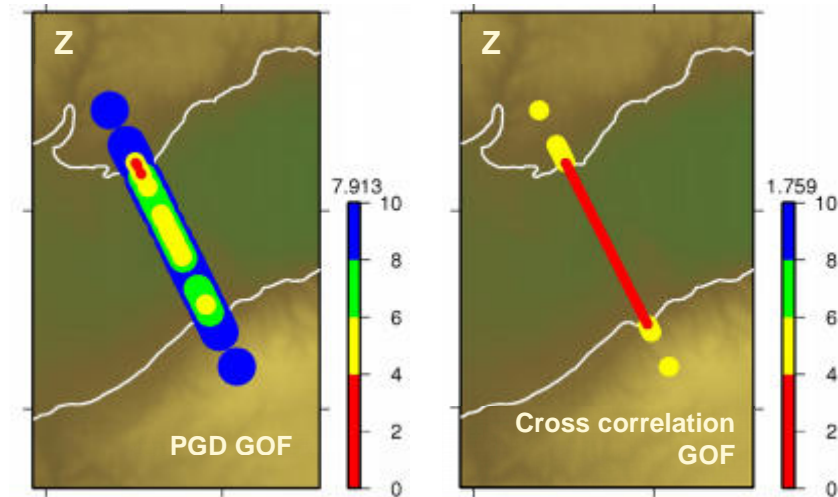


Figure 61: Maps of goodness-of-fit (GOF) scores on the vertical component for PGD (left) and cross correlation (right) comparing 2D elastic computation by team 2D03 in the laterally homogeneous vertical gradient model with the same computation in the laterally heterogeneous vertical gradient model of the Mygdonian basin. Blue dots are for excellent fit ($GOF > 8$), green dots for good fit ($6 < GOF < 8$), yellow dots for fair fit ($4 < GOF < 6$) and red dots for poor fit ($GOF < 4$). The number on top of the color scale is the mean GOF score of the corresponding map.

6.5 WRAP-UP OF SENSITIVITY RESULTS

The results of all these sensitivity studies are summarized in Table 15 in terms of "engineering" goodness-of-fit scores. Only the average values, taking into account all available components (*i.e.*, 2 or 3, respectively, for 2D and 3D results) and receivers, are considered. It indicates that the key ingredients most influencing the goodness-of-fit are a) the way damping is implemented in the simulation code, and b) the description of lateral heterogeneities within the sediments. As the corresponding "engineering GOF" scores are comparable to the validation scores, they should be considered as high priority issues whenever using the numerical simulation approach:

- using a code with a proper implementation of damping;
- having a detailed enough knowledge of the internal structure of the sediments and of their lateral variability.

Table 15: Wrap-up of sensitivity results. GOF stands for "goodness-of-fit from Anderson (see part 3.3).

Sensitivity topic		Resulting "GOF"	Comment
Model geometry	effect of surface topography	in the valley: 9-10 on rock: 7-8	<i>may affect mainly reference motion on rock</i>
Damping	implementation (constant value / proportional to frequency)	6-8	<i>affects mainly total energy and duration, not so much peak values nor spectral acceleration</i>
	damping value ($V_s/20 - V_s/5$)	7-8	
Velocity model in rock	surface weathering in rock	9	<i>affects reference sites and relative amplification</i>
Velocity model in sediments	Poisson's ratio	8	<i>(not shown)</i>
	homogeneous vs gradient, including lateral heterogeneities	7-8	
	without lateral heterogeneities within sediments (vertical gradient)	6-8	<i>affects waveforms</i>

7 CONCLUSION OF E2VP PHASE 1 AND PERSPECTIVES FOR PHASE 2

7.1 CONCLUSION OF E2VP PHASE 1

Thanks to the participation of several "first-class" teams from various parts of the world, the E2VP-1 project allowed to achieve several major accomplishments, mainly in the field of verification of ground motion simulation codes. Certainly not all the initial objectives could be reached, not all the initial questions could be answered, as the in-depth understanding of the origins of discrepancies or agreement require time and deep personal investment, and these initial objectives were probably too ambitious. Thus, "verification" and "validation" fields still face a lot of open issues where further investigations are needed, but this project did allow building a solid group now sharing a common experience, and a common concern about what are the next frontiers and what should be the next goals to address.

In a nutshell, the main lessons from this 3-year long project could be listed as follows:

- Careful verification requires time and often to "go back to basics", while careful validation requires high quality data, *i.e.*, including rich and high quality metadata. This implies either not to be too ambitious when setting up the goals of future similar exercises, or to allocate significant amounts of money and manpower.
- No ground motion simulation code accounting for wave propagation in complex media can be considered as press-button, neither in the linear, 3D domain, nor in the non-linear 2D case (nor probably in the 1D, NL case). The most common case is that, without iterations and cross-checking, different codes provide different results when applied to the same case study. The immediate conclusions of engineering interest are that:
 - too fast applications of existing codes may yield VERY wrong ground motion estimates, potentially resulting in raising mistrust in end-users;
 - some codes presently used in engineering applications would deserve some significant improvements, or strong warnings on rather stringent validity limits, while even state-of-the-art codes (predominantly in the "academic" field) deserve constant upgrading.
- However, the existence of a very good agreement between several completely independent codes, with code-to-code differences much smaller than the predictions-to-observations distance, makes it possible and legitimate to include the numerical simulation approach in the toolbox for site-specific ground motion estimation, at least in the 3D linear case. The lessons and experience of E2VP-1 draw the attention on the following recommendations for a wise use of such numerical simulation codes:
 - One should never be satisfied with only one computation from one single team, but should request several teams (at least two) with different numerical schemes to perform parallel computations on the same case. And one can accept the results as reliable only if the corresponding results agree beyond some quantitative goodness-of-fit threshold.
 - These goodness-of-fit criteria should definitely be improved and agreed upon by the engineering community in order to reach an objective of transparent quantitative comparison, which should replace sentences such as "one can see the very good agreement on the figure"...
 - In the long run, it would be very valuable to assign a specific "quality label" to numerical codes and teams that did accept to run some of the now existing "canonical" cases with their own numerical code, which are freely available on some web pages such as <http://www.sismowine.org/>. Maintaining this kind of internet facility in the long run will be beneficial for the whole community.

- External peer reviews are always useful in assessing the quality of results derived from highly sophisticated numerical codes.
- Comparison with actual data (in-situ earthquake recordings), whenever possible, are always useful. Having sensitive in-situ instrumentation (continuously recording broad-band velocimeters or sensitive accelerometers) proves to be invaluable for checking the reliability of numerical simulation results.
- Similar efforts are still to be done as to the verification of the NL simulation codes especially as they are much more often used in engineering practice than 3D, linear simulation codes. Are reproduced below some of the partial conclusions reached at the end of the 2D verification section:
 - NL verification should be performed on the simplest possible cases (1D soil columns);
 - it should be performed on already instrumented sites having recorded large acceleration levels;
 - it should be associated with careful in-situ surveys and lab tests designed in tight connection with the needs of the rheological models implemented in the various NL codes.
- The validation exercise had to be limited to local, weak-to-moderate magnitude events with significant high frequency contents since no stronger local event has occurred in recent years. The satisfactory match of 'overall' characteristics (amplitude, envelope, duration, response spectra) should be balanced by the large differences in the details of waveforms, especially for frequencies beyond 1-2 Hz. The limitations to increase the maximum frequency of synthetics are now much more related to the uncertainties in source parameters and the capabilities of shallow geophysical surveys to provide an accurate 3D description of the actual underground structure at short wavelength, including some badly known parameters such as material damping. This is definitely the next challenge in view of deterministic simulation of ground motion at intermediate frequencies. It thus definitely deserves further investigations and pursuing efforts, with several high-priority issues:
 - How do uncertainties and/or variability of source parameters (x-y coordinates, depth and focal mechanism) map on the variability of site-specific ground motion from local earthquakes?
 - To which extent can the apparent robustness of site amplification (surface to downhole spectral ratios) observed at TST be extrapolated/generalized to other sites and other sources, including in particular extended sources?
 - What is the engineering importance of the local surface waves (time domain NL analyses, broadening effects on amplification spectra)? In other words, what is the engineering added value of more reliable 3D predictions compared to 1D common practice? Up to which levels of accuracy should they be modeled/accounted for by 2D and 3D models? This question is important for developers of numerical codes, since the canonical cases did show the much larger sensitivity to surface waves compared to body waves, in relation with mesh size and properties, and for geotechnical and geophysical surveys as well since the generation of surface waves is directly linked to geo-mechanical properties on valley/basin edges (underground slopes, heterogeneity wavelengths and velocity contrasts).
 - Finally, as already outlined, the small number of "candidate events" for validation is a typical situation of moderate/weak seismicity areas. Future validation events would certainly benefit from the possibility to include more distant events, which implies the use and/or the development of some "hybrid" numerical schemes coupling computations at different scales.

7.2 PERSPECTIVES FOR E2VP PHASE 2

The phase 1 of the E2VP project, complemented by the “canonical case” work allowed a major progress in verification. Even if improvements are still mandatory, we showed that after a few iterations, the match between simulations, realized on realistic cases (with attenuation) and formulated using engineer parameters, are very good. The procedure is still not a “press-button” formality (it will certainly be never the case) and it is still necessary to work with several teams. Nevertheless, the 3D simulation tools are now ready to be confronted to real data and to be used on real site effects studies.

The “validation work” of phase 1 has laid the groundwork of such a work. Some comparisons between real data and simulations were surprisingly good whereas other ones were terribly bad. The source of the mismatches is not yet clearly identified. Are they linked to the intrinsic variability of ground motion? Are they linked to a bad determination of seismic source parameters? Are they linked to an imperfect definition of the geological and geotechnical model? E2VP phase 2 intends to tackle these issues.

7.2.1 Estimation of the influence of geological and source parameter uncertainties on the numerical simulation uncertainties

During phase 1, we did not seek to optimize or modify geological model or source parameters: we took “as it was” the information provided by Aristotle University of Thessaloniki. We now want to work in these two fields.

On seismic source parameters (magnitude, position, depth, focal mechanism), we will introduce the data from the Euroseistest accelerometric network within the sources parameter determination procedure (only the data from national velocimetric network were previously used). This work will be applied on a larger earthquake database than the one used for phase 1.

This work will also help to better assess the uncertainties associated to the source parameters. In the validation procedures, sensitivity studies will be done in order to assess the effect of source parameter uncertainties on the ground motion simulation by introducing changes in the source parameter values within the uncertainties domain.

Concerning the geological model, the results of recent surveys that were not valorized in the previous model will be considered. A few new surveys will also be done to extend the geological model toward the West and toward the East in order to get a larger model. A new model will then be proposed, associated to several other alternative models, different but plausible and compatible with available data. Within the validation procedure, one can then evaluate the effect of reasonable changes in the geological model on the ground motion simulation results.

7.2.2 Estimating ground motion variability using simulations

The strict comparison between simulation and real data will be done typically on a dozen of earthquakes. The estimation of the whole variability and uncertainty requires a wider work. We propose to simulate a “large” number (to be defined) of earthquakes that could better address the estimation of the ground motion variability (magnitude, position depth, incidence angle, azimuth...). This wider set of results will be used (among other analysis) to estimate the “single-station sigma” from a numerical point of view.

7.2.3 Estimating “single-station sigma” with real accelerometric data

Complementarily, a work on the real accelerometric database will be performed in order to obtain a local GMPE and estimate the associated uncertainties and also “single-station sigma” from an empirical point of view.

The common analysis of the three work fields presented above, *i.e.*, 1/ comparisons between real data and simulation associated to sensitivity studies on seismic source parameters and geological model upon a set of a ten of earthquake, 2/ estimation of ground motion variability by simulations, 3/ estimation of

standard deviation derived from real accelerometric data base, should allow to answer the main issues raised by E2VP phase 1.

7.2.4 Other issues

In parallel with the central work described above and in connection with other studies done within the Cashima and Sigma projects, the following issues will also be addressed in E2VP-2.

7.2.5 Validation work on distant events

During phase 1, we worked only with earthquakes that occurred “inside the modeling box”. Indeed, if we want to apply the results of E2VP on low seismicity sites, we will have to deal with signals coming from distant earthquakes occurring far from the studied site: in most such cases, we do not have any record of local earthquakes. Thus, we want to test the validation procedure using earthquake that occurred outside of the local, highly-detailed modeling box. This is not trivial because we have to solve the issue about how to “transfer” the wavefield from the hypocenter to the border of the model.

7.2.6 Until which frequency are the deterministic modeling approaches relevant?

Even if modeling tools and computing capabilities have made major progress, we will not be able to perform reliable and representative “deterministic” simulations up to very high frequencies because the geological medium cannot presently be described with the required resolution. Using the results related to the sensitivity on the geological model, and of a few other studies, E2VP-2 will contribute to estimate the “cut-off” frequency above which deterministic simulations are no longer suitable.

8 REFERENCES

- Anderson J.G., **2004**, Quantitative measure of the goodness-of-fit of synthetic seismograms, *13th World Conf. on Earthquake Engineering Conference Proc.*, paper number 243.
- Chaljub E., C. Cornou, and P.-Y. Bard, **2006**, Numerical benchmark of 3D ground motion simulation in the valley of Grenoble, French alps, *Third International Symposium on the Effects of Surface Geology on Seismic Motion, Grenoble, France, 2006, August 30th–September 1st*, paper number SB1, vol. 2.
- Chaljub E., P. Moczo, S. Tsuno, P.-Y. Bard, J. Kristek, M. Käser, M. Stupazzini, and M. Kristekova, **2010**, Quantitative comparison of four numerical predictions of 3D ground motion in the Grenoble valley, France, *Bull. Seism. Soc. Am.*, 100.4, 1427–1455.
- Coutant O., **1990**, Programme de simulation numérique Axitra, *technical report*, Université Joseph Fourier, Grenoble, France.
- Hisada Y., **1994**, An efficient method for computing Green's functions for a layered half-space with sources and receivers at close depth, *Bull. Seism. Soc. Am.*, 84.5, 1456–1472.
- Jongmans D., K. Pitilakis, D. Demanet, D. Raptakis, J. Riepl, C. Horrent, K. Lontzetidis, and P.-Y. Bard, **1998**, EURO-SEISTEST: determination of the geological structure of the Volvi basin and validation of the basin response, *Bull. Seism. Soc. Am.*, 88.2, 473-487.
- Kristeková M., J. Kristek, P. Moczo, and S.M. Day, **2006**, Misfit criteria for quantitative comparison of seismograms, *Bull. Seism. Soc. Am.*, 96.5, 1836-1850, doi: 10.1785/0120060012.
- Kristeková M., J. Kristek, and P. Moczo, **2009**, Time-frequency misfit and goodness-of-fit criteria for quantitative comparison of time signals, *Geophys. J. Int.*, 178, 813-825, doi: 10.1111/j.1365-246X.2009.04177.x.
- Manakou M., **2007**, Contribution to the determination of a 3D soil model for site response analysis, the case of the Mygdonian basin, *PhD thesis, Department of Civil Engineering, Aristotle University of Thessaloniki*.
- Manakou M., D. Raptakis, P. Apostolidis, F.J. Chávez-García, and K. Pitilakis, **2007**, The 3D geological structure of the Mygdonian sedimentary basin (Greece), *4th International Conference on Earthquake Geotechnical Engineering, 2007, June 25th–28th*, paper number 1686.
- Manakou M., D. Raptakis, F.J. Chávez-García, P.I. Apostolidis, K. Pitilakis, **2010**, 3D soil structure of the Mygdonian basin for site response analysis, *Soil Dynamics and Earthquake Engineering*, 30, 1198-1211.
- Moczo P., J. Kristek, V. Vavryčuk, R.J. Archuleta, and L. Halada, **2002**, 3D heterogeneous staggered-grid finite-difference modeling of seismic motion with volume harmonic and arithmetic averaging of elastic moduli and densities, *Bull. Seism. Soc. Am.*, 92.8, 3042-3066, doi: 10.1785/0120010167.
- Papazachos B., D. Mountrakis, A. Psilovikos, and G. Leventakis, **1979**, Surface fault traces and fault plane solutions of May-June 1978 major shocks in the Thessaloniki area, *Tectonophysics*, 53, 171-183.
- Papazachos C.B., **1998**, Crustal *P*- and *S*-velocity structure of the Serbomacedonian Massif (Northern Greece) obtained by non-linear inversion of traveltimes, *Geophys. J. Int.*, 134, 25-39, doi: 10.1046/j.1365-246x.1998.00558.x.

- Pitilakis K., G. Manos, D. Raptakis, A. Anastasiadis, K. Makra, and M. Manakou, **2009**, The EUROSEISTEST experimental test site in Greece, *EGU General Assembly, Vienna, Austria, 2009, April 19th-24th*.
- Psilovikos A., **1977**, Paleogeographic development of the basin and lake of Mygdonian (Lagada - Volvi area, Greece), *PhD thesis, Department of Geology, Aristotle University of Thessaloniki*.
- Raptakis D., F.J. Chávez-García, K. Makra, and K. Pitilakis, **2000**, Site effects at Euroseistest-I: determination of the valley structure and confrontation of observations with 1D analysis, *Soil Dynamics and Earthquake Engineering*, 19, 1-22.
- Raptakis D., M. Manakou, F.J. Chávez-García, K. Makra, and K. Pitilakis, **2005**, 3D configuration of Mygdonian basin and preliminary estimate of its site response, *Soil Dynamics and Earthquake Engineering*, 25, 871-887.
- Sotiriadis L., A. Psilovikos, E. Vavliakis, and G. Syrides, **1983**, Some Tertiary and Quaternary basins of Macedonia / Greece, *Formation and Evolution, Clausthaler Geologische Abhandlungen*, pp. 21.
- Tsuno S., E. Chaljub, and P.-Y. Bard, **2006**, Grenoble valley simulation benchmark: comparison of results and main learnings, Third International Symposium on the Effects of Surface Geology on Seismic Motion, Grenoble, France, 2006, August 30th-September 1st, paper number SB2, vol. 2.



Review of Deliverable D3-38

Evaluation of the relevance of the numerical simulation approach for site effect estimation: lessons of the Euroseistest verification and validation project E2VP phase 1 and perspective for phase 2

Authors: E. Maufroy, E. Chaljub, P-Y. Bard, F. Hollender & many others

Reviewed by: R. Paolucci, Politecnico di Milano

In this deliverable a summary is made of the validation activity of numerical codes for 2D and 3D numerical simulation of seismic wave propagation in complex geological media. The activity was conducted in the first phase between autumn 2007 and June 2010 within the CASHIMA project, and, in the second phase, started in February 2012, in strict link with the SIGMA project.

The report is comprehensive, clear and well written and fully conveys the idea of the huge effort made not only by the participant teams of the experiments to provide solutions for such a large amount of numerical tests but by the organizers of the experiment to collect, homogenize and process uniformly the results. There is no doubt that this activity is having a major relevance to better understand the potential applications of high performance numerical codes for seismic wave propagation, their present limitations and their expected progress in the next future.

Probably the weak point of the report is that it should have been more stringent and detailed in the definition of the planned activities and perspectives for the Phase 2, as well as in pointing out its benefits in the framework of SIGMA project. Therefore, my review is mainly aimed at raising some points to support the planning of this phase.

a) Creating a web site to check the accuracy of numerical codes and to provide “quality labels” to the codes

I find that this idea, stated in the conclusion section 7 of the report, is very valuable and should be fully exploited in the next future. Each code should pass a series of “canonical” cases and be attributed a goodness of fit score for each case. My concern for this purpose is that the canonical cases devised by the organizers are too much demanding from a computational viewpoint. If we consider for example test CAN1, the requirement of a homogeneous halfspace with $V_s=200$ m/s extending 5x4 km in plan and 3 km in depth is not realistic and implies a huge numerical mesh and computational effort. If we want that such cases could be used as canonical benchmarks they should be based on simple albeit realistic configurations and initial conditions (including plane waves, double couple source, surface load), and should be run in a reasonable computer time.

The canonical cases should serve as a basis to update the “rule of thumbs” considered by the users of the different numerical codes to set the minimum spatial distance of nodes, the time step, the maximum velocity contrast between adjacent layers. Most often, these rules are blindly applied, especially by untrained users. Again, canonical case CAN1 is very meaningful because it implied for most teams the

onset of large numerical dispersion, mostly due to the fact that at the threshold frequency of 4Hz the frequency content of the excitation was not negligible.

For this purpose, I think that simpler benchmarks of engineering relevance should be devised, including vertical and oblique plane wave propagation, large velocity contrasts, linear visco-elastic attenuation, surface topography and non-linear effects.

b) Planning a benchmark for nonlinear site effects, based on a real case study

Differences of numerical predictions in the nonlinear case (section 4) emerged as one of the most disturbing results of the phase 1, and should be addressed carefully in the very next future. At least one well calibrated benchmark based on real accelerograms should be defined, at least for 1D and 2D numerical models. There are not many suitable examples (Wildlife array? results from centrifuge experiments?), but authors are invited to investigate the different options and make one or more proposals.

c) Planning a benchmark for larger magnitude earthquakes

The phase 1 activity clearly showed that working with real records poses a number of further problems with respect to canonical cases, such as the role of detailed modeling of the seismic source and propagation path. Calibration of 3D numerical codes against records of moderate-to-large seismic events (say of magnitude 5.5-6 or larger) allows one to provide answers for the engineering applications of such kind of numerical codes, typically to understand what is the large and small-scale detail of information, in terms of kinematic fault model and dynamic soil properties along the propagation path, required to provide satisfactory predictions of earthquake ground motion, not only in terms of peak values, but also in terms of duration, broadband frequency content, and spatial coherency. Comparison with real records allows one to clarify as well the role of the visco-elastic attenuation model, especially at large distances from the source, and of soil nonlinearity.

Recent earthquakes, such as L'Aquila and Christchurch, did provide a large number of data, in terms of records, geological and geophysical information, suitable to devise an alternative, albeit more meaningful, benchmark than the small earthquakes close to Volvi basin. Both earthquakes have magnitude, geological and tectonic conditions that may be interesting also for small-to-moderate seismicity regions.

d) Link with SCEC activities

Finally, I suggest the authors to make reference to a similar work on Ground Motion Simulation Validation (GMSV) that is in progress in the United States, and that can be partly documented through the following web site: http://collaborate.scec.org/gmsv/2012_Coordination_Workshop. I suggest that a stricter connection with the SCEC researchers, or even a joint workshop, could be very helpful within the SIGMA project.

Project SIGMA

Review of:
**Evaluation of the relevance of the numerical
simulation approach for site effect estimation:**
lessons of the Euroseistest Verification and Validation
Project (E2VP) – phase 1
and perspectives for phase 2.

(Ref : SIGMA-2012-D3-38)

Alain Pecker
May 20, 2012

1. Scope of the work reviewed

The object of the report is to present the results of a very comprehensive international benchmark which aimed at testing and comparing numerical simulation techniques that can be used to quantify site effects; comparisons were undertaken between several teams using different modeling techniques (finite element, finite difference, spectral element, discrete element, discontinuous Galerkin) on canonical tests and with real data collected from earthquakes recorded in the Volvi basin in Northern Greece. This report is part of Work Package WP4, "Improving Seismic Hazard Models".

2. General comments

This report, although the work has not been conducted within the framework of SIGMA, is essential for the project. It clearly points out the limitations and pit-falls of numerical analyses for evaluation of site effects even within the linear range on simplified geometries.

The detailed methodological approach that has been followed to identify the origin of initial discrepancies between different institutions should serve as a guide for further benchmarks on this topic: undertaking a verification phase which consists in comparing predictions by different numerical techniques on simplified test cases; once verifications are deemed satisfactory, a validation phase consisting in comparing predictions to recorded data. Furthermore the authors propose a quantitative assessment of the goodness of fit between different solutions. This goodness of fit criteria is based on ground motion parameters, like PGA, PGV, PGD, Arias intensity... or a combination of all. One recommendation would be that WP4 coordinates strongly with WP5 to choose the most relevant parameters for engineering purposes and evaluation of damages in structures. Detailed comparisons of

wave forms may possibly be too stringent for engineering applications and not worth spending too much effort on it, at least within the framework of SIGMA.

Essential in the approach is the necessity to quantify uncertainties related either to the source model or to the site characteristics (velocity profile, damping...) as it has been tentatively done. The next phase of E2VP is clearly oriented towards quantifying these uncertainties.

It must be realized, as clearly indicated in the report, that numerical simulation cannot be the final answer to quantification of site effects for engineering applications since they are limited to rather low to medium frequencies (4Hz in the report). This limitation is not due to computer limitations but to the accuracy with which the medium can be characterized and there is no hope that this limitation can be overcome in the future. Therefore, it is recommended that the authors investigate complementary approaches (like stochastic simulations) to complement the predictions at least up to 20Hz.

It is pointed out in the report that, during phase 1 of E2VP, nonlinear simulations have been attempted but were not really successful possibly because they were too ambitious at the beginning, bypassing in some way the verification process. This effort should be pursued because safety margin assessment of nuclear facilities require that the response be known at large input motions for which the linear assumption may no longer be valid.

It is essential, as indicated by the authors, that comparisons between 1D, 2D and 3D simulations be pursued as the degree of complexity in 3D calculations is likely to be beyond the capability of engineering projects, especially if nonlinear soil behavior is accounted for.

Several of the points listed above are already included in phase 2 of E2VP; the other may be considered.

3. Specific comments along the text

- Tables 3 and 4: how are the attenuation values chosen? This is also relevant to the discussion on the effect of Q on the results in §6.2 where significantly higher values are used.
- For the canonical tests CAN1 and CAN2 why the discrete wave number solution is considered the reference solution? Is it better than others and free from numerical errors? Furthermore, it is mentioned later in the report that the discrete wave number solution has been computed with two different softwares (Hisada's code and Axitra); it would have been interesting to know how different the solutions were. Has a goodness of fit criteria applied to both solutions?
- In the verification of 2D nonlinear calculations (§4) it is indicated that the data provided consist in the G/G_{\max} and damping curves describing the shear nonlinear behavior. Other data are needed for a complete description of nonlinear behavior (see review of 2012-D3-39).
- In the same paragraph the very low threshold p_{ga} (0.05g) for which nonlinear behavior shows up in some models is very surprising and clearly needs further investigation as it is not supported by observations during earthquakes.

- The few 1D comparisons point out that amplification is overestimated with respect to observations. An explanation related to the destructive wave interference (in the field?) at the sediment basement interface is offered. It should be elaborated further because the damping value used in the simulation may also significantly impact the results at resonance in 1D calculations.
- In paragraph 6.5 which summarizes the results of the sensitivity analyses it is indicated that a proper implementation of damping is required. Several formulations were used in the benchmark (see table 2) and it would be useful that the authors indicate which implementation, in their opinion, is the best suited.